AIAA 2022-2023 Undergraduate Hybrid-Electric Regional Turboprop Design Proposal

A Technical Report submitted to the Department of Mechanical and Aerospace Engineering

Presented to the Faculty of the School of Engineering and Applied Science

University of Virginia • Charlottesville, Virginia

In Partial Fulfillment of the Requirements for the Degree

Bachelor of Science, School of Engineering

Darius Espinoza

Spring, 2023

Technical Project Team Members
James Caputo
Alexander Poley
Jannik Gräbner
Ryan Grant
Ryan Keller
Eun Park
Kangyi Peng
Alex Wang

On my honor as a University Student, I have neither given nor received unauthorized aid on this assignment as defined by the Honor Guidelines for Thesis-Related Assignments

Advisor

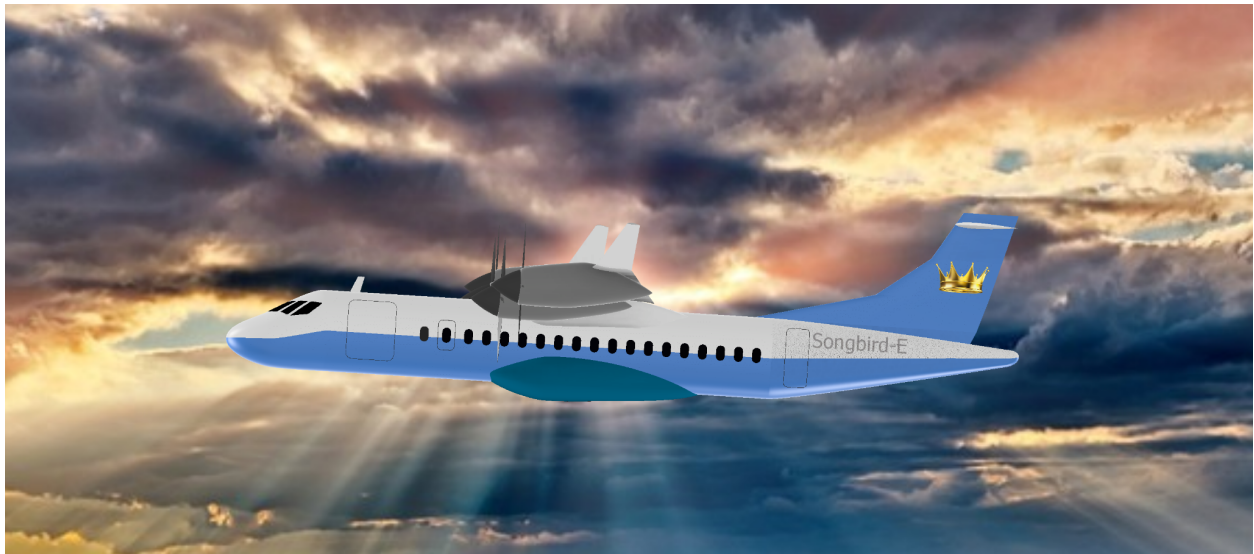Jesse Quinlan, Department of Mechanical and Aerospace Engineering

AIAA 2022-2023 Undergraduate Hybrid-Electric Regional Turboprop Aircraft
Final Design Report

James Caputo, Darius Espinoza, Jannik Gräbner, Ryan Grant, Ryan Keller, Eun Park, Kangyi Peng, Alexander Poley, Alex Wang

Department of Mechanical and Aerospace Engineering

University of Virginia School of Engineering and Applied Science, Charlottesville, Virginia, 22904

Conceptual Design of the Songbird-E
MAE 4650/4660 Aircraft Design I/II

Date of Submission: May 12, 2023

Meet the Team

James Caputo Stability & Control AIAA - 1402813	Ryan Grant, Team Co-Lead Configuration Aerodynamics AIAA - 1421496	Kangyi Peng Structures & Weights AIAA - 1422494
Darius Espinoza Geometry AIAA - 1422450	Ryan Keller Cost AIAA - 1422439	Alexander Poley (Team Lead) Mission Analysis & Performance AIAA - 1421588
Jannik Gräbner Subsystems AIAA - 1422528	Eun Park Electric Propulsion & Thermal AIAA - 1402251	Alex Wang Turboprop AIAA - 1373274

Dr. Jesse Quinlan, PhD (AIAA - 306245)
(Faculty Advisor)

Executive Summary

The SkyKings Aircraft Design team at the University of Virginia submits the Songbird-E, a hybrid-electric regional turboprop aircraft, in response to the 2022-2023 American Institute of Aeronautics and Astronautics (AIAA) Undergraduate Team Aircraft Design Request for Proposals (RFP). In this report, an in-depth analysis of the conceptual design of the Songbird-E is conducted. The Songbird-E seeks to revolutionize the turboprop market, enabling more efficient and environmentally-friendly air travel by means of electrification.

The Songbird-E demonstrates an in-depth understanding of the RFP and its requirements. The Songbird-E, shown again in figure ES1, features a turboelectric engine configuration. Most notably, addressing the figures of merit, the Songbird-E finds a reduction of 33.6% in block fuel over a 500 nmi mission, as compared to the current state-of-the-art, the ATR 42-600. By virtue of this, the design also features reductions in all emissions. The inboard engines are futuristic versions of the PW127XT-M, used on the ATR 42-600, on which our design is based. Attached to these engines is a generator, which diverts about 24% of its power to electric motors placed near the wingtips. Accordingly, the Songbird-E leverages improved aerodynamics, namely a weak DEP configuration with outboard power, and winglets. Future composites have enabled significant reductions in weight. Care has been taken to meet other requirements as well, including a 50 passenger capacity, a 1000 NMI design mission, a cruise speed of 275 KTAS at FL280, and the required field lengths. The Songbird-E also reduces direct operating cost by 14.2%. Assumptions made in the design were made carefully and conservatively, to ensure a viable entry into service by 2035. The use of futuristic subsystems paves the way for greater efficiency, usability, and maintainability, in addition to easier maintenance and a reduction in pilot workload. The Songbird-E makes green technology not only environmentally-friendly, but a smart economic decision too.
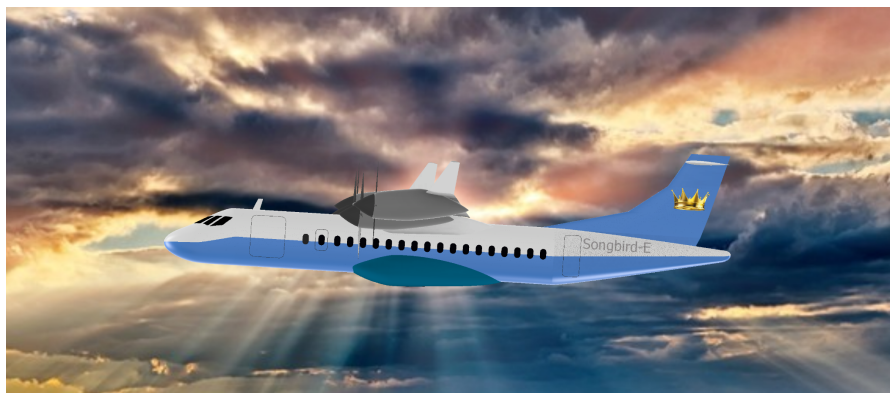
Figure ES-1. Songbird-E Hybrid-Electric Regional Turboprop Concept

Table ES-1. Aircraft Specifications

Crew	• 2 pilots • 1 flight attendant
Dimensions	• Height: 21.7 ft (no landing gear deployed) • Width: 91.9 ft • Length: 80.6 ft
Speed	• Cruise Speed: 275 knots
Range	• 1000 nmi design mission • 500 nmi economic mission • 1626 nmi ferry mission
Payload	• 50 passengers • 12000 lbs (200 lbs per passenger and 40 lbs luggage)
Engines	• 2x 2034-Technology PW127XTs (Turboelectric engines) • 2x 2034-Technology Electric Motors (based off STARC-ABL)
Weight	• Operating Empty Weight: 23305 lbs • Max Takeoff Gross Weight: 39840 lbs
Fuel	• Max Capacity: 5300 lbs • Design Mission: 4535 lbs carried, 3556 lbs expended • Economic Mission: 2811 lbs carried, 1855 expended
Ceiling	• Service: 30,500 ft • Absolute: 32,000 ft
Takeoff Distance	• Sea Level: 2578 ft • 5000' with ISA +18°F: 2907 ft
Landing Distance	• Sea Level: 2924 ft • 5000' with ISA +18°F: 3231 ft
Certifications	• VFR & IFR • Icing Conditions • FAA 14 CFR Part 25
Production	• Sale Price: $29.51 million • Direct Operating Cost: $2,960 per flight hour • Production Rate: 2 aircraft per month

Table ES-2 is intended to mimic the *Architecture-Level and Aircraft-Level Evaluation* table in the AIAA document titled *Guidelines for Analysis of Hybrid Electric Aircraft System Studies* [1]. Some values may be omitted. Delta percentages are computed as the increase or decrease from the ATR 42-600 reference value.

Table ES-2. Architecture-Level and Aircraft-Level Evaluation

Propulsion Architectural Schematic	Aircraft Concept
Songbird-E	
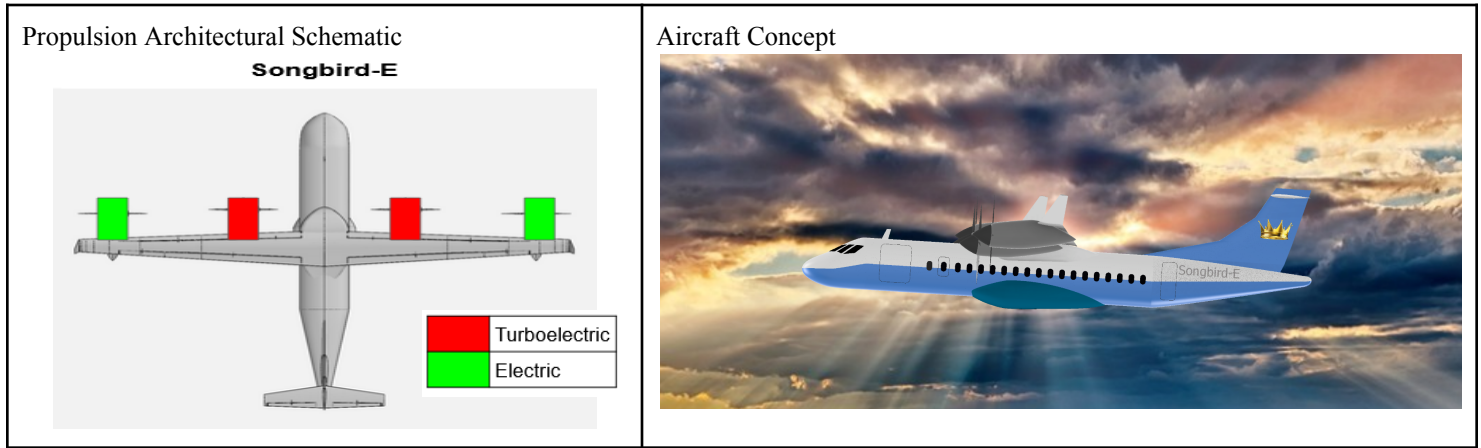
Propulsion Architecture Metrics	Songbird-E	ATR 42-600	Delta (%)
Specific Power (kW/kg)	4.442	4.206	+5.61%
Thrust Specific Fuel Consumption during Cruise*	0.391	0.498	-21.5%

*Values computed in FLOPS mission analysis during cruise

	Songbird-E Economic Mission (500 nmi)			ATR 42-600 Economic Mission (500 nmi)			Mission Deltas (%)	
Mission Stage	Segment Time (min)	Segment Fuel Burn (lbs)	Distance Covered (nmi)	Segment Time (min)	Segment Fuel Burn (lbs)	Distance Covered (nmi)	Segment Time	Segment Fuel
Taxi-Out	10.0	28	0	10.0	32	0	0	-12.5%
Takeoff	1.5	53	0	1.0*	40*	0	+50.0%*	+32.5%*
Climb	19.5	552	73.4	24.6	869	92.1	-20.7%	-36.5%
Cruise	76.6	1137	350.8	73.3	1769	353.0	+4.50%	-35.7%
Descent	22.9	56	75.8	15.6	52	55.0	+46.8%	+7.69%
Taxi-In	10.0	28	0	10.0	32	0	0	-12.5%
Total	140.5	1855	500	134.5	2794	500	+4.46%	-33.6%

*Takeoff time not calibrated to ATR 42-600.

Aircraft Design Weights	Songbird-E	ATR 42-600	Delta (%)
Max Take-off Weight (MTOW) (lbs)	39840	41005	-2.84%
Max Landing Weight (MLW) (lbs)	38246	40344	-5.20%
Manufacturer's Weight Empty (MWE) (lbs)	21105	23803	-11.3%
Operating Empty Weight (OEW) (lbs)	23305	25904	-10.0%

Max Payload Weight (lbs)	12000	11574	+3.68%
Max Zero-Fuel Weight (lbs)	35305	37478	-5.80%
Total Release Energy Weight (lbs)*	1855	2794	-33.6%
Release Fuel Weight (lbs)	1855	2794	-33.6%
Release Ancillary Energy Source Weight (lbs)	0	0	0

*Given for economic mission for comparison

Aircraft Sizing Parameters and Metrics	Songbird-E	ATR 42-600	Delta (%)
Wing Loading (lb/ft^2)	63.3	69.8	-9.31%
Wingspan (ft)	91.9	80.6	+14.0%
Reference Wing Area (ft^2)	629.8	586.0	+7.47%
Reference Wing Aspect Ratio	13.36	11.07	+20.7%
Number of Rotors Number of Blades for Each Rotor	4 4	2 6	
Maximum Mechanical Speed (RPM)	1200	1212	-1.00%
MWE/MTOW	0.5297	0.5805	-8.75%
OEW/MTOW	0.5850	0.6317	-7.39%
OEW/PAX (lb/PAX)	466.1	539.7	-13.6%
Release Energy Weight/MTOW	0.0466	0.0681	-31.6%
MLW/MTOW	0.9600	0.9839	-2.43%
Total Maximum Sea Level Thrust (lb)	9796.3	8302	+18.0%
AEO Thrust-to-Weight Ratio	0.4918	0.4048	+21.5%
OEI Thrust-to-Weight Ratio	0.2459	0.2024	+21.5%
AEO Max Power-to-Weight Ratio (hp/lb)	0.0722	0.0671	+7.60%
AEO Max Power Loading (lb/hp)	13.85	14.91	-7.11%
OEI Max Power-to-Weight Ratio (hp/lb)	0.0361	0.0335	+7.76%
OEI Max Power Loading (lb/hp)	6.924	7.455	-7.12%

Operational Performance	Songbird-E	ATR 42-600	Delta (%)
Take-off Field Length, MTOW, ISA, SL (ft)	2578	3632	-29.0%

TOFL (ft) Payload (lb) TOGW (lb) ISA Deviation (°F) Airport Elevation, AGL (ft)	2907 12000 39840 +18°F 5000		
Stall Speed and Flap Setting, MTOW, ISA, SL (KCAS)	85.6 [15°]	93.3 [15°]	-8.25%
Reference Speed and Flap Setting, MLW, ISA, SL (KCAS)	111.3 [30°]	121 [30°]	-8.02%
Landing Field Length, MLW, ISA, SL (ft)	2924	3169	-7.73%
NOX (lbs)	20.6	20.5	-0.485%
Minimum Rate-of-Climb (fpm) Specified Altitude (ft)	300 28000	300	
Time-to-Climb to Initial Cruise Altitude (min)	19.5	24.6	-20.7%
Initial or Fixed Cruise Altitude (ft)	28000	24000	+16.7%
Cruise Speed (KTAS)	275	289	-4.84%
Cruise Lift-to-Drag	16.2	13.7	+18.2%

Max PAX/Payload Economic Range	Songbird-E	ATR 42-600	Delta (%)
Range and PAX (nmi)	500 [50]	500 [48]	0% [+4.17%]
Payload (lb)	12000	11574	+3.68%
Block Fuel (lb)	1855	2794	-33.6%
CO_2e (lb)	6980	10512	-33.6%
Block Fuel per PAX (lb/PAX)	37.1	58.2	-36.3%
CO_2e per PAX (lb/PAX)	139.6	219.0	-36.3%
Specific Air Range (nmi/lb)	0.2695	0.1790	+50.6%
Percent Hybridization during Takeoff (%) Percent Hybridization during Cruise (%)	18.1% 24.1%	0% 0%	+18.1% +24.1%
Direct Operating Cost (USD/hr)	2960	3450	-14.2%
Direct Operating Cost per PAX (USD/hr-PAX)	59.20	71.88	-15.7%

4.71 ft

80°

91.9 ft

D=12.9 ft

11.4 ft

22.4 ft

3.25°

8.23 ft

1.59 ft

53.4 ft

26°

1.31 ft

80.6 ft

23.0 ft

5.58 ft

5.08 ft

16.3 ft

17.5 ft

3.58 ft

10.2 ft

13.5 ft

3.23 ft

6.35 ft

Figure ES-2. Detailed 3-View Drawing

Table of Contents

Acronyms & Nomenclature

AAA = Advanced Aircraft Analysis

AC = Alternating Current

ADS-B = Automatic Dependent Surveillance-Broadcast

AEO = All-Engines Operational

AIAA = American Institute of Aeronautics and Astronautics

AOA = Angle of Attack

APU = Auxiliary Power Unit

AR = Aspect Ratio

ATR = Avions de Transport Régional

CDR = Critical Design Review

CEF = Cost Escalation Factor

CG = Center of Gravity

CO_2e = Carbon Dioxide Equivalent

DC = Direct Current

dB = decibels

DEP = Distributed Electric Propulsion

DOC = Direct Operating Cost

EIS = Entry Into Service

EQN = equation

EVS = Enhanced Vision System

FADEC = Full-Authority Digital Engine Control

FBL = Fly-by-Light

FEA = Finite Element Analysis

FL = Flight Level

FLOPS = NASA Flight Optimization System

ft = feet (')

GD = General Dynamics

hp = horsepower

hrs = hours

HUD = Head-Up Display

IFR = Instrument Flight Rules

in = inches (")

kg = kilograms

ktas = knots true airspeed

kts = knots

kW = kilowatts

lbs = pounds

L/D = Lift-to-Drag Ratio

LE = Leading Edge

m = meters

min = minutes

MIT = Massachusetts Institute of Technology

nmi = nautical miles

OEI = One-Engine Inoperative

OpenVSP = Open Vehicle Sketch Pad

OEW = Operating Empty Weight

OML = Outer Mold Line

OPR = Overall Pressure Ratio

PAX = Passengers

PBW = Power-by-Wire

PDR = Preliminary Design Review

PRSEUS = Pultruded Rod Stitched Efficient Unitized
Structure

RDTE = Research, Development, Test, & Evaluation

RFP = Request For Proposals

RPM = Revolutions Per Minute

SAF = Sustainable Aviation Fuel

SOA = State-of-the-Art

SPL = Sound Pressure Level

SRR = System Requirements Review

STOL = Short Field Takeoff and Landing

TAWS = Terrain Awareness and Warning System

TE = Trailing Edge

TOGW = Takeoff Gross Weight

T/W = Thrust-to-Weight Ratio

VFR = Visual Flight Rules

VSPAero = Vehicle Sketch Pad Aerodynamics

W/S = Wing Loading

List of Tables

I. Introduction

The world is facing a crisis of pollution and emissions due to a rapid and continuing industrialization without much regard for the environment. Accordingly, climate standards are seeking to reduce carbon and other harmful emissions to improve air quality and mitigate other harmful environmental effects. The transportation sector emits roughly 37% of global carbon dioxide annually, with the aviation industry accounting for 2% of the global total [2, 3]. The demand for technologies with cleaner operations has increased substantially in recent years, and the aviation industry is no exception. Increasing efficiency and decreasing harmful emissions are not only better for the environment, but also for airlines' bottom lines. The Songbird-E pushes the boundaries of aviation technologies in order to provide a more efficient and environmentally-friendly means of regional air travel.

Designing this aircraft was a long and multifaceted process. It began with an in-depth review of the RFP and its requirements, along with a review of the regional turboprop market. Based on market research, the ATR 42-600 was chosen as the state-of-the-art comparator aircraft. Reviewing the requirements culminated in a System Requirements Review (SRR), demonstrating an intimate knowledge of the RFP. From there, nine initial concepts were designed in the aircraft geometry modeling software Open Vehicle Sketch Pad (OpenVSP), one by each group member [4]. All nine concepts were presented to the team, and three designs were down-selected using a ranked-choice vote. A rough initial analysis of the ATR 42-600 and all three concepts was then conducted. This included a constraint-based matching plot analysis, as well as preliminary airfoil, propeller, and subsystem selections, aerodynamic analysis using Vehicle Sketch Pad Aerodynamics (VSPAero), and propulsion system modeling in GasTurb [5, 6]. Cost models were also created in Advanced Aircraft Analysis (AAA) and thermal management was explored [7]. Mission and weights analysis of the three concepts was conducted using NASA's Flight Optimization Software (FLOPS) [8]. This preliminary analysis culminated in a Preliminary Design Review (PDR), to discuss the merits of the three concepts and down-select a single concept. The down-select was made both by ranking key characteristics of the concepts and ranked-choice voting, taking into consideration each team member's rationale. The overwhelming consensus was to use concept 1, which became the Songbird-E, with the recognition that the design would be subject to substantial change through trade studies. Following PDR, the ATR 42-600 and the Songbird-E models were refined by means of DARcorporation's FlightStream, weight verifications utilizing Part V of Jan Roskam's Aircraft Design series and *Fundamentals of Aircraft Design, Volume I*, by Leland

Nicolai & Grant Carichner, empennage and control surface sizing, and refined propulsion and costs modeling, [9, 10, 11]. After refining the analyses, several trade studies were conducted in operations, geometry, and propulsion. The final version of the Songbird-E was then brought forward for a Critical Design Review (CDR), and put forward in this report. These intermediate steps were much more comprehensive than summarized in this section and were extremely iterative in nature. The remainder of this report captures more detailed design information and explains many decisions, assumptions, and limitations in the design.

II. Concept of Operations, Requirements, and Mission Profile

This section will examine the requirements set forth by the AIAA. Developed from these requirements was a concept of operations and a mission profile to ensure the concept aircraft met the design requirements.

A. Requirements

The requirements for the Songbird-E were specified in the Request For Proposal (RFP) set by AIAA [12]. These requirements specify basic mission capabilities and design, and are summarized in Tables II-1 and II-2. The Songbird-E was designed to meet or exceed all mandatory requirements, in addition to some of the tradable requirements.

Perhaps most importantly, the AIAA defined two figures of merit. These were a 20% reduction in block fuel burn on a 500 nmi mission, and a reduction of emissions, as compared to current turboprops. The economic block fuel burn for the ATR 42-600 was found to be 2794 lbs through modeling in FLOPS. Reduction in emissions is suggested to include carbon dioxide (CO_2), NOX, soot, and more. The ATR 42-600 was estimated to produce 20.6 lbs of NOX during the economic mission.

Table II-1. Mission Requirements

Requirement	Comments
EIS by 2035, with engines that can be certified by 2034	Required
1000 nmi design mission	Required
46-50 passengers	Required
275 (350) ktas cruise speed	Required (Target)
Cruise at FL280 (28,000 ft)	Required
Category C approach speed, less than 141 kts	Required
Maximum takeoff and landing field of 4500 ft over a 50 ft. obstacle with ISA + 18°F day	Required
Demonstrate takeoff and landing performance at 5000 ft elevation with ISA + 18°F day	Required
Distance to cruising altitude must be less than 200 NMI	Required

Table II-2. Design Requirements

Requirement	Comments
Seat width of 17.2 (18) in	Required (Target)
Armrest width of 2 in	Required
Cabin stand-up height comparable to other transport-class aircraft	Required
Ergonomically-serviceable baggage compartment	Required
2 pilots and 1 crew, weighing 190 lbs, with 30 lbs and 4 ft^3 of baggage	Required
Passengers weighing 200 lbs with 40 lbs and 5 ft^3 of baggage	Required
Aisle width of 18 in	Required
ICAO Gate Code C (B) wingspan of less than 36 (24) m	Required (Target)
Meet 14 CFR 25.121 climb gradient requirements	Required
Capable of VFR and IFR flight with an autopilot	Required
Capable of flying in known icing conditions	Required
Meets applicable certification rules in FAA 14 CFR Part 25	Required
Provide systems and avionics architecture that will enable autonomous operations	Target

B. Concept of Operations

The RFP requests that this aircraft be designed to create a more efficient regional turboprop aircraft, in order to reduce the emissions and pollution caused by the aviation industry. The design is built and sized to improve efficiency and reduce emissions over regional passenger travel missions.

The key objectives of this design are to maximize efficiency and reduce emissions. while including a hybrid-electric propulsion system. Other design objectives include increasing reliability and maintainability, minimizing production costs, and producing a visually-appealing aircraft.

With the above requirements and objectives in mind, the Songbird-E was created. The Songbird-E is a hybrid-electric regional turboprop, with a design range of 1000 nmi. The Songbird-E features a conventional tube-and-wing architecture, with a high-mounted wing, and a high cruciform tail. The Songbird-E features a next-generation hybrid-electric propulsion system, with two turboelectric engines inboard, and two electric motors near the wingtips. Also featured is heavy use of the PRSEUS composite in the airframe, which reduces the airframe weight by over 9%. Futuristic subsystems, such as fly-by-light, power-by-wire, and full-authority digital engine control (FADEC) are integrated for increased usability, maintainability, and efficiency.

C. Mission Profile

The Songbird-E flies a conventional commercial mission: takeoff, climb to an altitude of 28,000 ft, cruise at 275 kts, descent, and landing at destination. The Songbird-E also satisfies the following reserve mission: missed approach and climb to an altitude of 12,500 ft, cruise at 275 knots, descent and land at alternate airport 100 nmi away. The Songbird-E is also equipped for a 30 min loiter at 1500 ft. This mission profile is depicted in Figure II-1.
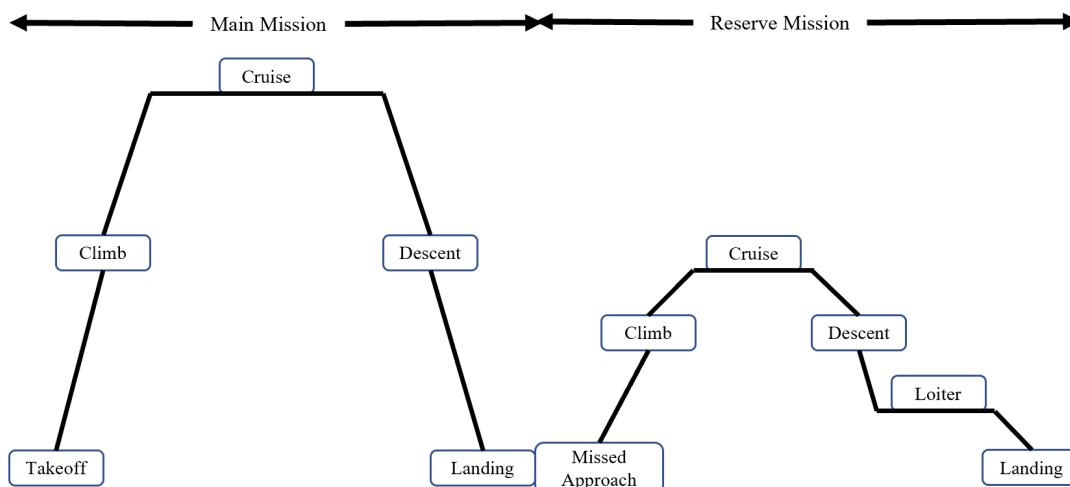
Figure II-1: RFP Mission Profile

III. Conceptual Designs/Configurations

After assessing key RFP requirements, nine concepts were produced. The following three concepts were then down-selected using ranked-choice voting. These concepts were generated using OpenVSP [4]. The three concepts, and the method of selecting a final concept, is described below.

A. Concept 1, LEEAP-50
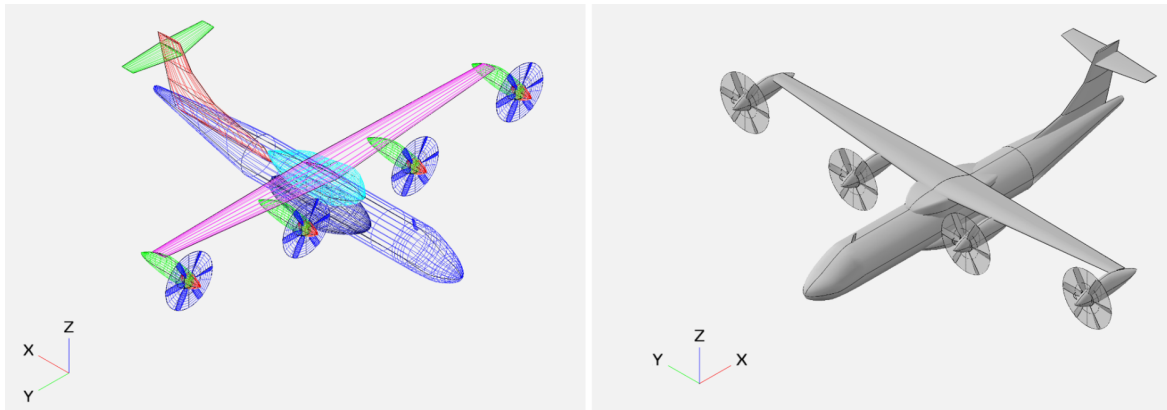
Figure III-1: Wireframe and Shaded Model of the LEEAP-50 (Concept 1)

Concept 1 is a 4-engine turboprop design, featuring a high-mounted wing tapered with a taper ratio of 0.35, to produce an optimal lift distribution, and a T-tail empennage. It was designed with a turboelectric architecture, with electric wingtip propulsors to be activated during takeoff and climb. This propulsion architecture was selected to reduce block fuel burn and overall emissions during the most intensive portions of the design mission. Concept 1, the LEEAP-50, would go on to become the final concept, the Songbird-E.

B. Concept 2, Hycraft
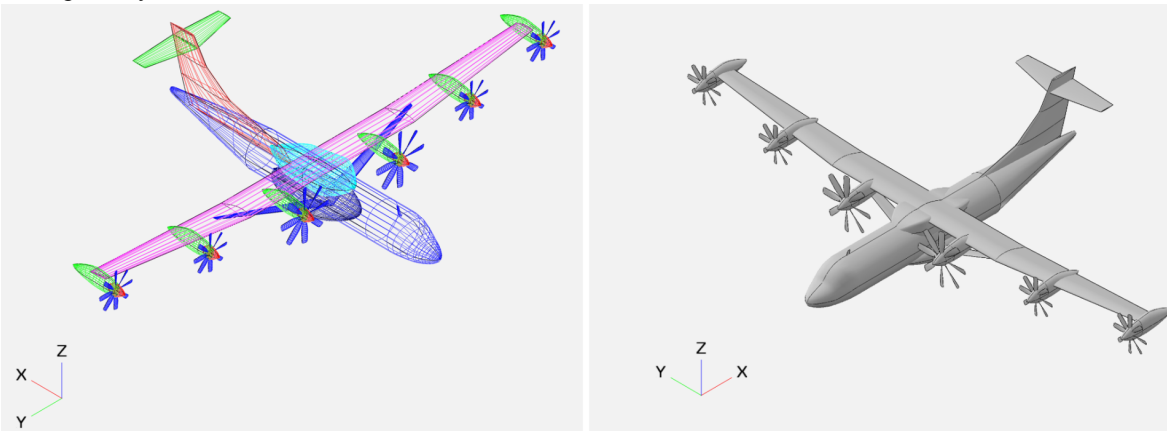
Figure III-2: Wireframe and Shaded Model of the Hycraft (Concept 2)

Concept 2 is a 6-engine turboprop design, featuring a high-mounted, truss-braced wing supported to enable a high aspect ratio design, and a T-tail empennage. It leverages distributed electric propulsion and parallel-series hybrid architecture with a lithium-ion battery. This propulsion architecture was selected to reduce block fuel burn and in-flight and overall emissions, using a scaled-down electrification approach afforded by the 6-engine design.

C. Concept 3, GreenWing-50
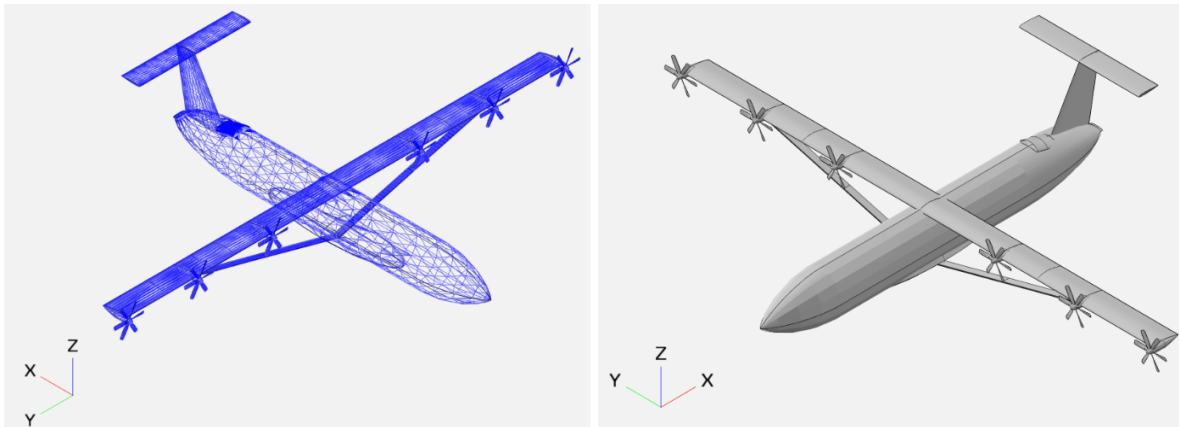
Figure III-3: Wireframe and Shaded Model the GreenWing-50 (Concept 3)

Concept 3 is a 6-engine turboprop design featuring a high-mounted, truss-braced wing to enable a high aspect ratio design, and a T-tail empennage. It leverages distributed electric propulsion and parallel-series hybrid architecture integrated with a Decalin fuel cell. This propulsion architecture was selected to reduce block fuel burn and overall emissions by using a scaled-down electrification approach afforded by the 6-engine design.

D. Down-Selection

To select between the concepts, a list of various key parameters were considered, such as the block fuel burn for the economic mission, max TOGW, and various costs. The tables below demonstrate key parameters for each design, as well as their comparative rankings.

Table III-1. Key Design Parameters of the Three PDR Concepts

LEEAP-50 (Grant) Key Parameters	
Max TOGW	42298 lbs
Max OEW	25302 lbs
Architecture	Turboelectric
Economic Block Fuel Burn	2227.3 lbs
% Reduction	20.134%
Wing Area	629.8 ft²
AR	13.36
C_L Cruise	0.575
C_L Max	2.4
Field Length	3190 ft
Battery/Fuel Cell Weight	0 lbs
TSFC (Cruise)	0.410
RDTE Cost	$1.073 Billion
Market Price	$22.548 Million
DOC	$3,138 / Hour

Hycraft (Espinoza) Key Parameters	
Max TOGW	46711 lbs
Max OEW	29790 lbs
Architecture	Parallel-Series
Economic Block Fuel Burn	2061.1 lbs
% Reduction	26.09%
Wing Area	851.8 ft²
AR	16.34
C_L Cruise	0.490
C_L Max	2.4
Field Length	2873 ft
Battery Weight	352.39 lbs
TSFC (Cruise)	0.355
RDTE Cost	$1.082 Billion
Market Price	$23.326 Million
DOC	$3,559 / Hour

GreenWing-50 (Keller) Key Parameters	
Max TOGW	46535 lbs
Max OEW	29824 lbs
Architecture	Parallel-Series
Economic Block Fuel Burn	1913.5 lbs
% Reduction	31.39%
Wing Area	708 ft²
AR	19.67
C_L Cruise	0.590
C_L Max	2.4
Field Length	3257 ft
Fuel Cell Weight	82.82 lbs
TSFC (Cruise)	0.313
RDTE Cost	$1.142 Billion
Market Price	$23.88 Million
DOC	$3,380 / Hour

Table III-2. Ranking Each Concept on Scorable Parameters

LEEAP-50 (Grant) Key Parameters	
Max TOGW	1
Max OEW	1
Economic Block Fuel Burn	3
% Reduction	3
Wing Area	3
AR	3
C_L Cruise	2
Field Length	2
Battery/Fuel Cell Weight	1
TSFC (Cruise)	3
RDTE Cost	1
Market Price	1
DOC	1

Hycraft (Espinoza) Key Parameters	
Max TOGW	3
Max OEW	2
Economic Block Fuel Burn	2
% Reduction	2
Wing Area	1
AR	2
C_L Cruise	3
Field Length	1
Battery Weight	3
TSFC (Cruise)	2
RDTE Cost	2
Market Price	2
DOC	3

GreenWing-50 (Keller) Key Parameters	
Max TOGW	2
Max OEW	3
Economic Block Fuel Burn	1
% Reduction	1
Wing Area	2
AR	1
C_L Cruise	1
Field Length	3
Fuel Cell Weight	2
TSFC (Cruise)	1
RDTE Cost	3
Market Price	3
DOC	2

The practicality of implementing each concept was also considered, to ensure a feasible and closed design. While the down-select was different due to early, low-fidelity models, concept 1 was chosen. There were a few reasons for its selection. First off, there were concerns about FLOPS underestimating the wing weights for the other two concepts, because FLOPS underestimates the wing weight of high aspect ratio (AR) wings. It was estimated that, even though concepts 2 and 3 demonstrated better economic block fuel burns, that the percent reduction could be overestimated by as much as 5.5%. There were also structural concerns of a high span and AR wing, especially with the inclusion of multiple engines along the span. There were also concerns about the number of engines. There

were additional concerns with a parallel-series propulsion system. Design 2 utilized batteries that are extremely heavy, and whose was underestimated heading into PDR. Conventional battery systems also present problems with charging, maintenance, and lifespan. Design 3 used Decalin fuel cells, which were uncertain of a 2035 EIS, and present concerns in regards to usage in modern airports. Design 1 was the most cost-effective design and met the 20% reduction in block fuel. Concept 1 also scored first in the most categories (6), as compared to the other concepts. As it was the best and most feasible design, concept 1 was selected by scoring and ranked-vote consensus.

IV. Sizing Analysis

This section of the report will detail an initial sizing and constraint analysis performed on the three concepts described in section III. Initial sizing analysis included TOGW estimation and a constraint analysis, using wing loading and thrust-to-weight ratio. Lastly, this section will examine the general sizing methodology for the final configuration of the Songbird-E.

A. Initial Sizing Analysis

An initial TOGW was estimated for each concept using the method described in chapter 5 of Nicolai & Carichner's *Fundamentals of Aircraft Design, Volume I* [11]. This method utilizes the Breguet range equation, along with weight fraction estimates for mission stages, and is based upon historical data. The lift-to-drag ratio (L/D) was found using data about the span and wetted area, and relations to known lift-to-drag ratios. Similarly, the SFC was taken from modern engines with similar thrust ratings. This data was used to create a total mass fraction, or ratio between the final and initial weights of the aircraft. Utilizing the calculated mass fraction, along with a payload weight calculated from RFP requirements, the fuel weight and available empty weight were calculated for a given TOGW. This empty weight describes the weight of the aircraft with no payload or fuel, and is the weight that can be changed directly by sizing the aircraft. Historical data shows a trend between TOGW and the required empty weight of historical aircraft. A script was used to calculate TOGW, from which the available empty weight was found using fuel fractions, and matched the required empty weight found from historical data. This yielded a TOGW of 48,112 lbs, which was used as an initial estimation.

B. Initial Constraint Analysis

After performing the initial sizing analysis, several stated and derived requirements from the RFP allowed for the determination of the feasible design space for the Songbird-E's. Critical constraints considered in the analysis

were the required takeoff and landing field lengths of 4500 ft, a minimum cruise speed of 275 knots, an approach

velocity of less than 141 knots, and a rate of climb speed derived from reaching FL280 in less than 200 nautical

miles (2.96 kts). Using methods discussed in Nicolai & Carichner, these constraints were converted into functional

forms and plotted in T/W vs W/S space. The resulting constraint diagram is depicted in Figure IV-1.
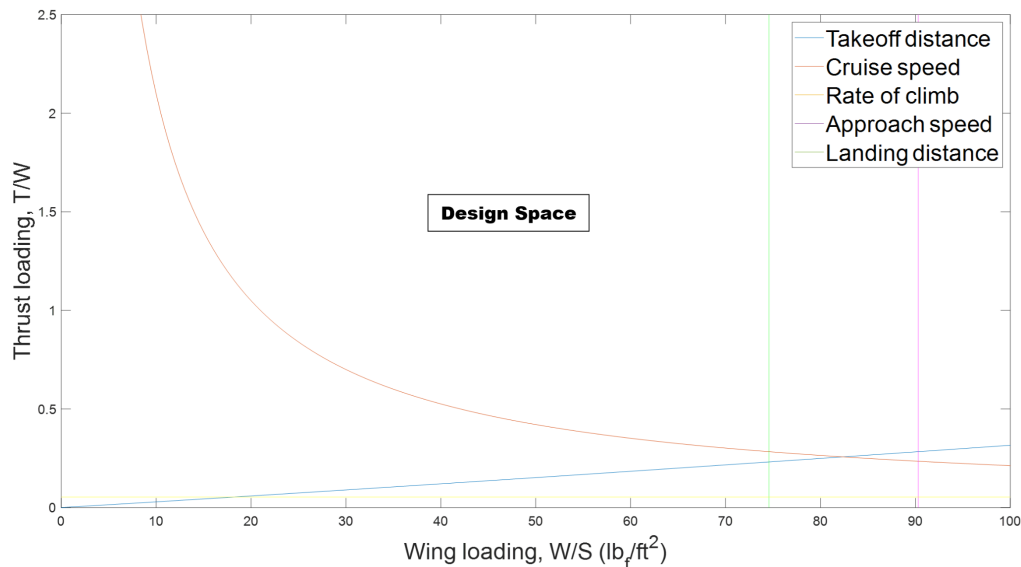
Figure IV-1. Constraint Diagram

C. Sizing Methodology

   After conducting TOGW estimation and matching plot constraint analysis, FLOPS input decks were

created. FLOPS will be discussed in-depth in section IX. The PDR weight of the Songbird-E came out to 42,298 lbs,

which was a 12.1% decrease from the initial TOGW sizing of 48,112 lbs. This is explained by FLOPS' employment

of more refined weight estimations that examine individual components and groupings. Following this analysis,

minimization of weight was pursued to drive down the block fuel burn. Weight reduction was pursued through

composite use in structural components, propulsion system refinement, and future subsystems and equipment. The

final weight of the Songbird-E, at 39,840 lbs, with an additional 5.81% decrease in TOGW.

   Other key drivers of this analysis were the wing area and thrust generation. The Songbird-E has a larger

wing area than the ATR 42-600, but couples this with an increase in span to yield a larger aspect ratio, ultimately

generating only 3% more induced drag, while also increasing lift by 24% at cruise, as compared to the ATR 42-600.

The propulsion system was sized to the original point of the ATR 42-600, as it was thought that the final Songbird-E

would not deviate much from the ATR 42-600, in terms of TOGW. As a method of verification of our design, the Songbird-E and ATR 42-600 were plotted on the initial constraint graph, which can be seen in Figure IV-2 below.
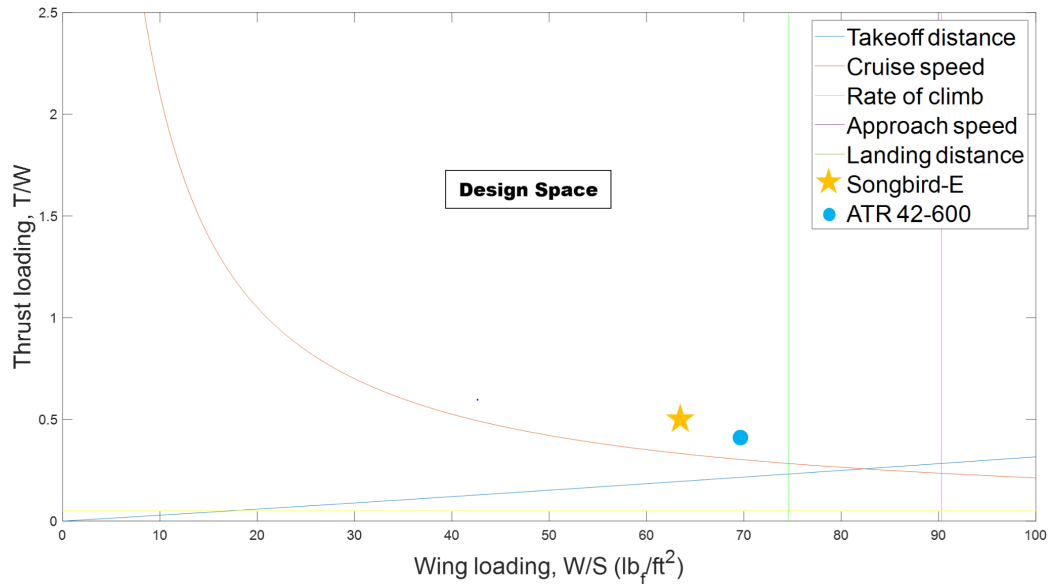
Figure IV-2. Songbird-E and ATR 42-600 Examined Under Initial Constraint Analysis

As shown in Figure IV-2, the Songbird-E's current design values of a T/W ratio of 0.4918 and a wing loading of 63.3 lb/ft^2 fall in the design space. The ATR 42-600 is graphed for comparison.

V. Configuration Layout

This section will showcase the Songbird-E's final configuration, and how it meets the design requirements.

A. General Configuration

The final design of the Songbird-E resembles the ATR 42-600, with notable differences, some of which include an increased number of engines, a longer fuselage and wingspan, and the addition of winglets. The increased number of engines allows the Songbird-E to take advantage of distributed electric propulsion, while also accelerating cleaner air away from the fuselage. The longer fuselage supports the passenger capacity increase, and the longer wingspan yields a higher aspect ratio and increased wing area, yielding a higher L/D. The electric nacelles were left long to account for room for other electrical systems and can be shortened in the future. A dimensioned drawing of the aircraft can be seen in Figure V-1.
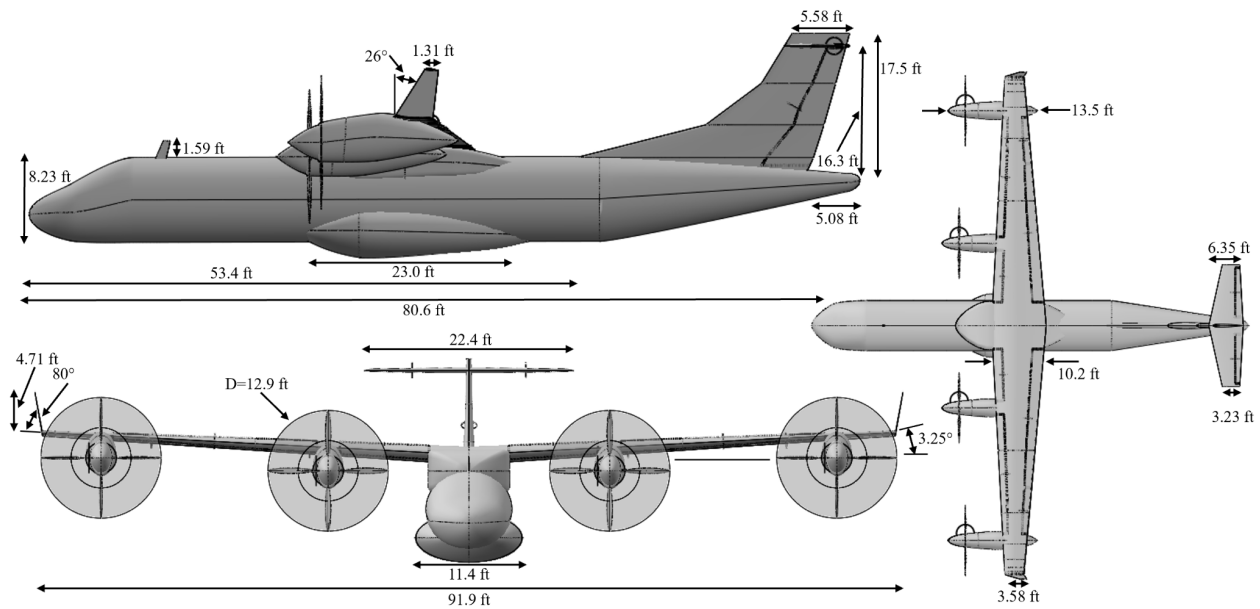
Figure V-1. 3-View Dimensioned Drawing of the Songbird-E

B. Aircraft Layout

The Songbird-E was designed to hold 50 passengers. The cabin layout can be seen in Figure V-2.

Floor Area | Cargo Area | Galley | Dead Space
Seating and Armrests | Door Location | Lavatory | Cockpit
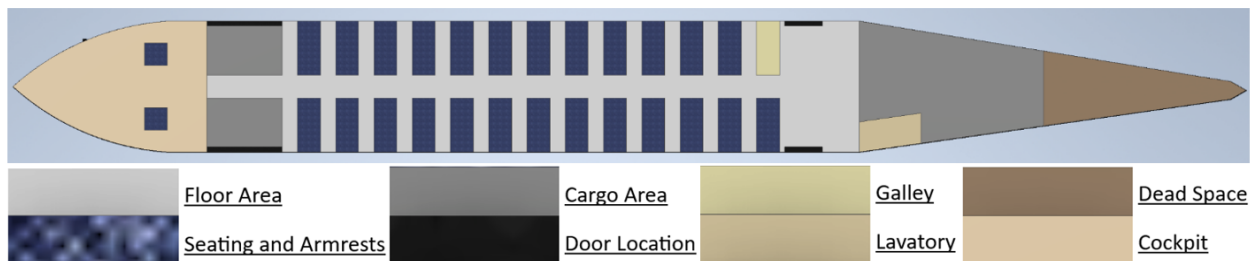
Figure V-2. General Layout of the Passenger Cabin and Cargo Storage Areas in Inches

There are two small cargo areas at the front of the plane and one larger one at the rear, that yield a total cargo volume of 283 ft³, exceeding the required volume of 262 ft³. Including these storage areas inside the cabin allows for easier access and use. Baggage stored in the cargo area will be stacked on top of each other. The decision to have a 2+2 seating configuration with the cargo above the floor came from a trade study between this configuration, a 2+1 seating configuration, and a 2+2 seating configuration with the cargo below the floor. The 2+1 configuration would have increased the fuselage length and decreased width, which would have increased weight and the fineness ratio. The 2+2 configuration with cargo below the floor would have decreased the fineness ratio as the result of increasing the fuselage height to meet volume requirements. Another drawback of storing cargo beneath the floor is that it

would shorten the fuselage, necessitating an increase in the size of the empennage to maintain controllability, especially in OEI conditions. As weight and an optimal fineness ratio were important for the downselect, the selected configuration provided a good compromise. A galley is located across from the last row of the passenger cabin, separated by walls from the seating area. A lavatory is located in the rear of the passenger cabin, behind the rear door on the port side. The cockpit contains the same layout and design of the ATR 42-600 with up-to-date glass panels and electronics, supporting 2 pilots. The placement of the seats in the cockpit can be seen in Figure V-2, and the general layout can be seen in Figure V-3 below [13].
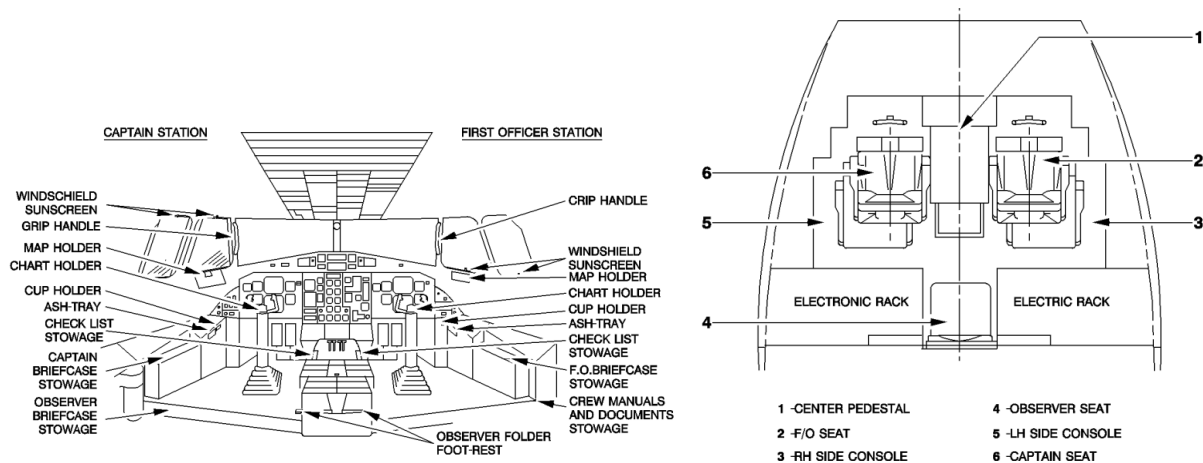
Figure V-3. Cockpit Diagram

This cockpit diagram is taken from the ATR 42-300 handling manual. The layout for the Songbird-E's cockpit will be the same, with up-to-date systems and electronics, including a fully glass cockpit, like the ATR 42-600 [13]. Cockpit subsystems will be discussed more in-depth later.

C. Doors

Cargo doors are located on each of the front cargo holds to assist in the loading of baggage. Each door is 60" by 50" [14]. General doors for crew and passengers are located on both sides of the aircraft, in the rear of the fuselage. Each door is 68" by 25" [14].

D. Seating / Passenger Configuration

To accommodate 50 passengers, a 2+2 seating configuration was selected due to its ability to limit the length of the fuselage and more cargo storage. A front-facing cross-section view of the fuselage can be seen in Figure V-4.
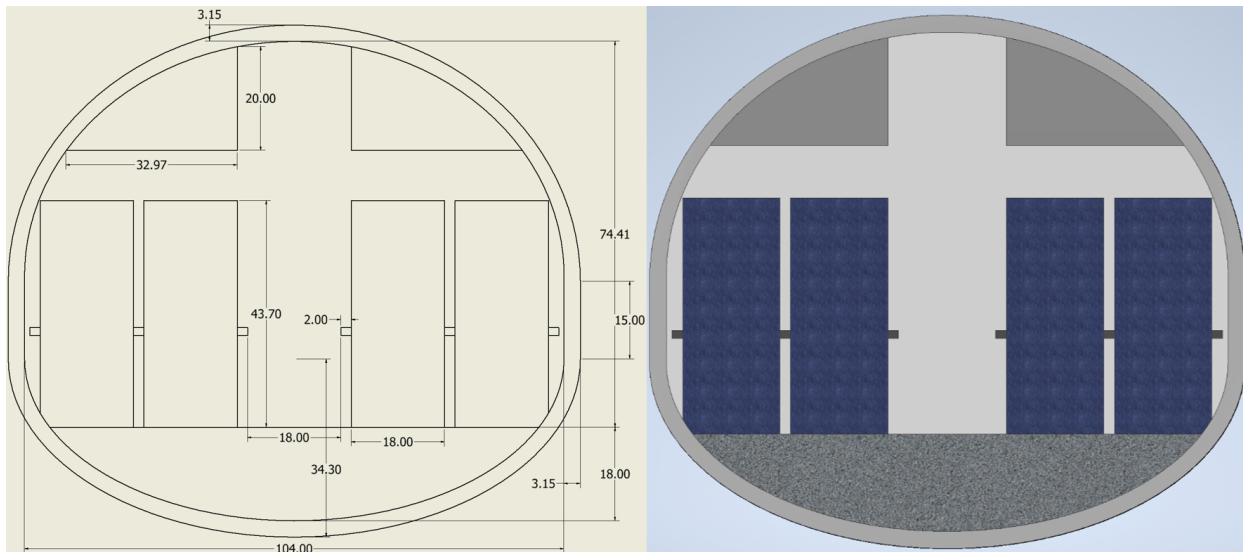
Figure V-4. Cross-Section of the Passenger Cabin (Dimensions in Inches)

For each seat, the width, height, and pitch are 18", 43.071", and 30" respectively. The armrests are 2" wide. The aisle is 18" wide. The stand-up height in the cabin is 74.409", same as the ATR 42-600 [13].

VI. Propulsion

This section of the report will examine the propulsion system design and architecture, as well as the selection and analysis of the propellers. Many trade studies to determine the specific configuration of the propulsion system were conducted, and will be discussed.

A. Propulsion Architecture

The propulsion system consists of four driven propellers, two on each side. The electrical architecture is partially turboelectric, with the inboard propellers powered mechanically from a gas turbine engine with a gearbox. Furthermore, the engines also supply power to an electric generator, which converts the mechanical energy to AC power, which is then converted into DC power through a rectifier. This rectifier is placed in the wing near the inboard engine. The DC power then travels through a cable along the length of the wing, to an inverter placed near the electric motor, where it is converted back to AC for the outboard electric motors. This conversion from AC to DC, and then back to AC allows the electric motors to operate at a wide range of RPMs, rather than specific multiples of the turbine RPM. A diagram of the propulsion architecture for one side of the aircraft can be seen in

Figure VI-1. The generator receives a constant 369 hp (275 kW) of power from the gas turbine across all stages of

flight. The decision to use a 369 hp electric motor was motivated by a trade study, discussed in section VI-E.
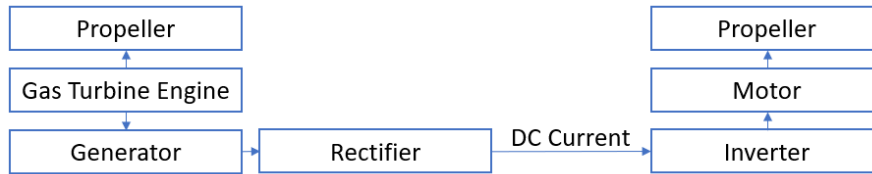
Figure VI-1. Diagram of the Turboelectric Architecture

B. Engine Modelling and Analysis

Propulsion analysis was done through a combination of data from GasTurb, XROTOR, and scripts written

in MATLAB. GasTurb is a turbine cycle simulation software that outputs various performance characteristics from a

list of inputs about the engine. XROTOR gives propeller performance data, and will be discussed in section VI-B.

Various engine decks depicting thrust, fuel consumption, and NOx emissions across a range of Mach and altitudes

were created as an input into FLOPS, which would then output key mission performance parameters. The baseline

engine selected for study was the PW-127XT, as it is the engine utilized by the ATR 42-600 [15]. Values for the

weight, mass flow, and overall pressure ratio were found and confirmed using various sources, and input into

GasTurb [16, 17]. Other parameters, mainly the turbine inlet temperature, were adjusted to match known values of

SFC, inter-turbine temperature, and power output [17, 18, 19]. Key values for the baseline PW-127XT engine at

static sea level conditions are shown in Table VI-1.

Table VI-1. Key Parameters of the Baseline PW-127XT

Parameter	Value from GasTurb	Known value
Weight, lb (kg)	1060 (481)	1060 (481)
Mass flow, lb/s (kg/s)	18.7 (8.49)	18.7 (8.49)
Total pressure ratio	15.77	15.77
Turbine inlet temperature, °F (°C)	2091 (1144)	
Inter-turbine temperature, °F (°C)	1446 (786)	1472 (800)
Mechanical power, hp (kW)	2741 (2016)	2750 (2023)
SFC, lb/(hp$\cdot$h) (kg/(kW$\cdot$h))	0.431 (0.262)	0.449 (0.273)
NOx emissions index (g/kg fuel)	14.6	

Using this baseline, a new engine was generated, as a prediction of a 2034 EIS engine of the same class. The main differences are in the turbine inlet temperature and the total pressure ratio. These values were adjusted based on a conversation with David Eames, a retired Rolls Royce propulsion expert. Furthermore, a weight reduction of 8% was assumed using trends for similarly-sized engines by NASA [20], and was counteracted by an increase in weight to account for the increased overall pressure ratio. Key values for the 2034 SOA engine at static sea level conditions are listed in Table VI-2.

Table VI-2. 2034 SOA Engine Specifications

Parameter	Value
Weight, lb (kg)	1046 (475)
Mass flow, lb/s (kg/s)	11 (5)
Total pressure ratio	22.2
Turbine inlet temperature, °F (°C)	2740 (1505)
Inter-turbine temperature, °F (°C)	2038 (1115)
Mechanical power, hp (kW)	2830 (2110)
SFC, lb/(hp·h) (kg/(kW·h))	0.370 (0.225)
NOx emissions index (g/kg fuel)	24.5

This new engine was used in GasTurb to generate a total power output at a range of Mach and altitude, which was then input into a MATLAB script, along with propeller maps generated by XROTOR. The MATLAB script then split the power across the inboard propeller and the electrical system. The outboard propeller's RPM was then optimized for each condition, with care taken to not exceed supersonic velocities at the propeller tip. Finally, the MATLAB script outputs a total thrust at each given condition for FLOPS. The efficiency of the electrical system was assumed to be 89.4%, based on individual component efficiencies taken from NASA's STARC-ABL analysis [21]. The one exception to this is the wire, which will be discussed later in section VI-D.

Table VI-3. Electric Component Efficiencies

Component	Efficiency (%)
Generator	96
Rectifier	99
Wire	99
Inverter	99
Motor	96
Total	89.4

The engine weights are listed in Table VI-4 below. The generator is included in the engine weights, and the weights are listed per turboelectric engine.

Table VI-4. Turboelectric Engine Weights Per Engine

Component	Weight (lbs)
Engine	1046
Engine Controls	26.3
Starting System	8.4
Propeller & Propeller Controls	273.7
Generator	75.8
Total:	1430

The weights for the engine controls and starting system were determined using EQNs 20.24 & 20.29 from Nicolai & Carichner's *Fundamentals of Aircraft Design, Volume I* [11]. Knockdowns of 50% were taken due to outdated technologies for the starting system and engine controls. More about this knockdown can be found in the systems section. Propeller and propeller control weights are combined and calculated using a MATLAB script with multiple empirical methods. These methods were the General Dynamics (GD) method, Torenbeek method, and an adjusted Torenbeek method from a TU Delft MS Thesis [10, 22]. These methods were calibrated to the ATR 42-600 propeller, since it is known and the empirical methods are calibrated to outdated, non-composite propellers. Following this calibration, the average of the three methods was taken. The weight of the generator is found based

on the power to weight ratio of 4.9 hp/lb (8 kW/kg) found in a modern generator [23]. The nacelle size from the ATR 42-600 was kept, to ensure that our engine would also fit.

C. Propeller Selection

The propellers were designed using XROTOR. XROTOR is an interactive program for the design and analysis of ducted and free-tip propellers, designed by Mark Drela (MIT) [24]. It uses key input parameters to design the shape of the propeller blades using Prandtl's lifting line theory. This means the rotor blades are treated as lifting lines and disk loading is assumed to be small.

There are four propellers on the plane, two for the inboard, turboelectric engines, and two on the outboard, electric engines. All four are variable pitch propellers, meaning that the pitch of the propellers is changed during flight to make them rotate at constant speed. To change the pitch, the propeller blades are rotated around their long axis. The pitch is controlled automatically to keep the speed at a constant 1200 RPM. The propellers all have a diameter of 3.93 m (12.9 ft), same as the ATR 42-600 propellers. The propeller diameter is limited by the maximum blade tip velocity. If those velocities enter the transonic area, propeller efficiency drops significantly. The propellers are optimized for cruise using an XROTOR function that optimizes the blade twist to reach a minimum induced loss. The airfoil used for the propeller blades is the NACA 6412, shown in Figure VI-2. Simulating different airfoils showed that the airfoil selection did not have a significant impact on the propeller performance. Nonetheless, the selected airfoil showed better results than other typical propeller airfoils.
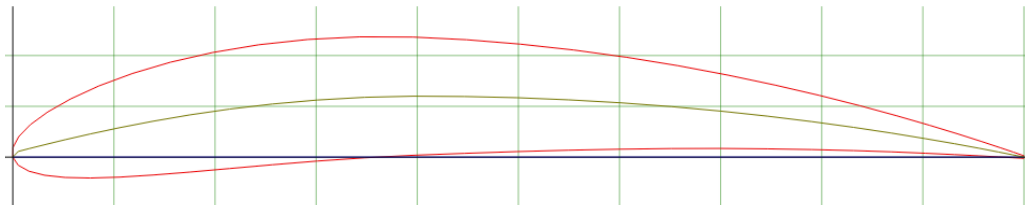
Figure VI-2. NACA 6412 Airfoil Used for Propeller Blades [51]

The propellers have 4 blades each. This was found to be a good compromise. More propeller blades leads to less vibration and noise, and produces higher thrust at a given RPM. However, fewer blades make the propeller lighter and more efficient. Each propeller has a hub radius of 0.295 m (0.968 ft) and a tip radius of 1.97 m (6.45 ft).

Table VI-5 shows the performance parameters of the propellers attached to the inboard, turboelectric engine and the outboard, electric engines during takeoff and cruise, respectively. The total thrust adds up to 24.2 kN for takeoff and 5.39 kN during cruise.

Table VI-5. Performance Parameters of the Propellers During Takeoff and Cruise

	Inboard		Outboard	
	Takeoff	Cruise	Takeoff	Cruise
Power [kW]	1898	785	247.5	247.5
RPM	1200	1200	1200	1200
Thrust [kN]	19.16	5.03	3.84	1.55
Efficiency	59.19 %	90.57 %	90.94 %	88.36 %

D. Electric Propulsion System

The hybrid-electric system requires many components for the movement of electricity from the inboard turboelectric engine to the electric motor near the wingtip. Below is a table showing the total electric system weights. The use of each component is described above in section B.

Table VI-6. Total Turboelectric System Component Weights

Component	Weight (lbs)
Rectifiers	60.9
Wiring	31.0
Inverters	59.7
Electric Motors	178.8
Thermal Management System	86.9
Extra Nacelles	67.1
Propeller & Propeller Controls	177.0
Total:	661

The propellers and propeller controls weights were determined using the same script as the main propellers. They weigh less as they are subject to less power. The two extra nacelles weights are calculated using the Torenbeek method, EQN 5.33 from Roskam's *Aircraft Design: Part V* [10]. They had to be added separately because FLOPS only allows for one type of engine input. The weight of the rectifiers and inverters were calculated assuming an equivalent power energy density, as used in NASA STARC-ABL analysis [21]. The electric motor weight was

calculated using a scaling law developed for high temperature superconducting motors and cooled similar to NASA's High-Efficiency Megawatt Motor [25, 26]. The resultant power density was 3.8 hp/lb (6.3 kW/kg).

The wiring was assumed to be aluminum for its combination of low density and high conductivity. The weight of the wiring was calculated using the following equation:

$$W_{Wire} = \frac{1}{4}\rho_{Al}\pi D^2 L$$
(EQN. 1)

where ρ is the density of aluminum (169 lb/ft³, 2700 kg/m³), D is the diameter of the wire, and L is the length. In this case, the length of wire for one side of the aircraft is twice the distance between the inboard engines and the outboard motors. The diameter of the wire affects not only weight but also the electrical efficiency of the wire, through the following equation:

$$\eta_{Wire} = 1 - \frac{4PR_sL}{\pi D^2 V^2}$$
(EQN. 2)

where P is the power of the electrical system, R_s is the resistivity of aluminum (3.28×10⁻⁸ Ω-m), and V is the voltage of the wire, assumed to be 270V, in order to give sufficient margin to the minimum voltage capable of creating an arc across an air gap, 327V [27]. These relationships in equations 1 and 2 give a relationship between weight per side of the aircraft and efficiency, which can be seen in Figure VI-3.
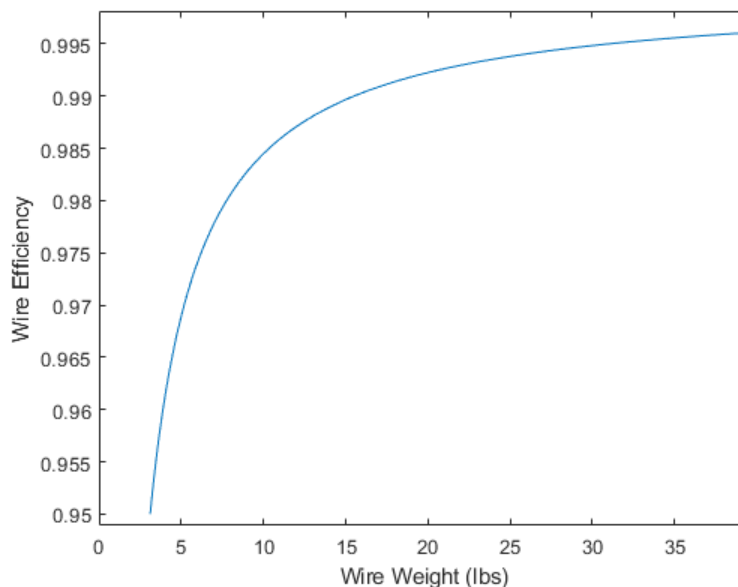
Figure VI-3. Wire Weight for One Side of the Aircraft vs. Efficiency for an Aluminum Wire with Varying Diameter

A diameter of 1.5 cm was selected since it results in high efficiency (99%) while maintaining realistic wire

diameters and relatively low weights (15.5 lbs per side).

The thermal management system (TMS) selected is outer mold line (OML) cooling, which uses copper heat

pipes to deliver low-grade heat to the aircraft's OML. At the OML, the heat is spread across the surface using

oscillating heat pipes. This was chosen due to high reliability and the lack of induced drag or power required.

The weight of the system was found by assuming the weight of the OML cooling system in the

STARC-ABL would scale proportionally to the surface area covered by the oscillating heat pipes [28]. This

assumption is good as the electrical systems are not far from the OML, and most of the weight is the oscillating heat

pipes. This results in an equation for the TMS weight as follows:

$$W_{TMS} = \rho_{TMS} \frac{P_{loss}}{\dot{Q}}$$
(EQN. 3)

where ρ_{TMS} is the weight of TMS per unit area, P_{loss} is the electrical system heat, and $\dot{Q}$ is the heat transfer rate. From

the electrical system power and efficiency, the heat output can be calculated to be around 74 hp (55 kW) of heat. The

weight of TMS per unit area of OML covered was found to be .98 lbs/ft^2 or 4.8 kg/m^2 from the STARC-ABL paper

[28]. The heat transfer coefficient was taken from the STARC-ABL's analysis using computational fluid dynamics

and adjusted for the different cruise conditions that the Songbird-E experiences. The adjustment assumed that the

heat transfer rate scales proportionally to the airspeed, the air density, and the temperature difference between the air

and the electrical components. This results in a total TMS weight of 86.9 lbs (39.4 kg).

E. Propulsion Trade & Sensitivity Studies

Several studies were conducted to show the aircraft performance's sensitivity to key parameters and

compare different possible propulsion system configurations. These include an electrical system efficiency

sensitivity analysis, and trade studies comparing different hybrid architectures, various methods of power

distribution, hybridization level, and overall pressure ratio of the turbine engine.

E.I. Electrical System Efficiency Sensitivity Study

A sensitivity study was conducted to analyze the sensitivity of our design to changes in our overall

electrical system efficiency. This was important as component efficiencies are subject to change as components are

developed and implemented. Engine decks were modeled using GasTurb and MATLAB, with electrical system

efficiency as an input, and were used in FLOPS analysis. Changing static sea level thrusts and thermal management system weights were also accounted for. While the thermal management systems have been refined since this study was conducted, the trend holds true. Other tweaks to the design have been made since, but no changes should affect the outcome of this study. A range of efficiencies were investigated between 85% and 95%, in 2.5% increments. Our actual system has an efficiency of 89.4%. The results of the study are displayed below in Figure VI-4 below.

Electric System Efficiency Trade Study
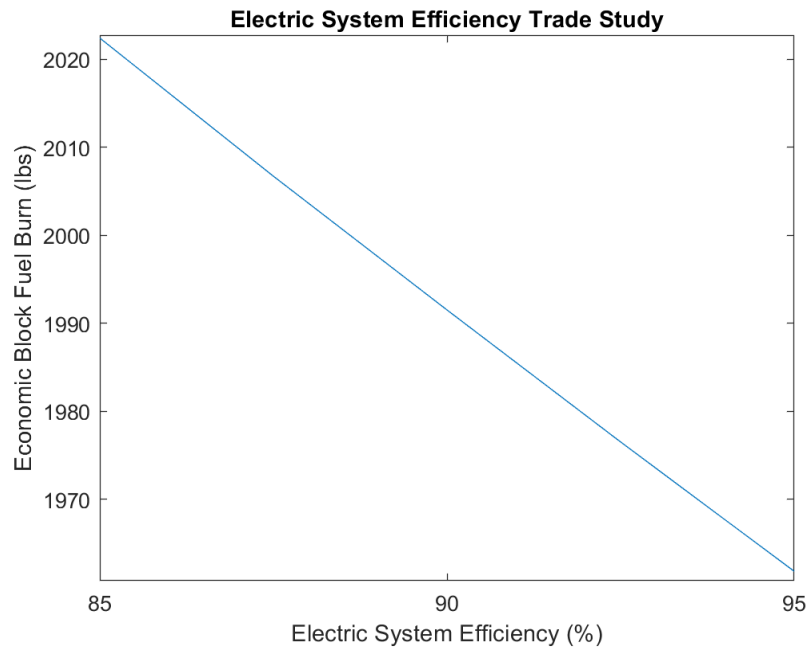
Figure VI-4. Electrical System Sensitivity Study

From a linear regression, block fuel burn on the economic mission increases by about 6.1 lbs per percent decrease in electrical system efficiency. Overall, our design is not extremely susceptible to reasonable shifts in electrical system efficiency.

E.II. Hybridization Architecture Trade Study

The architecture utilized was analyzed via a comparison between a partially-turboelectric architecture and a parallel-series architecture. The parallel-series architecture is very similar to the turboelectric architecture, but with an additional battery that can power the motor or be charged through the generator. A diagram of the parallel-series propulsion architectures is provided in Figure VI-5.
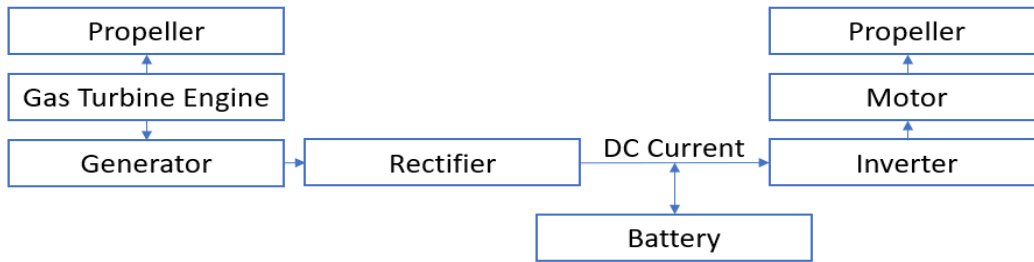
Figure VI-5. Diagram of the Parallel-Series Architecture Used in Trade Study

In the partially-turboelectric architecture, a constant power is taken from the generator at all points in flight, whereas the parallel-series architecture utilizes peak power shaving, meaning the motor is only active during takeoff and climb, and recharges during descent and at the gate. The propellers fold away during cruise and are assumed to be insignificant to the overall drag. The weights of the electrical system remain unchanged with the exception of additional battery and TMS weight. The weight of the battery was calculated using the following equation:

$$W_{bat} = \frac{P_{EM}}{\rho}(t_{takeoff} + t_{climb})\eta_{battery}\eta_{inverter}\eta_{motor} \qquad \text{(EQN. 4)}$$

where ρ is the battery energy density, P_{EM} is the power delivered to the electric motor, $t_{takeoff}$ and t_{climb} are the times to takeoff and climb, and $\eta_{battery}$, $\eta_{inverter}$, and η_{motor} are the electrical efficiencies of the battery, inverter, and motor respectively. A battery density of 250 Wh/kg was assumed. Furthermore, an increase to the TMS weight was also added to account for the heat generated from the battery. For this trade study, 470 hp (350kW) of power was used for each electric motor since it was the selected power during the time of the study. The turbine engine was also downsized, since the peak power needed is accounted for by the battery.
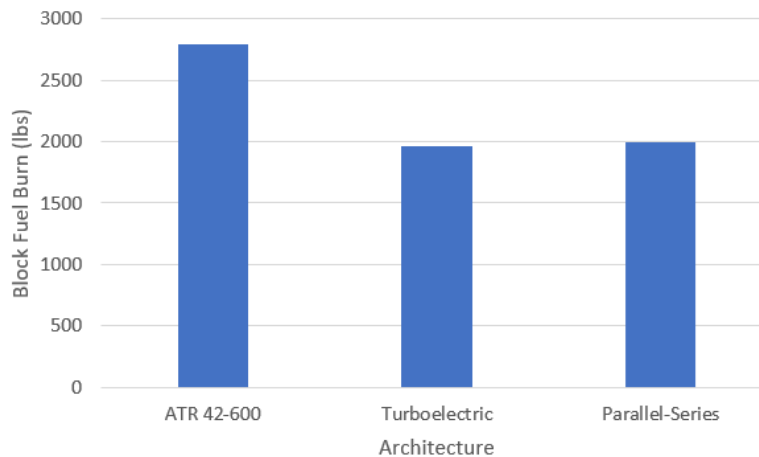
Figure VI-6. Comparison of Block Fuel Burns for Both Architectures, Compared to the ATR 42-600

The block fuel burn for each architecture, alongside the ATR 42-600's, can be seen in Figure VI-6. While both have significant improvements over the ATR 42-600, the parallel-series architecture results in a lower reduction in block fuel burn, without even considering the reliability of the battery, and making liberal assumptions about recharging. Thus, the turboelectric architecture was chosen for the Songbird-E.

E.III. Cruise Power Distribution Trade Study

To determine the optimal power distribution between the gas turbine and electric motor propellers, two different operating modes were investigated. The first option is always running the electric motor at full power. For the second option, the power ratio would stay the same as during takeoff. This means the power of the electric motor would decrease by the same percentage as the gas turbine propellers. Propellers optimized for each operating mode were designed and simulated for takeoff and cruise conditions. The results of that study are shown in Table VI-7. Note that the values do not match up with the current propulsion system, since the trade study was conducted on an earlier version of the propulsion system. However, the qualitative results transfer to our current architecture.

Table VI-7. Comparison of Operating Modes for Propeller Systems

	Option 1 (Electric Motor at Full Power)				Option 2 (Electric Motor Power Scaled)			
	Takeoff		Cruise		Takeoff		Cruise	
	GT	EM	GT	EM	GT	EM	GT	EM
Thrust (kN)	21.7	4.78	5.12	2.03	21.8	4.84	5.52	1.06
Efficiency	75.9%	90.0%	90.3%	92.5%	76.0%	91.1%	89.3%	92.8%
Total Thrust [kN]	26.48		7.15		26.59		6.58	

Looking at the results, option 1 increases the thrust during cruise by 8.7%, while only producing 0.42% less thrust during takeoff, in comparison to option 2. Hence, option 1 was selected for our propulsion system.

E.IV. Electric Motor Power/Hybridization Percentage Trade Study

In order to select the most efficient configuration, a trade study was conducted on the amount of hybridization, or the amount of power provided by the outboard electric motors. It was thought that there may be a "knee" in the curve, where our design would be most efficient. This study was extremely involved as many component weights and aerodynamic benefits depend on the power distribution. The components affected were the generator, main propellers, electric motors, rectifiers, wiring, inverters, electric motor propellers, small engine nacelles, and thermal management system. It is important to note that the way that the benefits of distributed electric

propulsion (DEP) are accounted for has been adjusted since this study was initially conducted. This change would only move the curve upward, increasing all block fuel burns proportionally. Electric motors were tested between 100 kW and 400 kW, in 25 kW increments. The results of the study can be found in Figure VI-7 below.
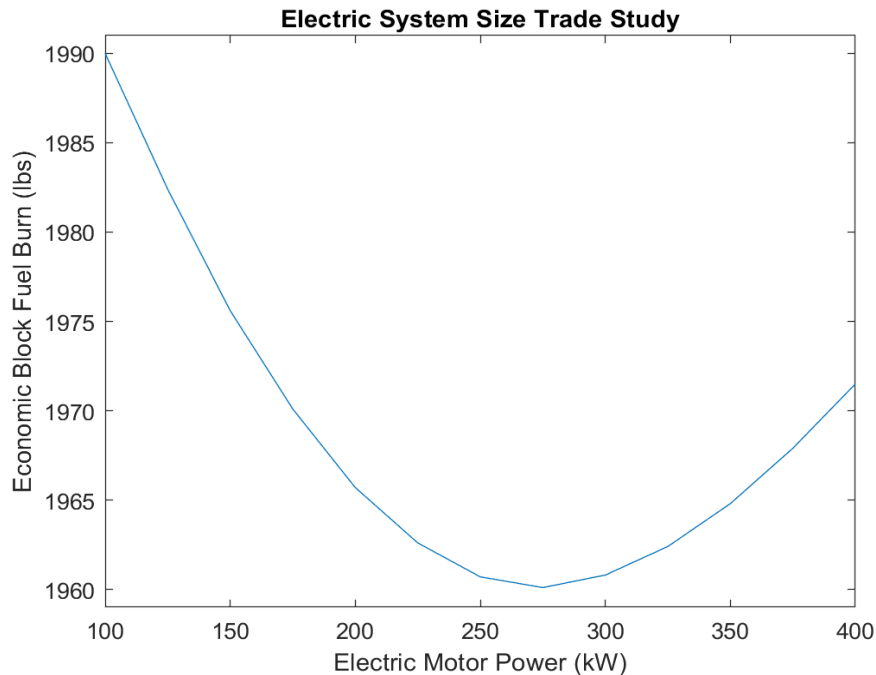
Figure VI-7. Electric Motor Power Trade Study Results

From conducting the trade study, it was found that the most efficient power configuration was very close to 275 kW, or 369 hp. This led to a change in our baseline design of the Songbird-E, which was initially sized to a 350 kW electric motor. The resulting configuration is a 76%-24% power distribution between the inboard turboprop and the outboard electric motor.

E.V. Overall Pressure Ratio (OPR) Trade Study

As part of accounting for a future engine, the overall pressure ratio of the turboelectric engine was studied. As the overall pressure ratio increases, so does the NOX output. According to the second figure of merit, a reduction in emissions, our concept became limited by the ATR 42-600 NOX output, of about 20.6 lbs of NOX per economic mission. From research, it was estimated that engine weight increases by about 3 kg (6.6 lbs) per unit increase in OPR. This was accounted for in the engine weights for this study. OPRs were tested from the current design point of 15.77 (same as the ATR 42-600) to 40, roughly in increments of 2.5. The results can be found in Figure VI-8.
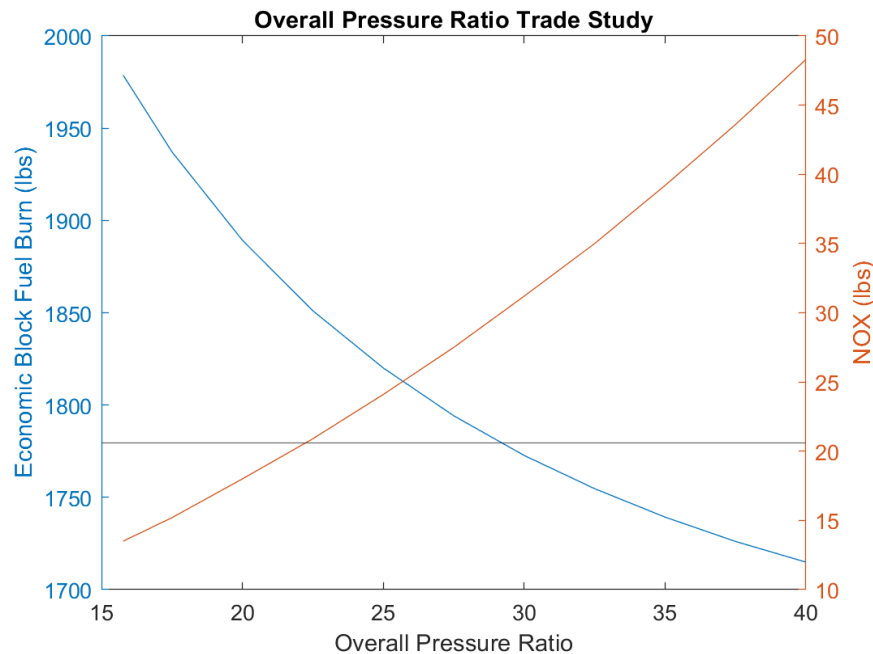
Figure VI-8. Overall Pressure Ratio Trade Study Results

In Figure VI-8, one can see the economic fuel burn and economic mission NOX plotted against the overall pressure ratio. The black line on the graph is the ATR 42-600 NOX output. From the NOX data, a quadratic regression was used to find the highest NOX that the Songbird-E could produce, while still yielding a reduction in NOX emissions. This point was found to be an overall pressure ratio of 22.2, leading to a change in our design, based on what is considered achievable by 2035, and the constraint supplied by the RFP. If that constraint were not present, the optimal design point would be where the two curves intersect, minimizing block fuel burn and NOX. As shown by Figure VI-8, the overall pressure ratio has a significant effect on the block fuel burn.

VII. Aerodynamics

This section will examine the aerodynamics of the Songbird-E. It includes information on the aerodynamic design process, including the selection process for the airfoil, wing design, and design of the high-lift devices and control surfaces. A full aerodynamic analysis of the Songbird-E was also conducted and is shown.

A. Airfoil Selection

As a consideration of the Songbird-E's aerodynamic design, it was essential that the selected airfoils yield an optimal performance throughout the mission. It was important to consider the effects of the chosen airfoils on the

aircraft's overall performance characteristics such as the lift, drag, and pitching moment coefficients. Since the Songbird-E is a transport aircraft, and will spend the majority of its mission time in the cruise phase, the optimal airfoils were those that optimized performance during cruise. Table VII-1 summarizes the key flow characteristics associated with this mission segment.

Table VII-1: Key Flow Characteristics of Cruise Segment

v_{oo} (ft/s)	h (ft)	ρ_{oo} (slugs/ft^3)	μ_{oo} (ft^2/s)	q_{oo} (psf)
464	28000	0.000958	0.00033	103

Six root airfoils were chosen for consideration: NACA 23018, NACA 33018, NACA 43018, NACA 53018, NACA 63$_3$-618, and NACA 64$_3$-618. The airfoils were analyzed at a Reynolds number of 9.5 million using XFLR5, an incompressible and time independent solver that utilizes the vortex lattice method [29]. Their respective aerodynamic performances were then compared at the design lift coefficient for cruise, which was calculated to be 0.5675. The resulting airfoil characteristics at cruise are summarized in Table VII-2.

Table VII-2: Performance Characteristics of Selected Airfoils at Cruise Lift Coefficient

Airfoils	α (deg)	C_d	C_m	C_l/C_d
NACA 23018	3.80	0.006	-0.01	92.2
NACA 33018	3.15	0.006	-0.001	93.6
NACA 43018	2.65	0.006	-0.005	90.1
NACA 53018	2.00	0.008	-0.012	74.4
NACA 63$_3$-618	0.05	0.004	-0.121	124
NACA 64$_3$-618	0.20	0.004	-0.121	129

As seen in Table VII-2, the NACA 64$_3$-618 has the largest 2D lift to drag ratio, followed by the NACA 63$_3$-618. Since an aircraft's lift-to-drag ratio is an indication of its aerodynamic efficiency, a high 2D lift-to-drag ratio is desirable in order to minimize the required fuel burn during a given mission. However, a key disadvantage regarding 6-series airfoils is a relatively high magnitude of pitching coefficient, which, as shown in Table VII-2, is more than an order of magnitude larger than the 5-series airfoils. This has major implications on an aircraft's longitudinal

stability, which must be addressed in the empennage design. Nonetheless, it was determined that maximizing the aerodynamic efficiency was of the highest priority, and thus the NACA 64_3-618 was selected as the optimal airfoil.

The airfoil distribution along the wing was chosen such that the root and tip airfoils had a max thickness to chord ratio of 18% and 13% chord, respectively. The root and tip section profiles are shown in Figure VII-1.

Root Airfoil: NACA 64_3-618   Tip Airfoil: NACA 64_3-613

Figure VII-1: Airfoil Profiles of Root NACA 64_3-618 and Tip NACA 64_3-613

B. Wing Design
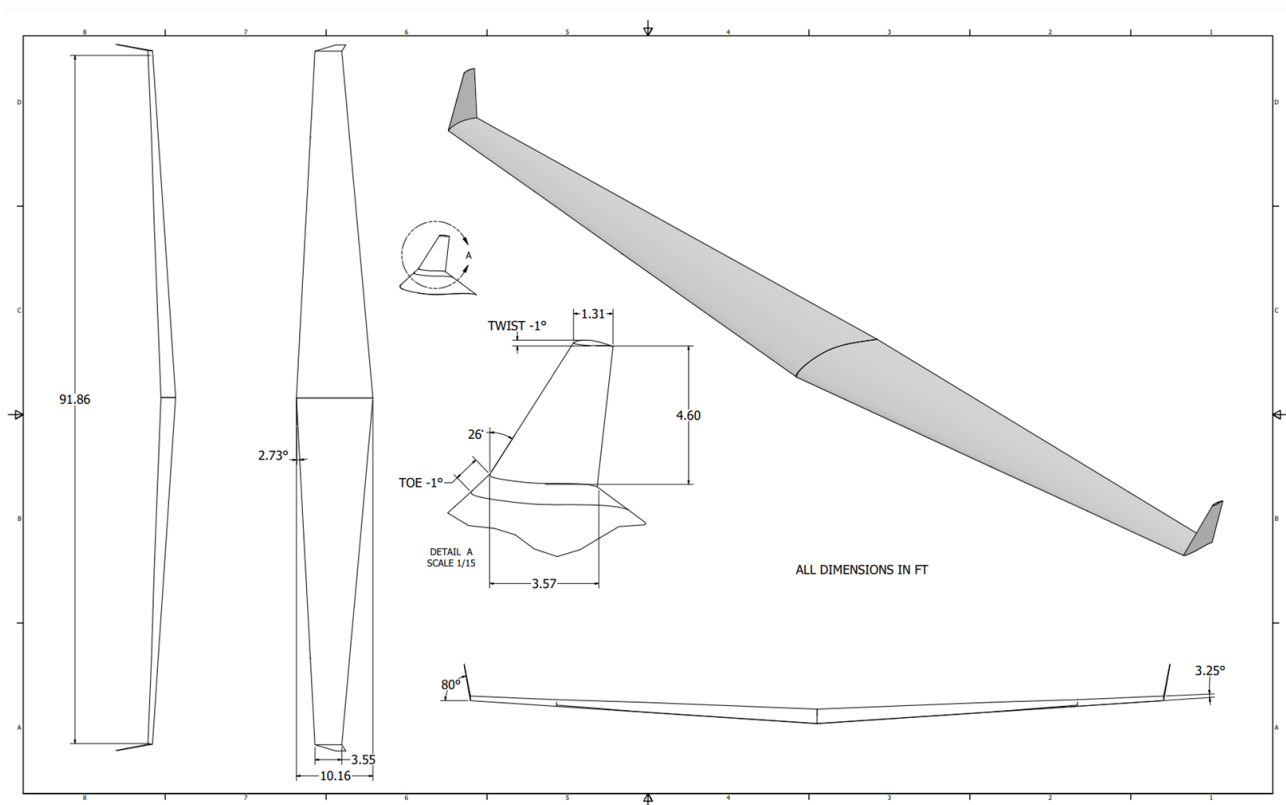
Figure VII-2: Wing Planform Geometry Excluding Control Surfaces

Table VII-3: Planform Characteristics

Parameter	Value
Wingspan	91.86 ft
Wing Area	629.8 ft^2
Aspect Ratio	13.36
Root Chord	10.16 ft
Tip Chord	3.55 ft
Mean Aerodynamic Chord	6.86 ft
Taper Ratio	0.35
Leading Edge Sweep	2.73°
Dihedral	3.25°
Incidence Angle	0°

Based upon Nicolai & Carichner's *Fundamentals of Aircraft Design* [11], the planform was designed with an optimal taper ratio of 0.35, in order to produce an approximately elliptical lift distribution along the wing. To maintain an elegant and visually-appealing design, a slight leading edge sweep of 2.73° was added as a result of the wing taper. The wing sweep, in addition to the included dihedral angle of 3.25°, both aid in the lateral stability of the aircraft. Since aerodynamic analysis indicated the wing produces sufficient lift during cruise at zero angle of attack, no incidence angle was required. By featuring a high aspect ratio design, coupled with an optimal taper ratio, the wing design of the Songbird-E yields optimal induced drag characteristics, minimizing the required block fuel burn.

C. High-Lift Devices and Control Surface Layout

To increase the planform lift characteristics during takeoff and landing, the Songbird-E implements both leading and trailing edge flaps. The leading edge flaps are split into 2 sections to accommodate the inboard engine nacelle, and cover 69% of the wingspan, with a chord ratio of 20%. The trailing edge flaps cover 56% of the wingspan, with a chord ratio of 25%. The trailing edge flap primarily serves the role of increasing C_{Lmax}, while the leading edge flaps primarily serve the role of delaying stall effects, and also increasing C_{Lmax} to a lesser extent. To permit lateral control authority of the aircraft, ailerons were added toward the wingtips, inboard of the electric motors. The ailerons cover 19% of the wingspan and have a chord ratio of 25%. Figure VII-3 demonstrates the control surface design.

	Chord Ratio	0.25
Aileron	Span Ratio	0.19
	Total Area	22.35 ft^2
	Max Deflection	$\pm$ 20°
LE Flaps	Chord Ratio	0.20
	Span Ratio	0.69
	Total Area	88.79 ft^2
	Max Deflection	30°
TE Flaps	Chord Ratio	0.25
	Span Ratio	0.56
	Total Area	98.59 ft^2
	Max Deflection	30°
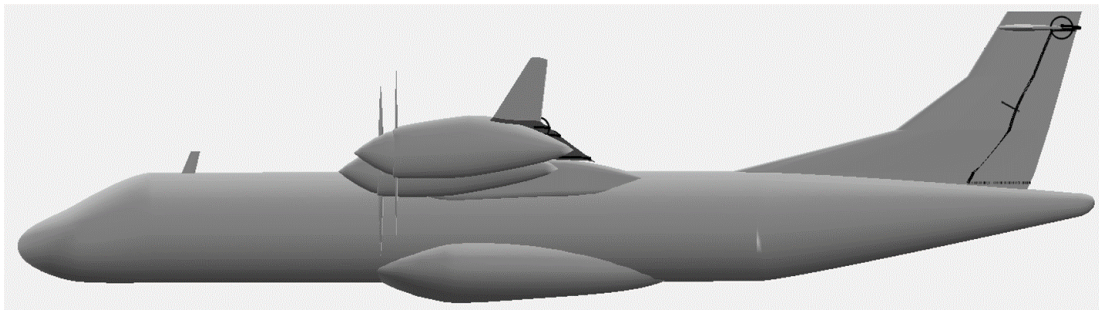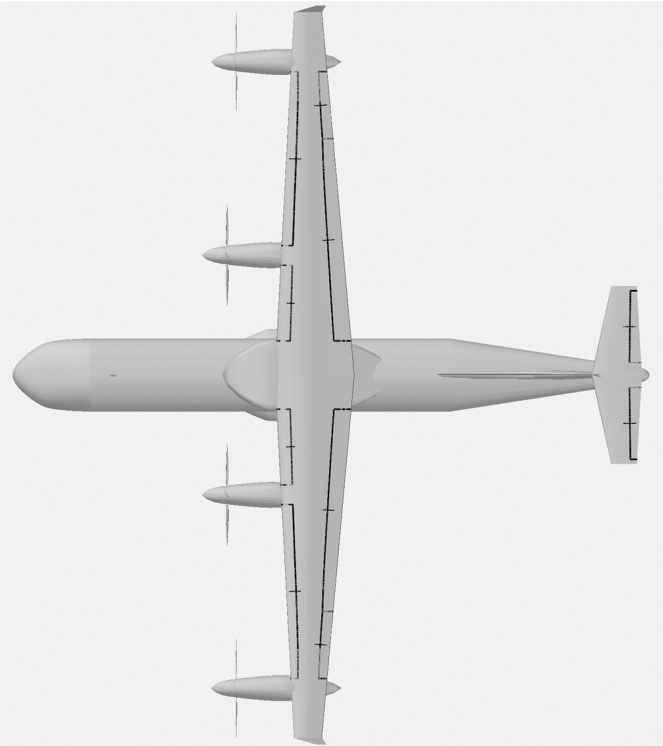
Figure VII-3: Aileron, Elevator, Flap, and Rudder Surfaces

D. Drag Build-Up

The parasite drag tool within OpenVSP was used to model the aircraft drag characteristics in its cruise configuration. The default settings within the parasitic drag tool were used, including the Blasius Laminar Flow C_f equation, the Schlichting Compressible Turbulent Flow C_f Equation, Hoerner Form Factor Equation, and Hoerner Streamlined Body Equation. The drag build-up was calculated component by component, at cruise conditions of 28,000 ft at 275 knots.
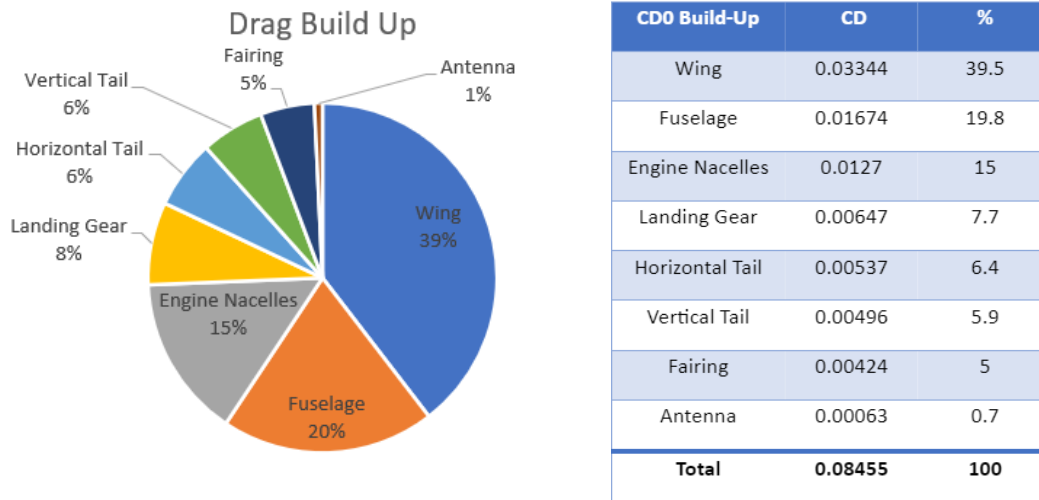
Figure VII-4: CD_0 Estimation of Drag Build Up

CD0 Build-Up	CD	%
Wing	0.03344	39.5
Fuselage	0.01674	19.8
Engine Nacelles	0.0127	15
Landing Gear	0.00647	7.7
Horizontal Tail	0.00537	6.4
Vertical Tail	0.00496	5.9
Fairing	0.00424	5
Antenna	0.00063	0.7
Total	**0.08455**	**100**

As seen in Figure VII-4, an estimate of overall parasite drag is obtained from OpenVSP. The wing causes the most drag in the design, which makes sense, as the wingspan is relatively large. The engine nacelles also have a large contribution to parasite drag. This is due to the 4 engines configuration change from the comparator ATR-42-600.

E. Aerodynamic Performance

Analysis of the aircraft's aerodynamic performance was conducted through the FlightStream. Developed by Research in Flight, FlightStream is a surface vorticity flow solver that incorporates unstructured meshing as a means of retaining the advantages of vorticity-based potential-flow solvers without compromising solver optimization [30]. Analysis of all mission segments was conducted. Thrust conditions were modeled in FlightStream's steady-state solver by mapping propellers as actuator disks under steady flow. Table VII-4 below characterizes the Songbird-E's performance at various altitudes and flight conditions.

Table VII-4. Songbird-E Aerodynamic Performance Data

	Takeoff	Climb 1	Climb 2	Climb 3	Cruise	Descent 1	Descent 2	Descent 3	Landing
Alt.	0	4880	8449	11909	28000	24963	14972	5002	0
Mach	0.170	0.283	0.293	0.316	0.470	0.408	0.328	0.271	0.160
AOA	8.000	8.000	8.000	8.000	0.000	-3.000	-3.000	-3.000	3.000
C_D	0.285	0.151	0.155	0.155	0.080	0.067	0.064	0.061	0.185
C_{Do}	0.058	0.031	0.031	0.031	0.031	0.032	0.030	0.030	0.042
C_{Di}	0.227	0.121	0.124	0.125	0.050	0.035	0.034	0.031	0.142
C_L	2.552	2.186	2.201	2.214	1.297	0.921	0.837	0.798	2.027
Max L/D	8.945	14.439	14.188	14.276	16.172	13.827	13.033	13.052	10.969

Takeoff and landing conditions were modeled using a high-lift geometry, depicted in Figure VII-5. Due to FlightStream's limitations of modeling the effects of leading edge control surfaces in lift generation, only the trailing edge subsurfaces were deflected. Takeoff and landing simulations were conducted with a deflection of 20 degrees.
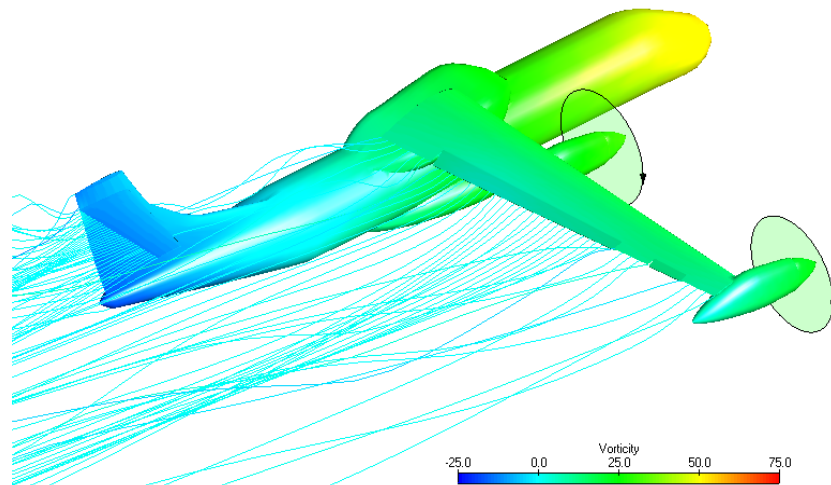
Figure VII-5. Streamline Profile of Songbird-E, High Lift Configuration

Climb and cruise flight conditions were conducted under the assumption of a clean wing, shown in Figure VII-6. For clean and high-lift configurations, the wingtips and radio transmitter on top of the fuselage were excluded, as the geometric additions were marginal in scale, significantly reduced convergence rates, and introduced meshing faults. The convergence threshold obtained for the Songbird-E in Figures VII-5 and VII-6 was at 1E-8 for Velocity and 1E-9 for Pressure residuals, of which the data in Table VII-4 was compiled.
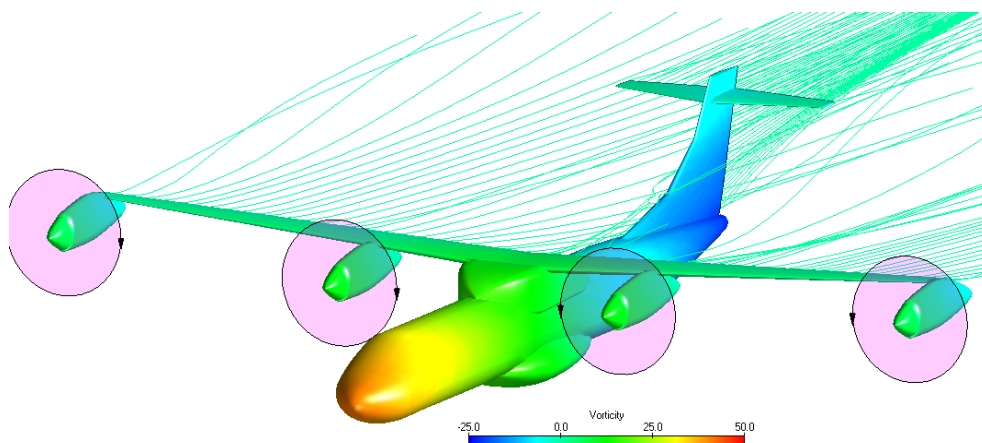
Figure VII-6. Streamline Profile of Songbird-E, Climb, Cruise Configuration

The addition of the winglets reduced the convergence thresholds to 1E-5 for Velocity and 1E-6 for Pressure residuals respectively, of which further grid control refinement and wing geometry adjustment in OpenVSP is necessary for better results. Table VII-5 summarizes the performance changes for the Songbird-E with respect to the ATR 42-600.

Table VII-5. Performance Comparison Summary, Scalable (Concept Performance/Reference)

	Takeoff	Climb 1	Climb 2	Climb 3	Cruise	Descent 1	Descent 2	Descent 3	Landing
Alt.	0	11604	16927	22696	28000	22709	16274	11601	0
AOA	8	8	8	8	0	-3	-3	-3	3
C_D	1.06	1.14	1.17	1.14	1.06	1.13	1.11	1.28	0.88
C_{Do}	0.91	1.82	1.93	1.91	1.1	1.26	1.22	1.2	0.98
C_{Di}	1.11	1.04	1.06	1.04	1.03	1.03	1.02	1.38	0.85
C_L	1.1	1.19	1.18	1.16	1.24	1.15	1.09	1.05	1.03
Max L/D	1.04	1.04	1.01	1.02	1.2	1.32	1.27	1.06	1.17

The aerodynamic performance comparison was conducted by matching flight speeds, altitude, and angle-of-attack conditions, of which empirical performance coefficients were derived for the Songbird-E's performance with respect to the reference aircraft. The reference geometry for the ATR 42-600 was sourced from OpenVSP Hangar and as such, aerodynamic performance comparison data must consider the possibility of inaccuracy with respect to operational aircraft. Necessary approximations of control surface positions and deflection angles for the ATR 42-600 resulted in potential variances in takeoff and landing data. The airfoil choice and additional propeller, as well as modifications to the tail sizing on the Songbird-E, resulted in an overall better performance than the reference ATR 42-600, as depicted in Table VII-5. Major improvements in C_L and maximum L/D were sourced from the engine calibration as the electric motor configured to constantly operate at maximum power provided an overall improvement to C_L by a maximum of 19% during climb and 24% during cruise conditions. For the Songbird-E, sweep analysis was performed, of which developments in C_L, C_{Di}, C_{Do}, and C_{My} were observed with respect to changes in angle-of-attack and sideslip angles. The results are characterized in Figure VII-7 for the climb/cruise configuration, and Figure VII-8 for the high-lift takeoff configuration.
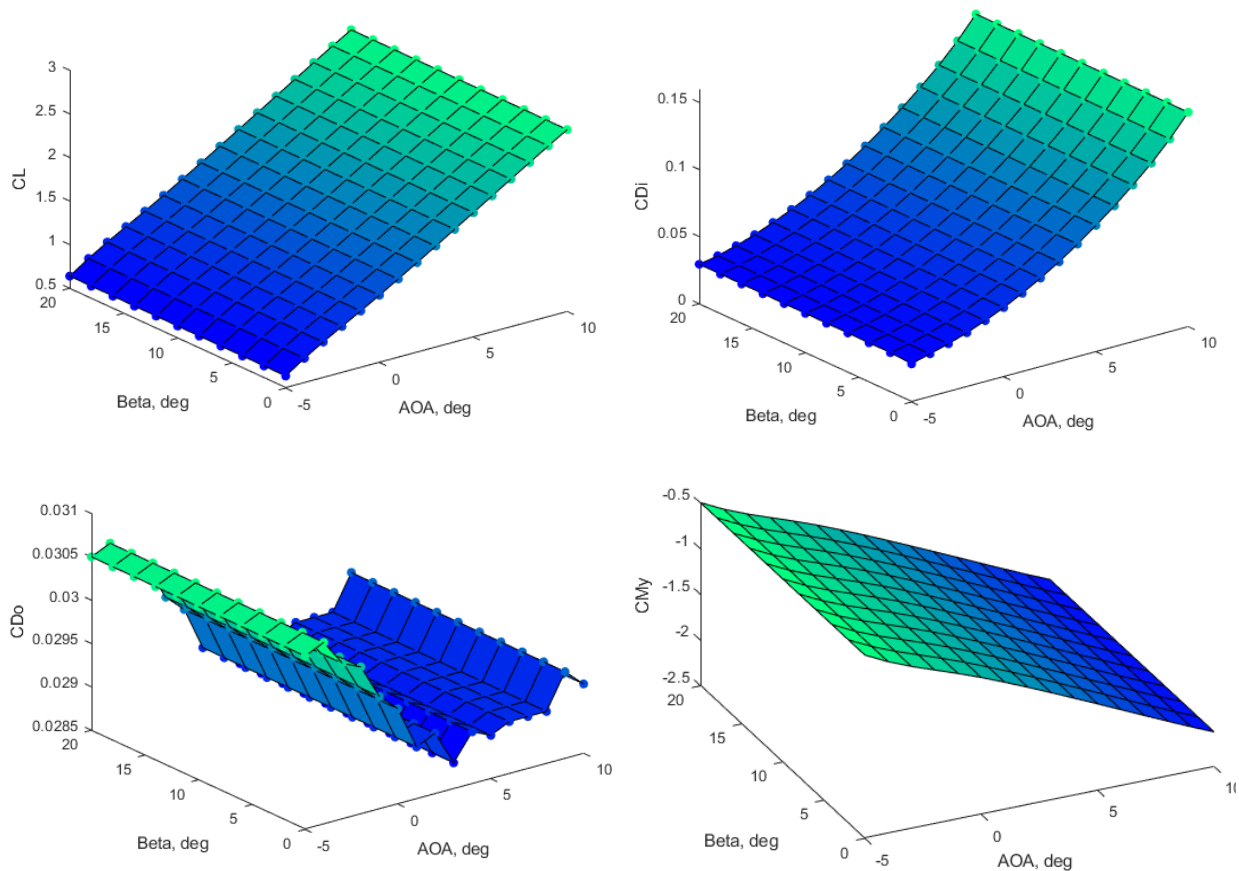
Figure VII-7. Surface Mapping, Songbird-E Climb/Cruise Configuration

The surface maps for the clean configurations were obtained with good convergence thresholds of 1E-8 for Velocity and 1E-9 for Pressure residuals. Surface profiles did not exhibit any discontinuities, gaps, or peaks for increasing sideslip angles for any designated angle-of-attack, indicating an aerodynamically stable and streamlined geometry for common operating conditions. The implementation of control surfaces deflected at 20 degrees resulted in disrupted geometry along the trailing edge, thus increasing the roughness of flow and drag generation in the presence of sideslip. At angles of sideslip above ±10 degrees, flow separation was observed along the deflected subsurfaces and increased proportional to the sideslip angle. The above surface maps are summarized in the L/D profile of the clean configuration in Figure VII-9. Aerodynamic sweeps of the configuration indicate that both clean and high-lift configurations are capable of providing the necessary C_L for takeoff, climb, and cruise for sideslip conditions upwards of ±20 degrees, with performance improvements, as compared to the ATR 42-600.
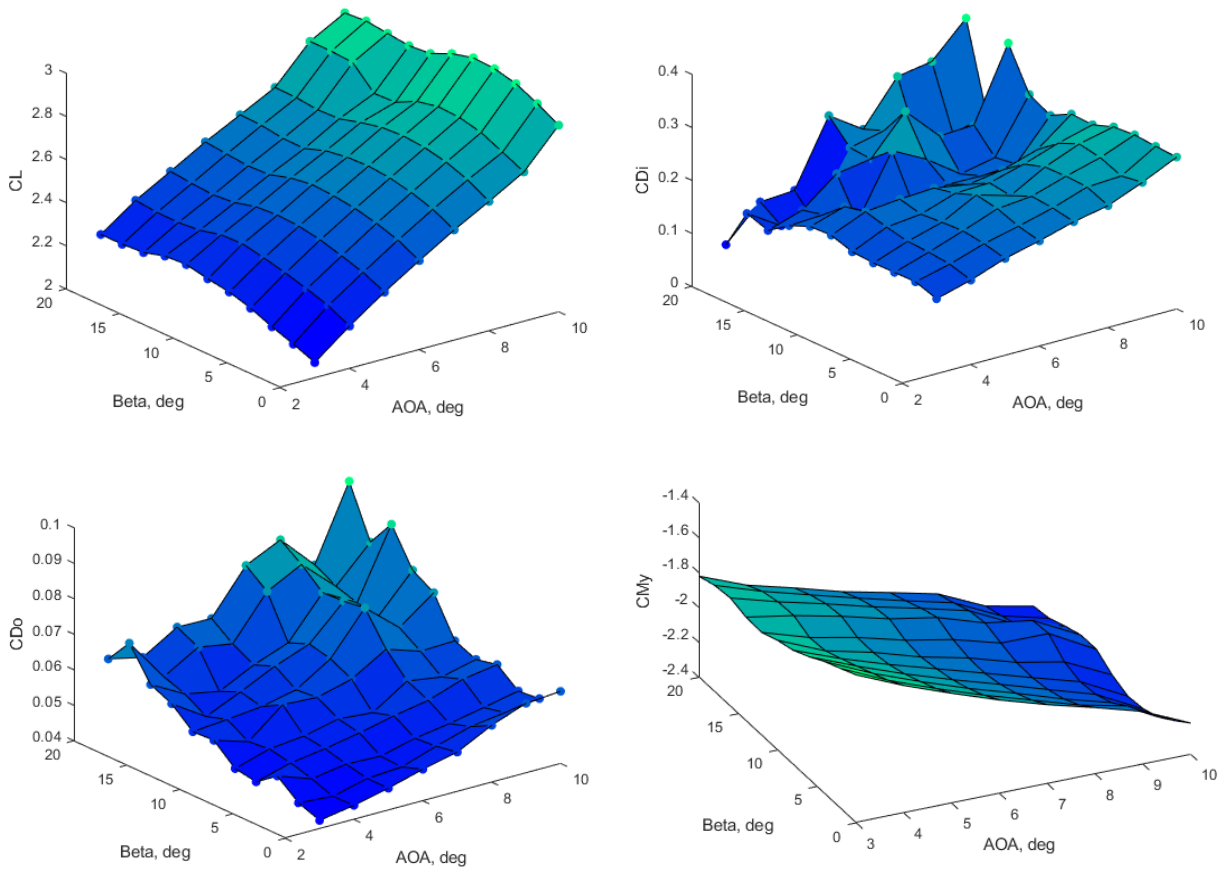
Figure VII-8. Surface Mapping for the High-Lift Configuration
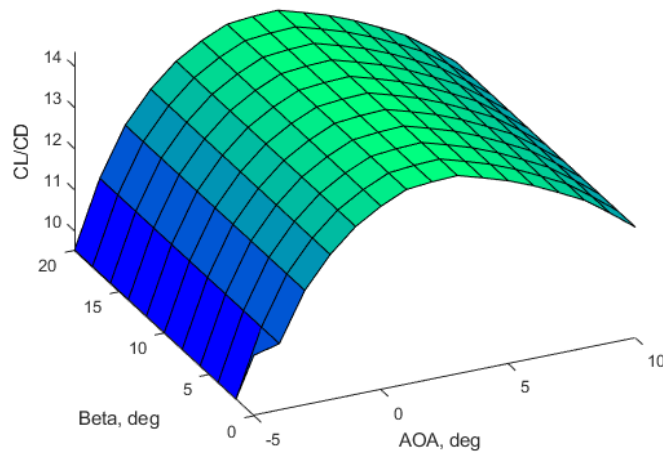
Figure VII-9. L/D Distribution for Clean Configuration

F. Aerodynamics in Mission Analysis

The Songbird-E leverages three main aerodynamic benefits in its current configuration, namely weak distributed electric propulsion (DEP) configuration, the acceleration of air further from the fuselage, and winglets.

From a paper by researchers at TU Delft, it was found that, for an aircraft that covers 53% of the span in propulsors, aerodynamic coupling increases the aero-propulsive efficiency by 9% [31]. Though the aircraft considered is slightly larger than the Songbird-E, sized for 75 passengers with a 1500 nmi design range, and uses an over-the-wing-distributed-propulsion system, this paper provides a good basis for exploring the aerodynamic effects of a distributed propulsion system. The Songbird-E covers approximately 56% of its span with its 4 propulsors. Using a proportional relationship, the Songbird-E claims a 9.5% benefit to fuel flow factor.

Air away from the fuselage is cleaner and more efficient. Thus, by placing propulsors towards the wingtips, aerodynamic benefits to induced drag are achieved. To quantify these benefits of the Songbird-E, a paper written by Nathaniel Blaesser at NASA Langley on their PEGASUS concept was examined [32]. Mr. Blaesser found that, as compared to a clean wing, an inboard propulsor provided a 5% decrease in induced drag, and a wingtip propulsor provided a 9% decrease. Since our design doesn't place the outboard propulser on the wingtip, but pulls it in enough to contain the propeller diameter within the wingspan, the 9% benefit was scaled down to 8.58% based on the distance between the inboard and outboard engines. As the PEGASUS concept is a similar size, such a move should be reliably accurate. Accounting for this benefit in FLOPS was a bit difficult, as FLOPS can only take in one type of engine on a wing. The inboard turboprop was placed in its proper position, so it was assumed that FLOPS had already accounted for a 5% benefit due to the inboard turboelectric engine. Thus, a scaling rule was developed:

$$5\% * (fraction\ of\ inboard\ power)\ +\ 8.58\% * (fraction\ of\ outboard\ power)\ -\ 5\% \quad \text{(EQN 5)}$$

Applying EQN 5 to the Songbird-E, with 24.1% of its power coming from its outboard electric motor, a reduction of 0.86% induced drag was claimed. This was thought to be a conservative estimate for the induced drag benefit.

Lastly, winglets were added to the Songbird-E. The aerodynamic benefits of winglets were estimated from papers on the addition of winglets to the Jetstream 31 and the A320neo. The effect of winglets on the Jetstream 31 was studied by Ilias Lappas and Akira Ikenaga from the University of South Wales and Airbus UK Future Projects Department, respectively [33]. They found a 1.19% benefit to total drag by use of winglets. In regards to the A320neo, research was conducted by Dieter Scholz of the Hamburg University of Applied Sciences [34]. Mr. Scholz found a 4% benefit to total drag by adding sharklet winglets to the A320neo. The benefit to the Songbird-E was

estimated by interpolating between the span of both designs. From this interpolation, the Songbird-E claims a 2.92% reduction in total drag. The weight of the winglets was accounted for and will be discussed later.

G. Aerodynamics Trade Studies

This section will examine the two trade studies conducted on the aerodynamic configuration of the Songbird-E, which are the ICAO Gate Code B and engine placement trade studies.

G.I. ICAO Code B Wingspan Trade

The Songbird-E features a 28 m (91.86 ft) wingspan with a wing area of 58.5 m^2 (630 ft^2), resulting in an aspect ratio of 13.36. This meets the mandatory gate requirement of ICAO Code C, specified in the RFP, which stipulates that the wingspan must be <36 m. However, meeting the tradeable requirement of ICAO Code B, which requires a wingspan of <24 m, would allow the Songbird-E to service smaller airports. Thus, the trade of meeting ICAO code B was explored, to assess the tradeoffs between airport accessibility and aircraft performance.

Key considerations in this study were economic block fuel burn reduction, the impact of a lower aspect ratio on induced drag, the impact of shorter span on the distributed electric propulsion benefit, and competitor planform characteristics. A span that met the gate code target was designed to the characteristics in Table VII-6.

Table VII-6. Summary of Planform Changes

Design	Span (m)	Area (m^2)	AR (ul)	Root Chord (m)	Tip Chord (m)	Taper Ratio	Sweep (°)
Current	28	58.50740	13.36	3.10	1.08	0.35	2.73
Gate Code B	24	51.98556	11.04	3.21	1.12	0.35	2.73

An analysis of this study in FLOPS indicated a decrease in economic block fuel burn reduction of 3.53% for the Code B wing. It was also determined that meeting ICAO Code B was deemed insignificant by ATR, as the ATR 42-600 has a wingspan of 24.6 m [35], just failing to meet this specification. From our market analysis, it was found that smaller Code B airports simply don't provide a market for aircraft so large. Thus, the original planform, with a 28 m (91.86 ft) wingspan, was preserved to maximize the economic block fuel burn reduction.

G.II. Distributed Electric Propulsion and Winglet Coupling Trade

In order to achieve the most aerodynamically-efficient concept, a trade study was conducted on the engine locations. This study considered the impacts of wingtip propellers, winglets, distributed electric propulsion (DEP),

and power distribution. The aerodynamic benefits of the wingtip propulsors were found by taking the 9% benefit from the previous power distribution discussion, though this may be a conservative estimate based on other papers.

Four configurations were studied. These were inboard electric motors with wingtip turboprops, inboard turboprops with wingtip electric motors, and inboard turboprops with outboard electric motors contained within the span, with and without winglets. From early analysis, it was found that using outboard turboprops would be infeasible. The vertical tail size would not converge and was still increasing double the vertical stabilizer area, due to the OEI condition. Thus, only the latter three configurations were studied.

The configurations showed the following benefits: The wingtip electric motor, which was the baseline at the time, showed a 27.5% reduction in economic block fuel burn. The DEP design without winglets found a benefit of 29.3% reduction, and the DEP design with winglets had a benefit of 30.9% block fuel reduction. All such reductions are as compared to the ATR 42-600. This study led to two conclusions. First, winglets do buy their way onto our aircraft, even after accounting for its weight, yielding another 1.6% in block fuel reduction. Second, the DEP benefit far outweighed the baseline wingtip propeller configuration. It is important to note, though, that this study was conducted prior to correcting EQN 5 by 5%, due to FLOPS' accounting for the inboard engine induced drag reduction versus the clean wing. This would make the benefits closer together, but should scale down the benefits of all three configurations, as they all utilize that equation. This study concluded by changing the configuration of the Songbird-E, from a wingtip propulsor, to utilizing a stronger DEP configuration.

VIII. Mass Properties

This section will showcase the weight analysis of the Songbird-E, by research, and analysis in FLOPS. This section also includes information on the center of gravity and the weight sensitivity of our design.

A. Weights

Much goes into the weight estimations for our concept, as weight estimation is holistic in nature. To start, the weights of the ATR 42-600 components were estimated. It was necessary to tune various structural and subsystems weights in FLOPS to match known weights of the ATR 42-600, such as maximum payload weight, operating empty weight (OEW), maximum zero fuel weight, and maximum takeoff gross weight (TOGW) [15]. These tuned values for the ATR 42-600 were then used as the basis of our concept. These weights were tuned as multipliers on individual components, such as fuselage, electrical, furnishings, etc.

A few other important elements of the ATR 42-600 were crucial. A paint weight was assumed, according to EQN 7.51 in Roskam's Aircraft Design, Part V, of about 150 lbs [10]. The weight of the PW127XT engines was found to be 1046 lbs from the propulsion section of this report. The propeller and propeller system weights were calculated as described in the Propulsion section. Also noteworthy is that the ATR 42-600 does not utilize an auxiliary power unit (APU), but rather uses an engine brake on the starboard engine, operating the engine in what is known as "hotel mode" [36]. While it is louder and less efficient, it can save as much as 300 lbs of weight.

Once the model was tuned, the Songbird-E weights could be further calibrated. The basic subsystem weights were further verified against Nicolai & Carichner's *Fundamentals of Aircraft Design* and Roskam's *Aircraft Design: Part V* [10, 11]. These methods include General Dynamics (GD), Cessna, and Torenbeek methods, among others. The subsystem weights will be discussed more in the subsystems section.

The weights of the aircraft structure were all computed by the empirical methods in FLOPS, with the exception of the wing. Due to FLOPS' issues with estimating wing weight when AR is >10, a correction factor was employed. Upon speaking with Dr. Jesse Quinlan, Branch Head of the Aeronautics Systems Analysis Branch at NASA Langley, a correction factor of EQN 6 was suggested, for aspect ratios between 10 and 16.

$$1 \ + \ 0.15 \ * \ \frac{AR-10}{6} \hspace{3cm} \text{(EQN. 6)}$$

This correction factor was verified against the Torenbeek method (EQN 5.7 in Roskam's *Aircraft Design: Part V*) [10]. The correction factor was found to be highly accurate for our wing, yielding a wing weight only 0.17% less than the Torenbeek method. About 160 lbs were added to account for winglets, as scaled from the Boeing 737-900 OEW [37]. This was accounted for by using a multiplier on the wing weight to achieve the necessary increase.

Futuristic aircraft glass was also utilized to reduce weight. In June 2015, Aviation Glass & Technology made history with the first-ever aviation authority approval of its ultrathin, lightweight aircraft glass [38]. Their glass is 50% thinner and 25% lighter than traditional polycarbonate products. Using the General Dynamics method cited by Jan Roskam, 50 passengers of windows was estimated to weigh about 250 lbs, which led to a weight reduction of about 60 lbs, credited to the fuselage weight.

As previously indicated, the use of composites played a significant role in reducing the structural weight of the aircraft and will be discussed more in-depth in the materials subsection of this report. The final structural weights are given in Table VIII-1 below.

Table VIII-1. Structural Weights for the Songbird-E

Component	Weight (lbs)
Wing	3085
Horizontal Tail	264
Vertical Tail	314
Fuselage	5140
Landing Gear	1782
Turboprop Nacelles	181
Paint	157
Total:	10923

The crew and payload/passenger weight was calculated from RFP requirements, 190 lbs and 30 lbs of baggage per crew member, and 200 lbs and 40 lbs of baggage for passengers. Passengers are also accommodated by 712 lbs of passenger service. In order to allow for growth in the weight of our conceptual aircraft, especially in a futuristic hybrid-electric propulsion architecture, an empty weight margin of 250 lbs, or about 2.7% of the aircraft's OEW, was selected and included. The itemized weights are listed in Table VII-2.

Table VIII-2. Itemized Songbird-E Weights

Grouping	Weight (lbs)	Total Weight %
Structures	10923	27.42
Propulsion	3699	9.28
Systems & Equipment	6233	15.65
Empty Weight	21105	52.97
Operating Empty Weight	23305	58.5
Payload	12000	30.12
Zero Fuel Weight	35305	88.62
Fuel Weight	4535	11.38
Gross Weight	39840	100

Though mentioned in the RFP in section 6b, the Songbird-E has not been designed for freighter or maritime surveillance variants, though we are confident that the Songbird-E could be outfitted for such purposes.

B. Center of Gravity (CG)

The center of gravity (CG) was calculated using the in-depth weight breakdown from FLOPS, and placing each individual component in the aircraft, estimating a component CG for each. This included all elements of the structural, propulsion, and systems and equipment, as well as fuel and payload. The CG is given by Figure VIII-1.

| 33.16 ft |
| 35.97 - 36.11 ft |
| 38.22 ft |
| 43.32 ft |
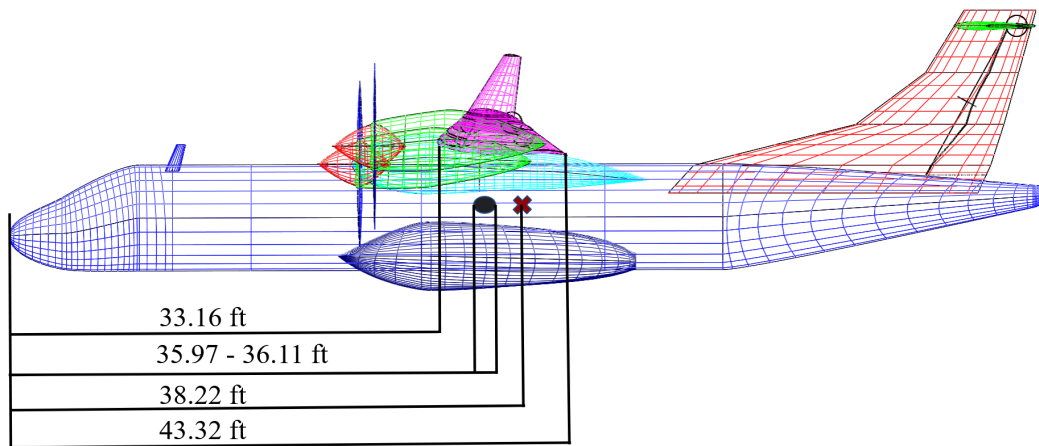
Figure VIII-1. CG Diagram with Range

At max passenger capacity, with sufficient fuel for a 1000 nmi mission, the CG is 36.11 ft from the aircraft's nose. At zero fuel with maximum passengers, the CG is found to be 35.97 ft from the same reference. The latter point is unrealistic to achieve since aircraft rarely tap into their fuel reserves, but it shows the absolute limit of the CG range. The CG range is small because the fuel is stored very close to CG. Since the aircraft is symmetrical, there was no need to calculate a CG on the port-starboard axis. No CG was calculated in the vertical direction either. It was assumed to be within normal parameters for the current analysis.

C. Weight Sensitivity Study

A weight sensitivity study was performed on the Songbird-E, to examine the impacts of weight growth on our design. This study was conducted by increasing the empty weight margin from 0 to 1000 lbs, in increments of 250 lbs. By performing a linear regression on the data, with a high R^2, it was determined that per 1 pound of empty weight margin increase, OEW increases 1.11 lbs, TOGW increases 1.23 lbs, economic block fuel burn increases 0.05 lbs, and the block fuel percent reduction decreases 0.0017%. It is important to note that the empty weight margin is directly included in the OEW and TOGW increases.

IX. Performance

This section examines the performance of our aircraft, and its abilities to meet and exceed the RFP requirements. First, the mission requirements are refreshed. The economic mission and the Songbird-E's improvements over the ATR 42-600 are examined, specifically in the context of the RFP. A stepped walkthrough of the design progress will be discussed, in order to break down our design's benefits. An analysis of the takeoff and landing capabilities of our aircraft is demonstrated, along with an examination of the design mission. The payload-range diagram is discussed, as well as a trade study on the cruise speed and altitude used by the Songbird-E. Lastly, the flight envelope is examined and an acoustic analysis of our concept is shown.

A. Requirements and Approach

The RFP sets out many mission requirements that will be addressed in various subsections. The mission requirements can be found in Table II-1. The economic mission will be discussed in subsection C, the takeoff and landing performance in subsection E, and the design mission will be discussed in subsection F. A trade study on the cruise speed and altitude requirements was also conducted, and will be discussed in subsection G.

All mission analysis was conducted for this design using NASA's Flight Optimization System (FLOPS) [8]. FLOPS was created in the mid-1980s, and has been used and maintained for conducting mission and performance analysis on aircraft concepts by NASA's Langley Research Center in Hampton, VA. FLOPS is run out of the command line using text input and output files. It is built on Fortran. There are six main modules in FLOPS, namely weights, aerodynamics, propulsion data scaling and interpolation, mission performance, takeoff and landing, and program control. Propulsion data is fed through an engine deck, created from propulsion modeling outputs.

FLOPS has served three primary purposes: providing detailed component masses, sizing our aircraft, and examining mission performance. The comparator ATR 42-600, the three PDR concepts, and the Songbird-E were all modeled in FLOPS. FLOPS has been invaluable to the design and analysis process.

B. FLOPS Calibration

In order to calibrate the FLOPS model of the ATR 42-600 and our concepts, model settings were adjusted to meet the published block fuel burn values published by ATR [15]. The primary metric calibrated to was ATR's published value for a 400 nmi economic mission, but data given on 200 and 300 nmi missions was also used. By adjusting the spanwise efficiency, induced drag, total subsonic drag, and fuel flow factor, our FLOPS model of the

ATR 42-600 was calibrated to the block fuel burn for 200, 300, and 400 nmi missions, with errors of -2.09%, 1.3%, and 1.09%, respectively. The calibrated values of our ATR 42-600 model were then applied to the other decks, given the similar sizing point. Later in the design process, the FLOPS' aerodynamics were calibrated to information from VSPAero and FlightStream aerodynamic simulations of the ATR 42-600 and the Songbird-E.

C. Economic Mission, Figures of Merit, & Requirements

This section analyzes the economic mission to demonstrate our aircraft's performance under the figures of merit, namely the 20% reduction in block fuel burn on a 500 nmi mission, and a reduction in emissions, including CO_2e and NOX. The detailed performance of the Songbird-E on the economic mission is given in Table IX-1.

Table IX-1. Songbird-E Economic Mission Performance

Segment	Initial Weight (lbs)	Fuel (lbs)		Time (min)		Distance (nmi)		Mach Number		Altitude (ft)	
		Part	Total	Part	Total	Part	Total	Start	End	Start	End
Taxi Out	38088	28	28	10.0	10.0	0	0	0	0	0	0
Takeoff	38060	53	82	1.5	11.5	0	0	0	0.2	0	0
Climb	38007	552	633	19.5	31.0	73.4	73.4	0.2	0.462	0	28000
Cruise	37455	1137	1770	76.6	107.6	350.8	424.2	0.462	0.462	28000	28000
Descent	36318	56	1827	22.9	130.5	75.8	500.0	0.462	0.2	28000	0
Taxi In	36233	28	1855	10.0	140.5	0	500.0	0	0	0	0

From Table IX-1, the Songbird-E's performance against the requirements can be analyzed. First, the Songbird-E has a total block fuel burn of 1855 lbs. This achieves a 33.6% reduction from the 2794 lbs of block fuel burn found to be expended by the ATR 42-600 on a 500 nmi mission. The RFP also calls out economic block fuel burn per seat. In this metric, our aircraft further exceeds the ATR 42-600, as the Songbird-E adds two extra seats. The ATR 42-600 has an economic block fuel burn per seat of 58.2 lbs/seat, compared to the Songbird-E's 37.1 lbs/seat. This results in a 36.1% reduction in economic block fuel burn per seat. The Songbird-E not only meets these economic block fuel burn figures of merit, but well-exceeds them.

In regards to emissions, CO_2e, or carbon dioxide equivalent, and NOX were examined. CO_2e is a combination of pollutants that contribute to climate change, adjusted based on their respective global warming potential [39]. Researchers from NASA Langley and NASA Glenn state that 3.7625 lbs of CO_2e are produced per pound of fuel consumed. Thus, the relationship between block fuel burn and CO_2e are directly proportional. As our

design reduces block fuel burn by 33.6%, our design reduces CO_2e by the same amount. Total emissions could also be reduced by the use of sustainable aviation fuels (SAFs). In a press release from June 2022, ATR made history by performing the first 100% SAF-powered test flight on a commercial aircraft [40]. The press release claims that SAF can reduce life cycle greenhouse gas emissions by 80%, as compared to jet fuel. It is likely that the Songbird-E would be able to utilize full SAF flight 12 years from now, as the ATR 42-600 may be able to in the near future.

In order to paint a more complete picture of emissions, direct NOX output was also examined. This is because the overall pressure ratio was varied to minimize block fuel burn. The Songbird-E was found to produce 20.5 lbs of NOX, compared to the ATR's 20.6 lbs. More on the NOX output can be found in the overall pressure ratio trade study in the propulsion section. From CO_2e analysis and achieving a 0.5% reduction in NOX, the second figure of merit has been achieved. A more detailed and direct comparison can be found in the Table X-3 on the intermediate baselines comparison

Turning attention to the requirements, all of the mission requirements are met. The cruise speed is approximately 0.4624 Mach, which translates to a cruise speed of 275 kts at 28,000 ft. This yields a mission time of 2.34 hours. The cruising altitude is also set at FL280. In the climb section of Table IX-1, the distance to cruising altitude is shown to be 73.4 nmi, which is significantly below the RFP minimum of 200 nmi to cruising altitude. A reserve mission is also accounted for, as defined in section II-C. The Songbird-E stores an extra 1007 lbs of fuel for that purpose on the economic mission.

D. Intermediate Baselines

In order to demonstrate the benefits of specific aspects of the Songbird-E, intermediate baselines were developed. They can be seen in Figure IX-1 and will be explained below.

Baseline ATR 42-600

ATR 42-600 with 2034 Turboprops

	PW127XT-M
	2034 SOA Turboprop
	Turboelectric
	Electric

Songbird-E with 2034 Turboprops

Songbird-E
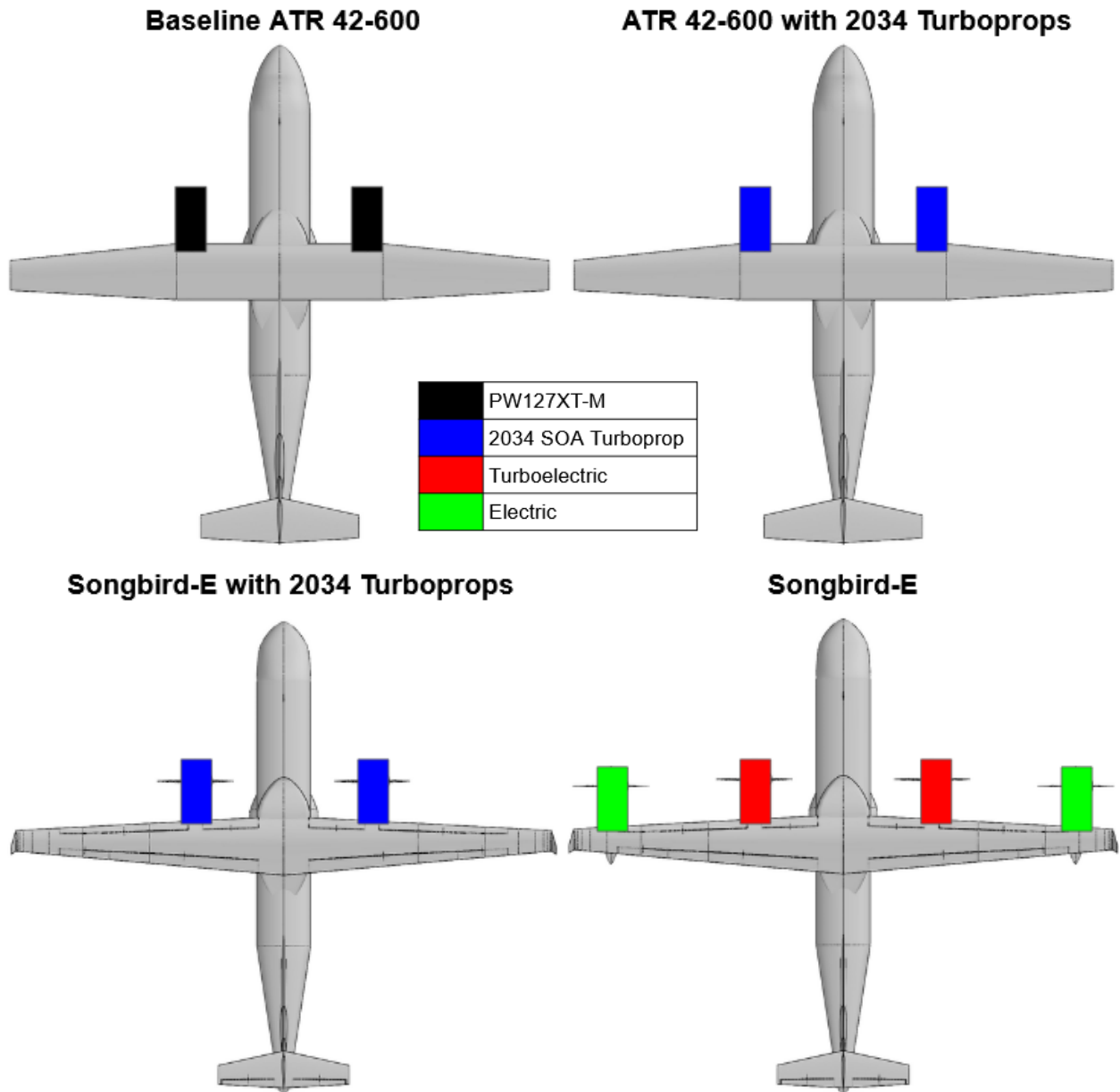
Figure IX-1. Intermediate Baselines

The stepped process begins with the baseline ATR 42-600. A 2034 EIS ATR 42-600 was developed, with the only change from the baseline being the swapping of the PW127XT engines on the ATR 42-600 with a similarly-sized futuristic turboprop engine that would be expected given technological advancements. More about this engine can be found in the propulsion section of this report. The next intermediate baseline was the Songbird-E's outer mold line (OML), but with the same engines and engine configuration as the 2034 ATR 42-600 model. This baseline utilized two futuristic turboprop engines on our outer mold line. Lastly, the Songbird-E concept

is shown, demonstrating the full performance characteristics of our concept. These intermediate baselines allow us to step through our design to show the benefits of future turboprop engines, improved aerodynamics and geometry, and our hybrid-electric propulsion architecture. Shown in Table IX-2 below are key figures of merit from each of the baselines.

Table IX-2. Intermediate Baseline Comparative Performance

	ATR 42-600	ATR 42-600 with 2034 Engines	Songbird-E with 2034 Engines	Songbird-E
Max TOGW (lbs):	41005	41005	39361	39840
Economic Block Fuel Burn (lbs):	2793.8	2498.4	2016.3	1855.2
Percent Change from ATR:		-10.6%	-27.8%	-33.6%
Economic Block Fuel Burn per Seat (lbs/seat):	58.2	52.1	40.3	37.1
Percent Change from ATR:		-10.5%	-30.8%	-36.3%
Economic Block Fuel Burn per Seat per NMI (lbs/seat-nmi):	0.116375	0.1041	0.080652	0.074208
Percent Change from ATR:		-10.5%	-30.7%	-36.2%
CO_2e (lbs):	10511.7	9400.2	7586.3	6980.2
Percent Change from ATR:		-10.6%	-27.8%	-33.6%
Econ NOX Emissions (lbs):	20.6	31.0	22.4	20.5
Percent Change from ATR:		50.5%	8.73%	-0.485%

A few important notes on the above table must be provided. First, the ATR 42-600 is typically run in a 48 seat configuration whereas the Songbird-E was configured for 50 passengers. Second, all values shown are in reference to the 500 nmi economic mission, as this was given for the primary figures of merit. Lastly, the 2034 engine and hybrid-electric engine utilize an increased overall pressure ratio, from 15.77 to 22.2, as is supported by research into current and future engine technologies. Lastly, the Songbird-E cruises at an altitude of 28,000 ft, whereas the ATR 42-600 is designed to cruise at 24,000 ft [15]. To show the block fuel burn reduction growths, the waterfall chart is provided below as Figure IX-2.
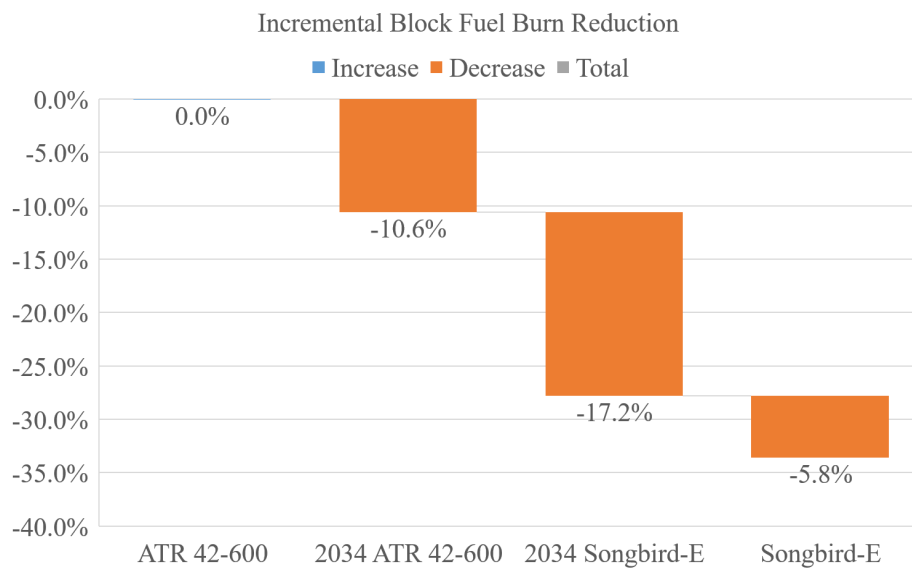
Figure IX-2. Incremental Reduction in Block Fuel Burn Across Intermediate Baselines

As can be seen from the waterfall chart, by simply replacing the PW127XT-M with a projected 2034 turboprop

engine, block fuel burn is reduced by 10.6%. By improving the aerodynamic characteristics of the aircraft, moving

from the ATR 42-600's OML to the Songbird-E's, a further 17.2% reduction is achieved. Lastly, the transition from

the ATR 42-600's propulser configuration to our hybrid-electric configuration yields an additional 5.8% reduction,

leading to a total reduction of 33.6% in block fuel.

E. Field Length Analysis

From the requirement specification, the Songbird-E is required to meet a maximum field length of 4500' at

5000' airport altitude, and an approach speed that does not exceed the category C limit of 141 kts.

In order to analyze the takeoff and landing performance of the aircraft, FLOPS was used, in conjunction

with Nicolai & Carichner's *Fundamentals of Aircraft Design Volume I* [11]. FlightStream simulations found the

high-lift C_L at takeoff to be 2.55. This value is an underestimate, as FlightStream is unable to model our leading edge

flaps. This value was input to FLOPS, which was prioritized, as it had more information and the ability to calculate

these parameters. The takeoff field length values yielded by FLOPS were found to be reasonable, but the landing

field lengths seemed unlikely high. The same problem also occurred in the ATR 42-600 FLOPS model. In

MATLAB, the simple takeoff and landing formulas from Nicolai & Carichner were coded (EQNs 6.3 & 6.5 in the

textbook). These formulas take wing loading (lb$_f$/ft^2), air density ratio at sea level to altitude (1 at sea level), takeoff

C_L, thrust-to-weight ratio, and approach angle. While the textbook's simple takeoff formula output yielded incorrect

results, the percent increase for the altitude change from 0 to 5000' was used to correct the FLOPS value for altitude. The textbook's landing field formula was found reliable. The stall, takeoff, and landing speeds were also estimated using Nicolai & Carichner (EQNs 6.1 & 10.2). The performances are outlined in Table IX-3 below.

Table IX-3. Takeoff and Landing Performance Analysis

Takeoff and Landing Performance			
Takeoff Performance		Landing Performance	
TOGW (lbs):	39840	Max Landing Weight (lbs):	38247
Field Length Requirement (ft.):	4500	Field Length Requirement (ft.):	4500
Calculated Sea Level Takeoff Field Length with ISA + 18°F day (ft):	2578	Calculated Sea Level Landing Field Length with ISA + 18°F day (ft):	2924
Calculated Takeoff Field Length at 5000' elevation with ISA + 18°F day (ft):	2907	Calculated Landing Field Length at 5000' elevation with ISA + 18°F day (ft.):	3231
Takeoff Speed (kts):	102.7	Approach Speed (kts):	111.3

As can be seen from the table, the Songbird-E exceeds all takeoff and landing performance requirements. In addition to the above values, the stall speed was found to be 85.6 kts. Table IX-4 below shows the Songbird-E's takeoff and landing performance as compared to the ATR 42-600 and its short field takeoff and landing (STOL) variant, the ATR 42-600S. The ATR 42-600 and ATR 42-600S values are taken directly from ATR's website [15, 41].

Table IX-4. Takeoff and Landing Comparison to ATR 42-600 & -600S at Sea Level

	Songbird-E	ATR 42-600	ATR 42-600S
TOGW (lbs):	39840	41005	41005
Takeoff Field Length (ft.):	2578	3632	2625
Landing Field Length (ft.):	2924	3169	2657
Takeoff Speed (kts):	102.7	112	112
Approach Speed (kts)	111.3	121	121

The Songbird-E improves on the takeoff and approach speeds, due to its higher takeoff lift coefficient. By using the provided stall speed from ATR, as well as other information, the ATR 42-600 was found to have a takeoff coefficient of lift of 2.37. Our performance is similar to the STOL variant of the ATR 42-600, which utilizes more powerful engines to increase their thrust to weight ratio, thus decreasing their field length. These relatively-low field lengths,

even those of the ATR 42-600 and -600S, are very important to airlines, especially those operating at home and abroad in more-remote areas. Air Tahiti, for example, purchased ATR 42-600 aircraft, partially because of their ability to operate from airstrips shorter than 1200 m (3937 ft), making the Songbird-E more marketable [42].

F. Range Performance

The Songbird-E is sized to the design mission requirement of 1000 nmi. Table IX-5 shows the design mission performance.

Table IX-5. Songbird-E Design Mission Performance

Segment	Initial Weight (lbs)	Fuel (lbs)		Time (min)		Distance (nmi)		Mach Number		Altitude (ft)	
		Part	Total	Part	Total	Part	Total	Start	End	Start	End
Taxi Out	39840	28	28	10.0	10.0	0	0	0	0	0	0
Takeoff	39812	53	82	1.5	11.5	0	0	0	0.2	0	0
Climb	39759	608	689	21.5	33.0	82.0	82.0	0.2	0.462	0	28000
Cruise	39151	2782	3471	183.8	216.8	842.2	924.2	0.462	0.462	28000	28000
Descent	36369	56	3528	22.9	239.7	75.8	1000	0.462	0.2	28000	0
Taxi In	36285	28	3556	10	249.7	0	1000	0	0	0	0

As the ATR 42-600 has a design range of 726 nmi, there is no comparison to make for the design mission [15]. Addressing the figures of merit for this mission, the Songbird-E expends 3556 lbs of fuel, while producing 13380 lbs of CO_2e, and 35 lbs of NOX.

The Songbird-E still fulfills all requirements set forth in the RFP, cruising at a speed of 275 kts at FL280. This yields a mission time of 4.16 hours. The distance to cruising altitude is shown to be 82.0 nmi, which is well-within the limit of 200 nmi.

G. Payload-Range Diagram

A payload-range diagram of the Songbird-E was also computed. The points were analyzed by FLOPS, which has settings for such analysis built in. The diagram is shown below, in Figure IX-3.
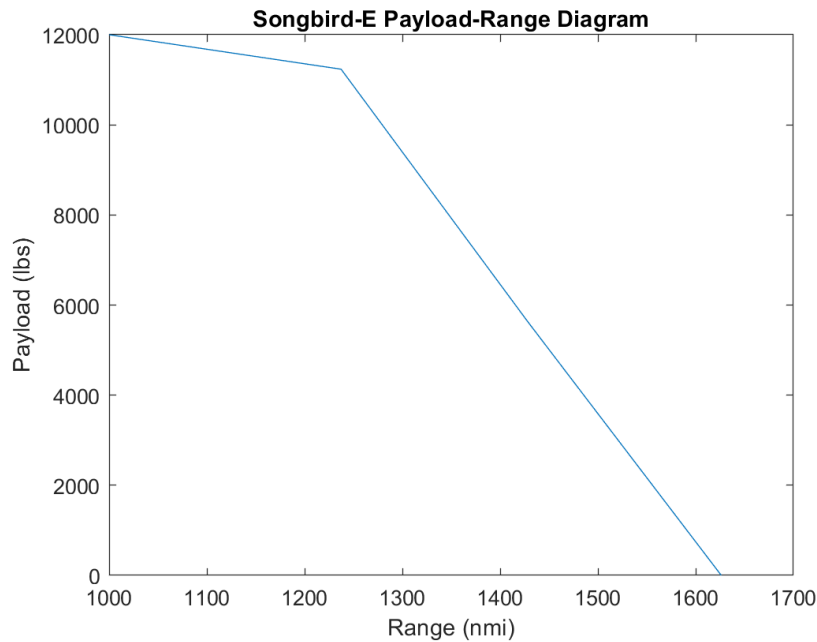
Figure IX-3. Payload-Range Diagram for the Songbird-E

The Songbird-E is sized to the leftmost point, that is, full payload for a 1000 nmi design mission. The design mission carries 4535 lbs of fuel. At the maximum fuel capacity of 5300 lbs, the maximum payload that can be carried is 11235 lbs. This produces a range of 1237 nmi. An intermediate point, with 50% payload, was also computed, but it falls on the second linear section of the graph and provides no new interesting information. With no payload and the maximum fuel capacity of 5300 lbs, the Songbird-E achieves a ferry mission of 1626 nmi.

H. Flight Envelope

Given the RFP requirement, the Songbird-E will cruise at FL280 (28,000 ft). The decision to meet, and not deviate from this requirement, will be further discussed in subsection I. The service and absolute ceilings were calculated using a rerun of FLOPS. Another cruise schedule was defined and flown, with varying higher altitudes, to learn where excess power hit 100 ft/min and 0 ft/min for the service and absolute ceilings, respectively. The service ceiling, beyond which a 100 ft/min rate of climb is no longer possible, is around 30,500 ft. The absolute ceiling, where rate of climb is no longer possible, is about 32,000 ft. This envelope is sufficient to ensure safe operations.

I. Cruise Speed & Altitude Trade Study

To investigate the target requirement of a cruise speed of 350 kts and the increase in cruising altitude from the ATR 42-600, a trade study was done by examining economic block fuel burn and mission time while varying cruise speed and altitude. The goal was to test cruise speeds from 250 kts to 350 kts, in increments of 25 kts, and to

test altitudes from 24,000 ft (FL240) to 30,000 ft (FL300), in increments of 2,000 ft. Upon attempting to complete the study in this configuration, it was found that the model would not close for any altitude below cruise speeds of 260 kts or above 305 kts. Even still, at 29,000 ft, 260 kts would not close, and at 30,000 ft, 260 kts and 305 kts would not close. Thus, the structure of the study changed, to examine cruise speeds from 260 kts to 305 kts, in increments of 15 kts. The altitudes stayed the same, except data was also taken at 29,000 ft. Figure IX-4 below shows the outcomes of the study, which was run in FLOPS.
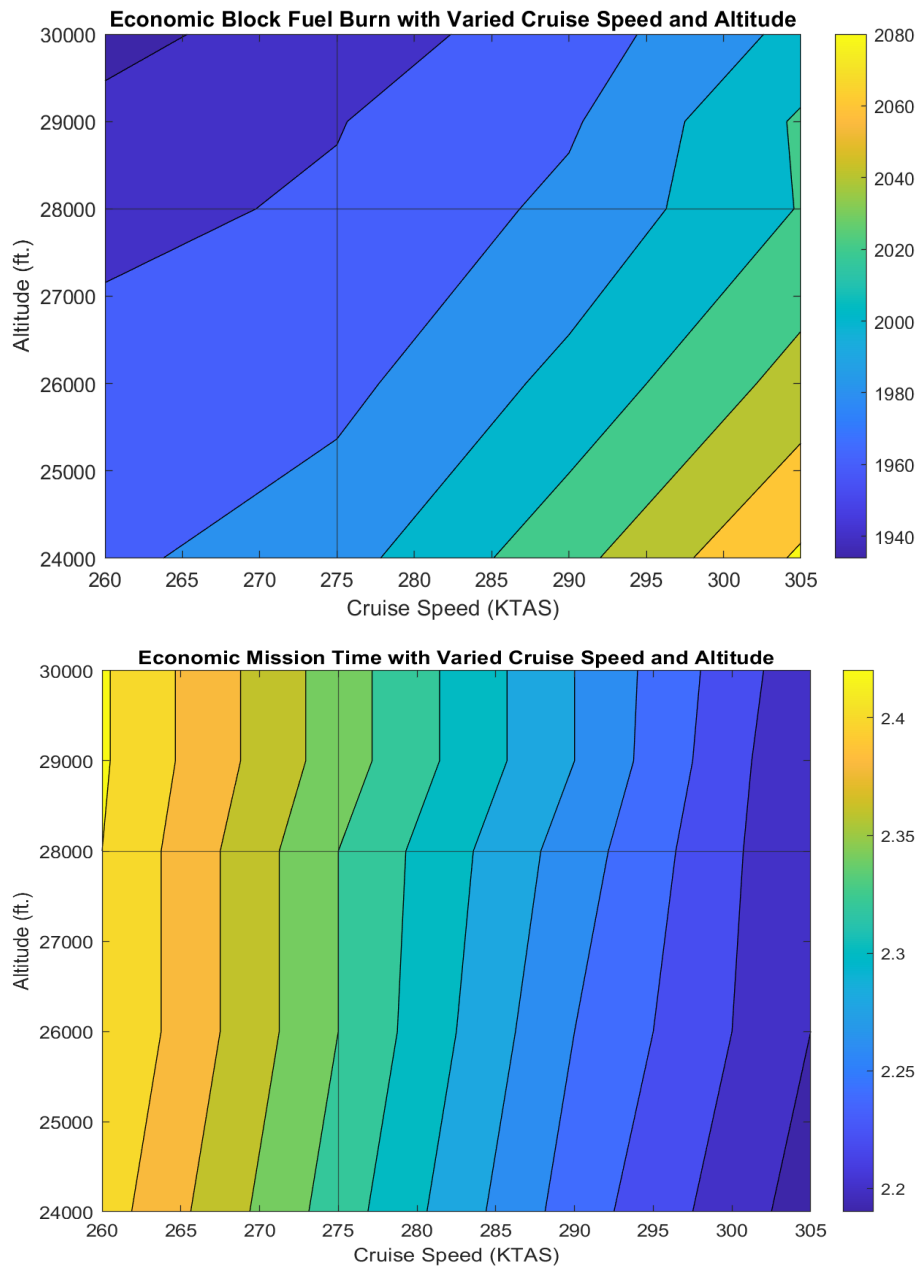
Figure IX-4. Economic Block Fuel Burn (Top) and Time (Bottom) with Varied Cruise Speed and Altitude

The two graphs show the economic block fuel burn and time graphed against the cruise speed and altitude. The minimum speed and altitude constraints are graphed using the black lines, with the intersection being the minimum design point. To fill in the study points that would not close the design, a MATLAB community function called "inpaint_nans" was used to interpolate missing values [43]. The study suggested no significant reason to deviate from the RFP, but it is noted that increasing the cruise speed would create faster missions, allowing airlines to conduct more flights, and increasing cruise altitude would generate greater efficiency, but at the expense of some mission time. There could potentially be an optimal cruise altitude to be found,, but given the issues of closing the design, that area was not studied. Furthermore, given the service and absolute ceilings discussed in subsection G, it would be unrealistic to fly the Songbird-E much higher, given the need for a safety margin, even if it were more efficient.

J. Acoustics

The implementation of an additional propeller near the tip of the wing requires acoustic analysis of the aircraft. This analysis is conducted via FlightStream's unsteady solver, of which the solver mode uses unsteady formulation of surface vorticity and time-dependent wake propagation methods to shed vorticity as a parametric function, of which the requisite temporal pressure fluctuations are generated for the unsteady flow solution [44]. Due to FlightStream's ability to prescribe motions directly onto the boundary surfaces of the geometry, the results generated are true, time-dependent solutions. For aeroacoustic analysis, the Aeroacoustics Toolbox in FlightStream was utilized, of which the unsteady flow equations are assessed under source time-dominant algorithms, with respect to designated observer positions, to obtain changes in ambient Sound Pressure Level (SPL) at defined ranges near the aircraft. Figure IX-5 displays the SPL distribution along the X-Y plane, 5 meters below the aircraft.
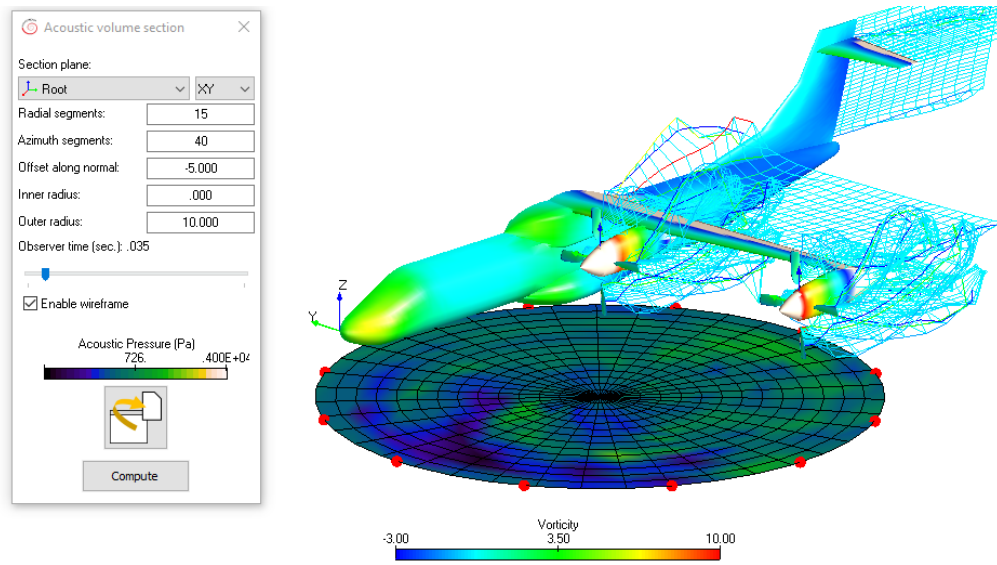
Figure IX-5. Sound Pressure Level Distribution, XY Plane

The average acoustic pressure observed from the aircraft's CG provides a displacement of 726 Pa, and 3980 Pa directly below the propellers. Assessment of the propellers on the Y-Z plane yielded a periodic SPL of 532 kPa, about the flowstream disturbed by the propeller movement, with an initial maximum of 2.2 MPa when the propellers start rotating, characterized by Figure IX-6.
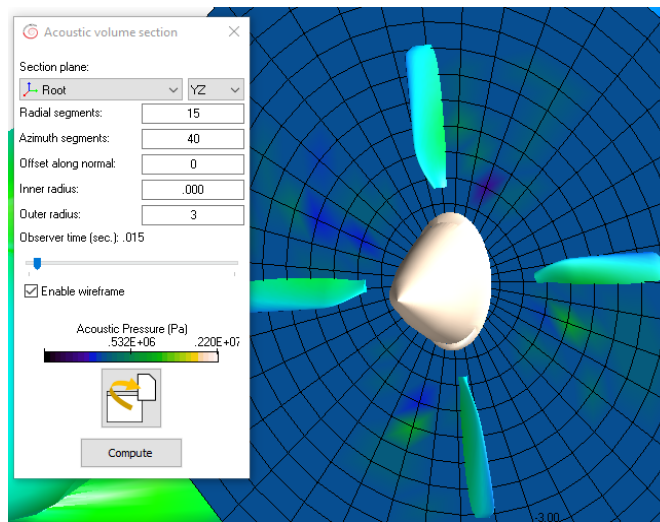
Figure IX-6. Acoustic Assessment of Propellers

Observers located 5 m below the propellers on the X-Y plane observed SPL differentials incurred by propeller rotation resolve into the ambient within 0.25s. Observers located directly on the YZ plane indicated ambient resolution thresholds of 0.3s to 0.4s, depending on their relative position. Complementing propeller analysis was a component acoustic analysis conducted at cruise conditions, the data of which is characterized under Table IX-6. A

component acoustic analysis sweep was conducted under the assumption of small perturbation effects, simulating

minor increments to sideslip and angle-of-attack.

Table IX-6. Sound Pressure Level Proportional Factor, Small Perturbation

Component	SPL Factor		
	AOA	Beta	Cruise
Fairing	0.028	0.023	0.023
Fuselage	0.046	0.039	0.09
Main Wing	0.138	0.135	0.13
Root Nacelle	0.018	0.017	0.023
Tip Nacelle	0.009	0.008	0.02
Vertical Tail	0.092	0.087	0.09
Stabilizer	0.046	0.045	0.03
Antenna	0.009	0.009	0.01
Root Prop	0.399	0.415	0.35
Tip Prop	0.215	0.223	0.23

For small perturbations of angle-of-attack and sideslip divergence of 5 degrees or less, the root propeller

observed an increase in SPL generated by 14-18.5% from the observation position at the aircraft's CG. Disturbances

in flowstream conditions corresponded to a decrease in SPL from the tip propeller, as the acoustic pressure

attenuated before reaching the observer's position. The Songbird-E increased the number of propellers along the

wing and reduced the propeller blades per hub. Accordingly, a comparator acoustic analysis on the ATR 42-600 was

conducted, characterized by Figure IX-7.
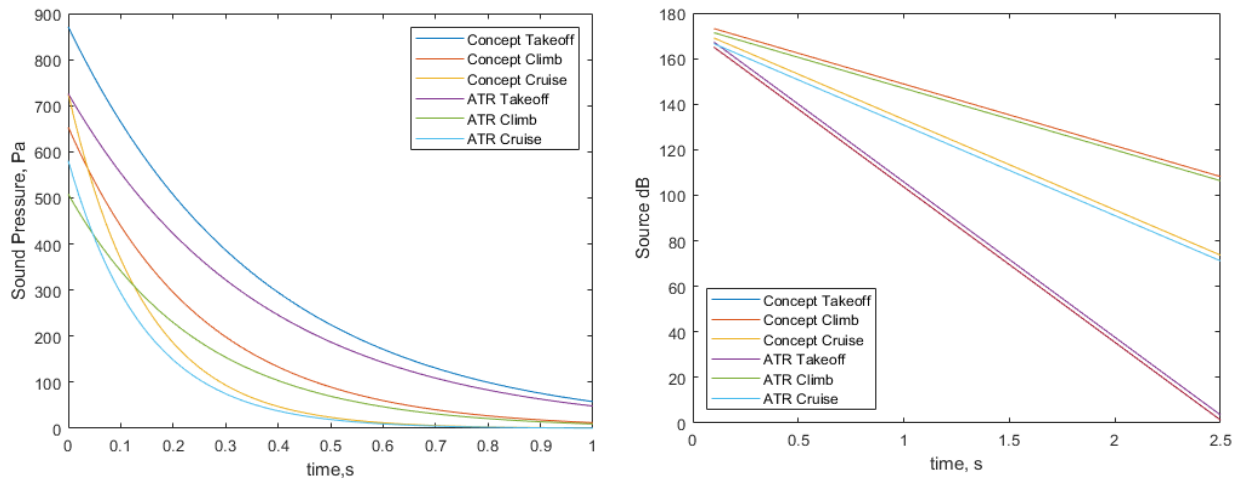
Figure IX-7. Acoustic Comparison, Flight Condition, CG Observer, SPL (Left), Decibels (Right)

Preliminary overviews of the aircraft's components do not indicate any acoustic sources that may exceed 10,000 HZ, including internal turbine engine components or shaft generator subsystems. Thus, Stokes' law of sound attenuation was used to approximate the attenuation of sound pressure generated by the aircraft, applying the assumption of an isotropic and homogeneous medium during all phases of flight. Figure IX-8 displays the change in attenuation coefficient with respect to altitude, and characterizes the SPL differentials between the aircraft in decibels.
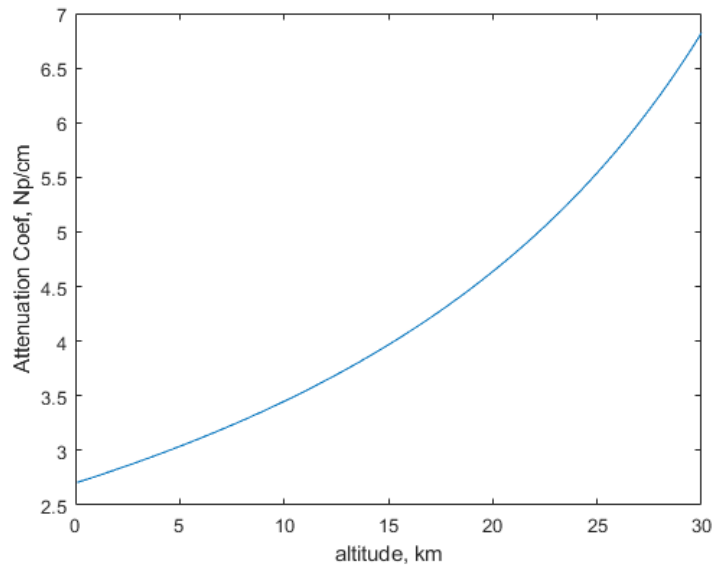
Figure IX-8. Attenuation Coefficient wrt Altitude

The Songbird-E does not adopt major geometric alterations compared to the ATR 42-600, and accordingly, the acoustic comparison is mostly dependent on the changes to the engines and propellers. General flight conditions observed a sound level increase of 1.832 dB for takeoff conditions, 2.51 dB during climb and 2.23 dB during cruise, as compared to the ATR 42-600. Observers located at the aircraft CG observed ambient resolution times of 2.5s for cruise, 3.5s for climb, and 5s for takeoff conditions. At 200 meters from the aircraft, acoustic resolution to ambient conditions was reduced to within 1 second for the X-Y plane. Observers located beyond 300 meters away did not observe any significant SPL differentials. Preliminary acoustics analysis indicates that the Songbird-E does not encounter any acoustics issues as compared to its reference aircraft, to be validated by certification studies.

X. Stability and Control

This section discusses the stability and control of the Songbird-E. This includes both the design of the empennage and the control surfaces.

A. Empennage Design
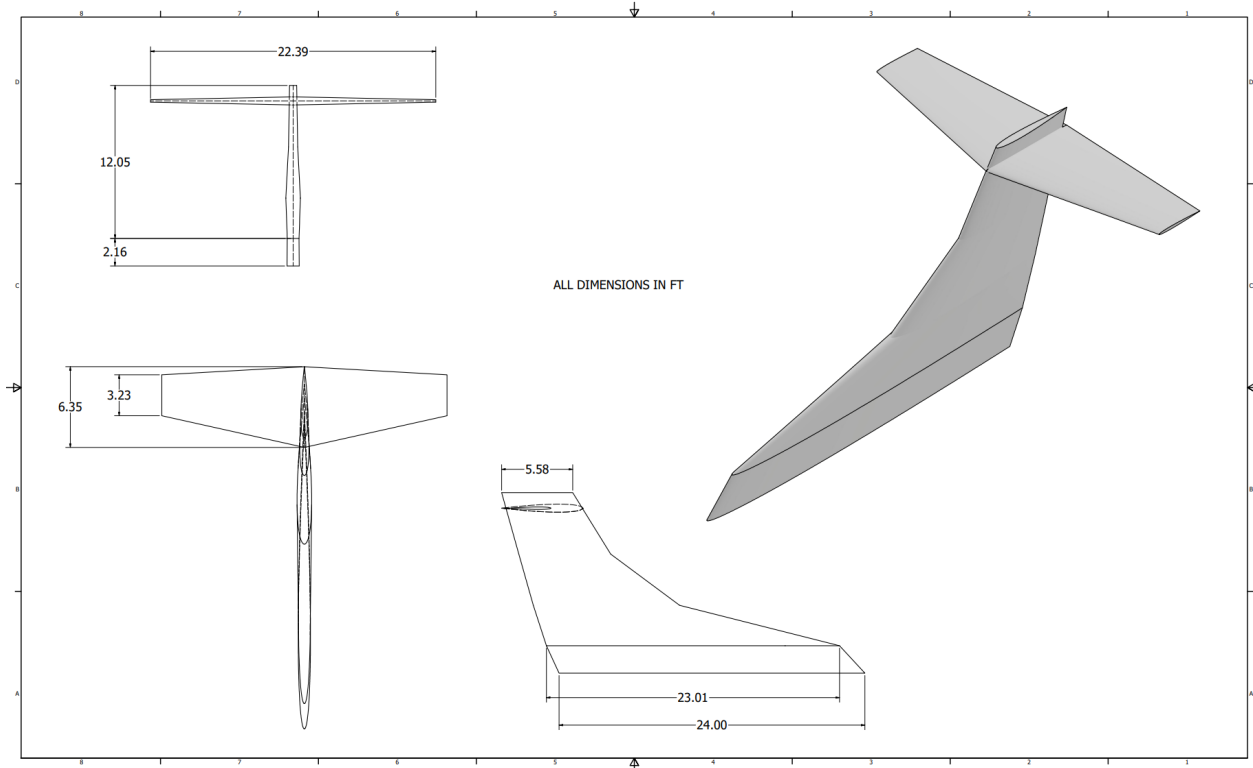
Figure X-1. Empennage Geometry Excluding Control Surfaces

The empennage of an aircraft serves the role of trimming the aircraft and ensuring both longitudinal and lateral-directional stability and control. As is common for regional turboprop aircraft, such as the ATR-42-600 and Dash 8-Q300, the Songbird-E features a T-tail configuration. Benefits of this configuration include a reduction in vertical stabilizer area due to the end plate effect, and the ability to position the horizontal stabilizer further away from the wing wake, increasing the effectiveness of the elevator. Table X-1 summarizes the key characteristics of the empennage.

Table X-1. Parameters of Horizontal and Vertical Stabilizers

Parameter	Horizontal Stabilizer	Vertical Stabilizer
Span (ft)	22.39	14.21
Area (ft^2)	107.2	136.1
Aspect Ratio	4.68	1.48
Taper Ratio	0.51	0.63
Moment Arm (ft)	38.70	20.95
Volume Coefficient	0.961	0.049
Sweep (°)	12.53	53.68
Incidence Angle (°)	0	0
Airfoil	NACA 0008	NACA 0007

B. Horizontal Stabilizer Sizing

The horizontal stabilizer was sized by considering the longitudinal stability of the aircraft. To satisfy

longitudinal stability, the static margin must be positive, where a low static margin indicates high longitudinal

maneuverability. This corresponds to controllability. Thus, the optimal static margin will vary depending on the

aircraft requirements, where a lower static margin is desirable for more maneuverable aircraft, such as fighters, and a

higher static margin is desirable for transport aircraft. Since the Songbird-E is a regional transport aircraft, stability

is favored. Thus the static margin fell within the upper end of the typical range for stable aircraft, which is defined to

be between 5% and 40% [45]. It was also important to verify that the horizontal stabilizer results in an acceptable

trim angle, which is defined according to Napolitano's *Aircraft Dynamics* to be between -1° and +3° [46]. The static

margin and trim angle were calculated using VSPAero to be 0.3 and 1.6° respectively.

C. Vertical Stabilizer Sizing

The vertical stabilizer was primarily sized by ensuring sufficient controllability in the event of engine

failure. During engine failure, yawing moments are generated by the resulting asymmetrical thrust vector and drag

produced by the failed engine. Thus, the vertical tail must be sized such that the rudder can be deflected to counter

these moments. The critical condition for a 4-engined aircraft is failure of both engines on the same side. Thus

failure of both the gas turbine engine and the electric motor were considered in this analysis. By calculating the

minimum control speed of 1.2 times the stall speed, and assuming a maximum rudder deflection of 25°, a process

detailed in Roskam's *Airplane Design: Part II* was utilized to iteratively size the vertical stabilizer [47].

D. Control Surfaces

The Songbird-E employs ailerons, a rudder, and an elevator in order to ensure sufficient control authority

about the lateral-directional and longitudinal axes. The parameters for each control surface are given in Table X-2.

Table X-2: Aileron, Rudder, and Elevator Parameters

Aileron	Chord Ratio	0.25
	Span Ratio	0.19
	Total Area	22.4 ft^2
	Max Deflection	+/- 20°
Rudder	Chord Ratio	0.25
	Span Ratio	0.84
	Total Area	38.7 ft^2
	Chord Ratio	+/- 25°
Elevator	Span Ratio	0.25
	Total Area	0.81
	Max Deflection	21.1 ft^2
	Chord Ratio	+/- 25°

E. Stability and Control Characteristics

To ensure the stability and controllability of the design, three conditions must be met: sufficient static

margin, acceptable cruise trim angle, and overall design static stability. These parameters were calculated using the

embedded VSPAero solver within OpenVSP. VSPAero is a vortex lattice solver. It simulates the lifting surfaces of

the OpenVSP model as infinitely flat plates, and applies discrete vortices to the surfaces. It then sums over the entire

model to calculate aerodynamic data, such as lift and drag. However, as it is a vortex lattice solver, it cannot

simulate viscous drag or stall characteristics. VSPAero proved useful, as it is much faster than FlightStream.

Based on the PEGASUS design, the acceptable static margin range should fall within 0.23 and 0.38 [48].

This ensures that the design is stable, but not so stable that it is difficult to control. VSPAero simulated the aircraft in

cruise conditions, and calculated the neutral point of the aircraft. Based on the neutral point, center of gravity, and the mean aerodynamic chord, the static margin was computed to be 0.3, well-within the required envelope.

To reach an acceptable trim angle, some design changes were made. An acceptable trim angle should be between -1° and +3° [46]. In the initial design, the cruise trim angle of the aircraft was found to be -2°. To combat this, the incidence angle of the horizontal tail was introduced, at -2.25°. However, upon reaching a final design, the trim angle was found to be 5°, outside of the acceptable range. The incidence angle of the horizontal tail was then set to 0°, to achieve an acceptable trim angle of 1.6° (Figure X-2).

Static Margin	0.3
Longitudinal Stability Derivative (wrt α per rad)	-1.96
Trim Angle (deg)	1.6
Lateral Stability Derivative (wrt β per rad)	-0.204
Directional Stability Derivative (wrt β per rad)	0.040
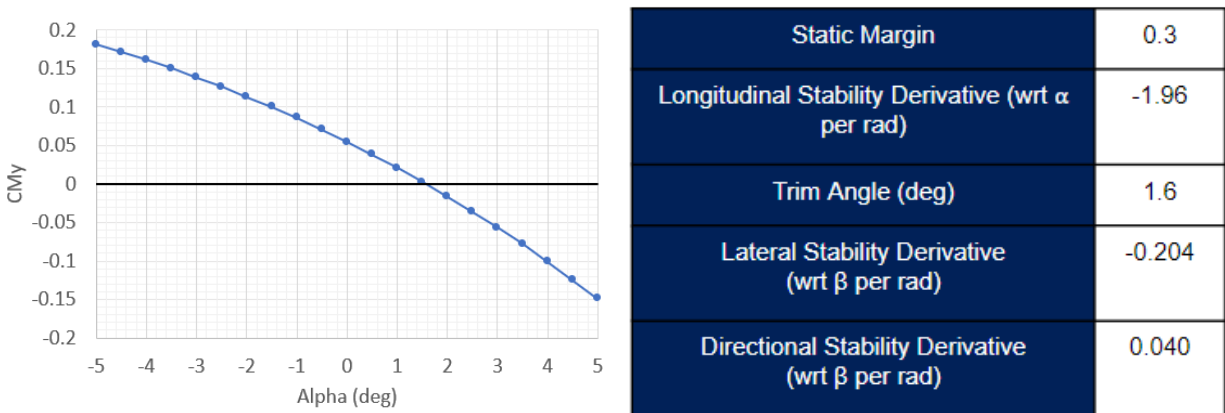
Figure X-2. Graph of Moment Coefficient vs Angle of Attack and Stability Evaluation

Finally, the design had to meet the criteria for static stability. There are three conditions to achieve static stability: a negative longitudinal stability derivative, a negative lateral stability derivative, and a positive directional stability derivative. Using VSPAero, these stability derivatives were calculated, as shown in Figure X-2. The calculated stability derivatives meet the criteria for static stability; therefore, the design is stable in flight. Again, it is important to note the shortcomings of using VSPAero's low-fidelity modeling, especially in regards to the calculation of stability derivatives. However, the directions of the stability derivatives will be correct, and since the design meets the necessary stability derivative directions, it can be considered statically stable. As the three conditions are met, our design is ensured to be both stable and controllable in flight.

XI. Structures and Loads

This section will examine the structural loading of our aircraft. The V-N diagram is given in this section to show the flight limits of our aircraft. A wing loading and structural analysis is also conducted by utilizing finite element analysis (FEA). This section also includes a materials and landing gear discussion.

A. V-N Diagram

The V-N diagram represents the maximum loads the aircraft can sustain in different flight conditions, following FAR Part 25 guidelines, with a load factor ranging from -1 to +2.5. The V-N diagram's maneuvering and gust envelope were both constructed with aircraft weight at the end of economic cruise at FL280 with flaps retracted. The end of the economic cruise mission was chosen because it is the lowest weight experienced prior to descent, resulting in the most constraining scenario for the gust loads. Methods in Roskam's *Aircraft Design: Part V* were used for the calculation [10]. At FL280, the maneuvering envelope is as follows: stall speed with full flaps is 129 knots, design maneuvering speed is 204 knots, cruise speed is 275 knots, and the maximum dive speed is 344 knots. Maximum gust load factor at cruising speed for FL280 is ± 0.63, and the gust load factor at maximum dive speed is ± 0.50. This places the gust load envelope firmly inside of the maneuvering envelope, meaning as long as the aircraft operates within +2.5 to -1 load factor, as specified by the FAR 25 regulations, the gust loads are null factors under normal flight conditions. The V-N diagram for the Songbird-E can be found in Figure XI-1.
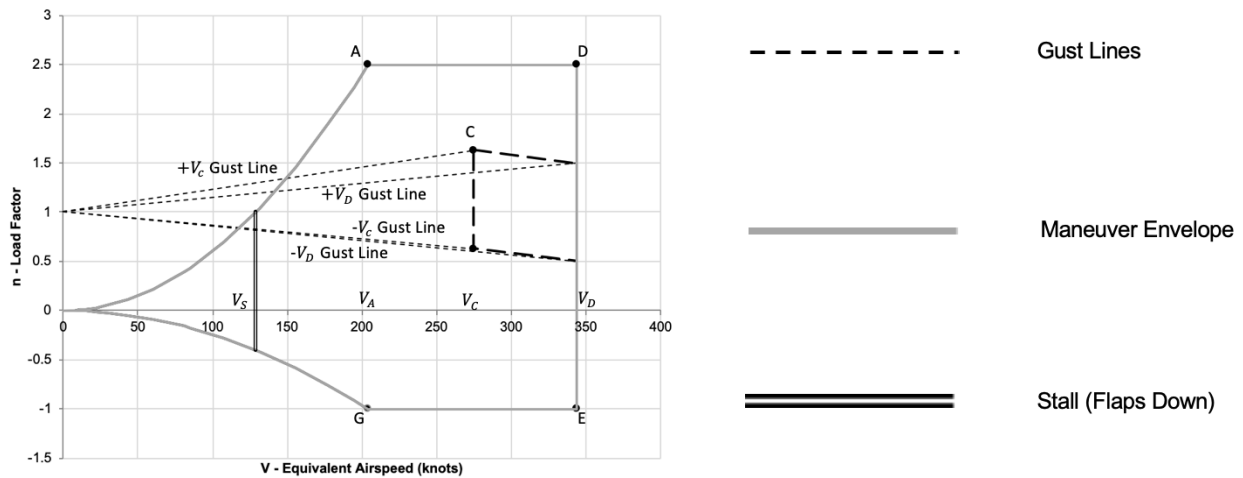
Figure XI-1. V-N Diagram

B. Wing Loading and Structural Analysis

Preliminary FEA analysis of the wing structure assumed a triple-spar configuration, depicted below in Figure XI-2. The initial design considers the fuel tank to be integrated as an auxiliary support structure in stress analysis.
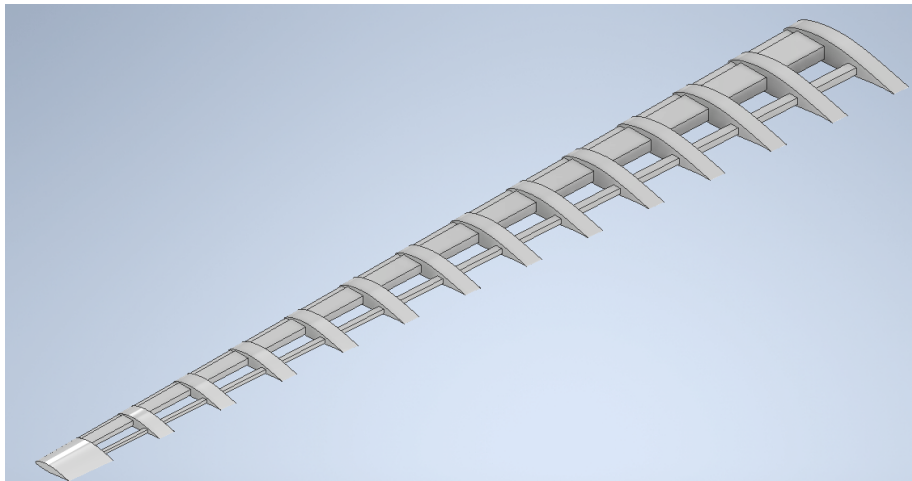
Figure XI-2. Theorized Wing Structure

The fuel tank, primary, and secondary spars were lofted with base dimensions characterized as follows: 300 mm x 500 mm fuel tank, 220 mm x 90 mm primary spar, and 150 x 115 mm for the rear spar. There are also 14 ribs. A uniform thickness of 10 mm was assigned for the fuel tank to avoid stress concentrations near the wingtip, as a preventative means against rupture. Baffles were also utilized to minimize sloshing of the fuel during maneuvering. Elliptical loads were applied across the length of the wing to match the maximum possible lift force experienced by the wing at takeoff of 600 kN, and engines were regarded as point loads. Figures XI-3 and XI-4 characterize the von-Mises stress and vertical displacement across the structure.
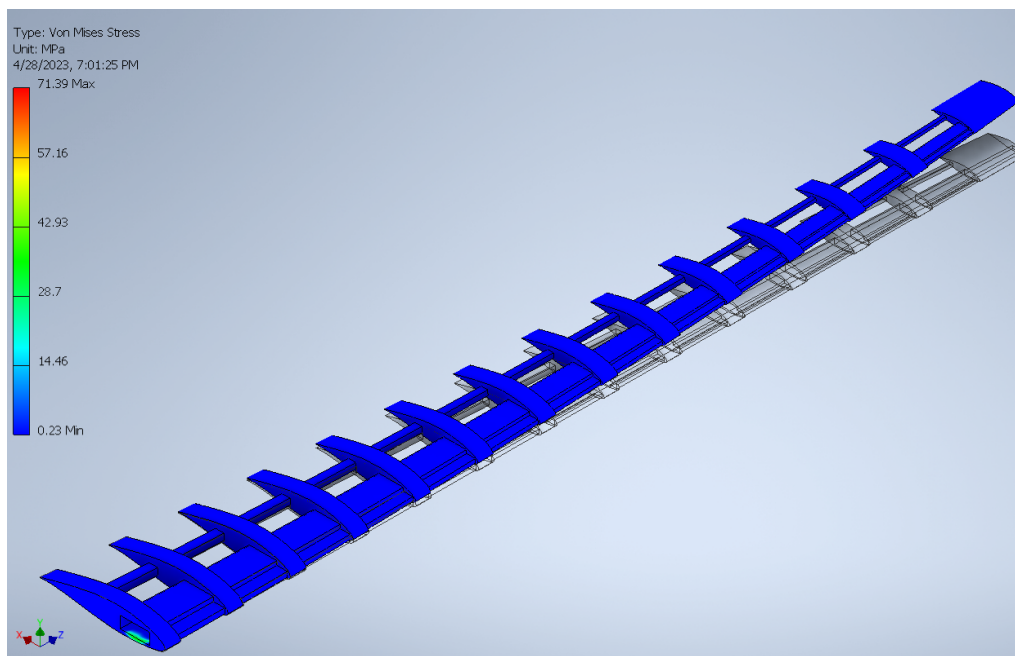
Figure XI-3. Von Mises Stress Distribution Across Theorized Wing Structure
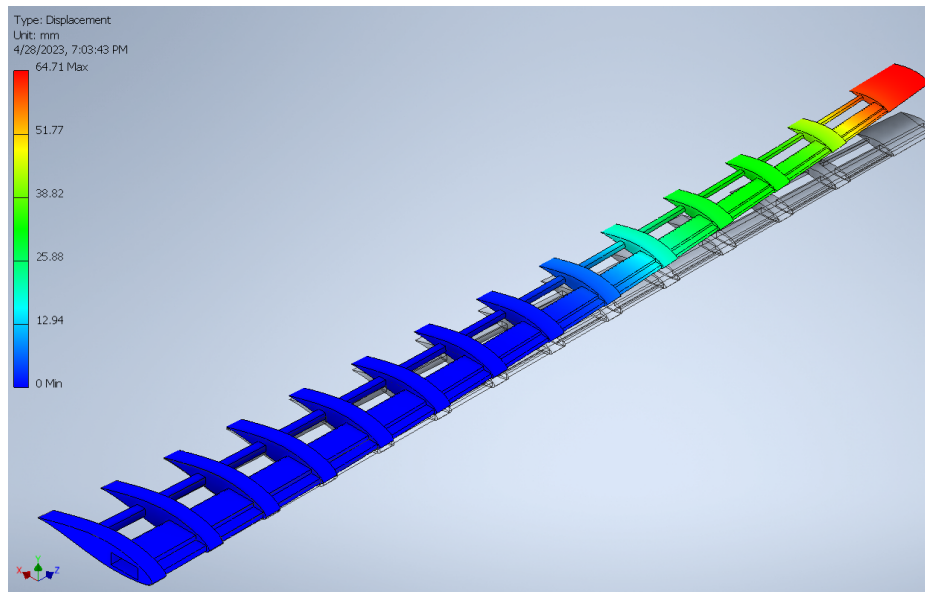
Figure XI-4. Y-Displacement of Theorized Wing Structure

Stress concentrations were observed at the root of the wing structure, and the vertical position of the fuel tank was not balanced with respect to the applied loads. As such, future iterations of FEA analysis need to consider raising the vertical position of the fuel tank. For the iterated design, preliminary modal analysis was conducted to observe the frequency modes corresponding to the applied stresses. Figure XI-5 and XI-6 characterize the common stress-response modes observed in the FEA model.
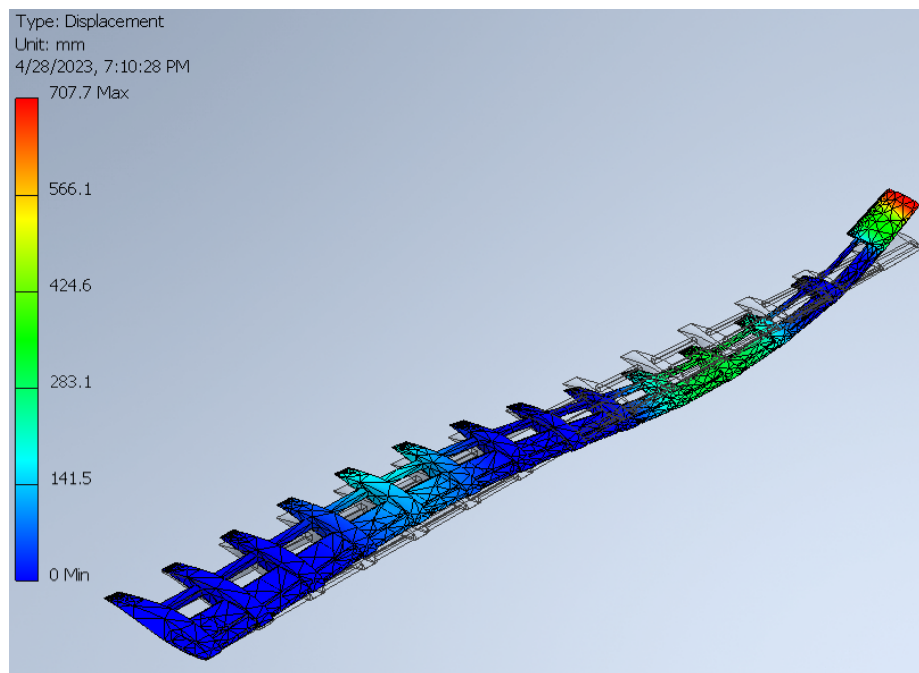
Figure XI-5. Vertical Buckling Mode of Theorized Wing Structure
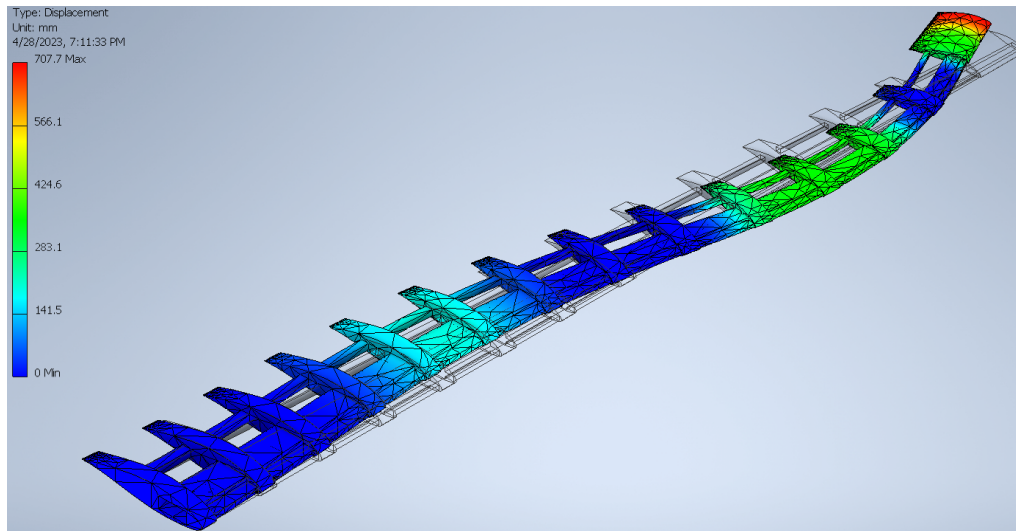
Figure XI-6. Horizontal Buckling of Theorized Wing Structure

Preliminary modal analyses were conducted under an applied frequency range of 1-100 Hz, of which 15 modal responses were collected. Under the modal response, vertical displacement increased to a maximum of 707.7 mm, and horizontal displacement was considered at a maximum of 7.325 mm. Table XI-1 characterizes the qualitative assessments of the frequency modes observed.

Table XI-1. Frequency Modes Observed, Qualitative

Modal Response Type	Initial Frequency Mode	Corresponding Initial Hz
Vertical Displacement	1	1.02
Horizontal Displacement	3	6.51
Vertical Buckling	4	10.26
Horizontal Buckling	6	22.11
Twisting	7	27.91
Twisting + Buckling	8	30
Tip elongation	13	73.74
Structure elongation	15	90.04

The material assumed for the FEA study was 6061 Aluminum with a defined yield strength of 240 MPa. From a safety factor analysis, and the above von-Mises stress distributions, it is evident that the structure material far exceeds the pure strength requirements as the distributed load corresponding to the maximum lift force resulted in a minimum safety factor of 3.85. With solid primary and rear spars, the total weight estimation was 957 kg, with

reductions available for our composite-configured wing. The aluminum weight matched the estimated aluminum wing weight, which was found using a FLOPS correction factor and verified using the Torenbeek method, as described previously. The structural loading does not appear to be a limiting factor. An aeroelastic flutter analysis could potentially allow us to reduce the wing structure and weight. Active flutter control systems could potentially be integrated to counteract the potentially-destructive results of a lower wing weight, and allow us to reduce more wing structural weight. An important consideration for future FEA analysis is the modal response beyond frequencies of 20 Hz. The introduction of mixed modal responses of twisting and buckling can prove catastrophic to the structural lifespan and performance, in the case of turbulence or moderate to large-scale perturbation. Future FEA analysis will require the incorporation of damping substructures and materials as preventive means for such modal responses.

C. Materials

The ATR 42-600 takes heavy advantage of composites. A broad assumption was made that all composites provided a 30% reduction in weight as compared to aluminum, when tuning the ATR 42-600 model. A breakdown of the ATR 42-600's use of composites can be seen below in Figure XI-7 [49]. Estimates made in FLOPS came from research and eyeballing and tuning the ATR 42-600 model. Though eyeballing is extremely imprecise, the simple approximation is verified by the given weights breakdowns.
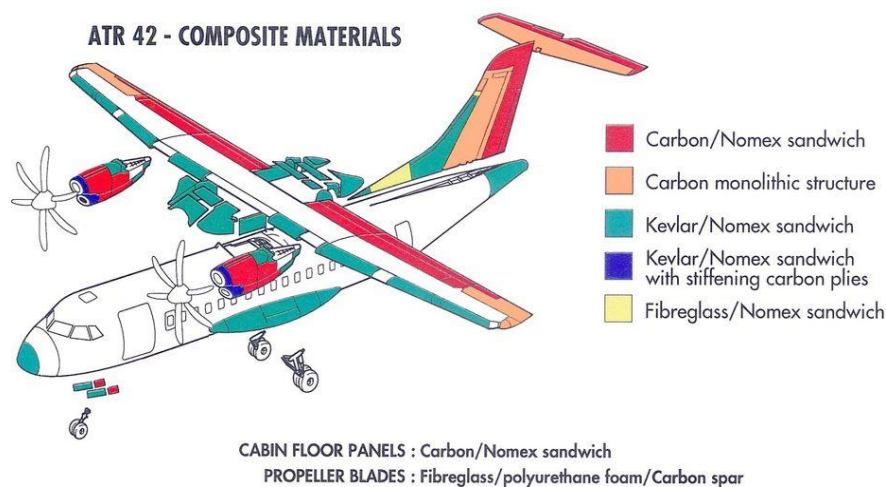
Figure XI-7. ATR 42-600 Use of Composite Materials

The Songbird-E makes full use of the PRSEUS composite in its airframe. PRSEUS, or the Pultruded Rod Stitched Efficient Unitized Structure, is a NASA-Boeing partnership for a composite material that provides both in-plane directions [39]. This means that PRSEUS can support both flight loads and internal pressure loads. It is

manufactured using a stitched, resin-infused process. PRSEUS' use was found promising, as it was successfully tested to the FAA's required pressure and bending loadings in 2015. This paper, written by Craig Nickol and William Haller of NASA Langley and NASA Glenn, respectively, outlines reductions in wing, empennage, and fuselage weights, as compared to full use of traditional composites. For the wing, this was accounted for in FLOPS by using the full composites factor for the wing, and then applying the specified weight reductions to the wing weight terms. The listed weight reduction factors were also applied directly to the horizontal and vertical stabilizers, as they already utilized full composites. Though the fuselage was not already made entirely of composites, in order to gain a more conservative estimate, the listed 5% reduction was applied as-is. The PRSEUS composite resulted in a 9.1% reduction to the airframe weight, by means of 16.8% reduction to the wing weight, 21.5% reduction to the empennage weight, and 5% reduction of the fuselage. The PRSEUS composite could potentially be applied to other areas of the structure, such as parts of the landing gear and the engine nacelles, for further weight reduction. Though the FEA analysis was conducted using aluminum, the composite was shown to handle aircraft-certification-grade stresses, ensuring little performance difference between the aluminum and the PRSEUS composite.

D. Landing Gear

The Songbird-E utilizes a tricycle type landing gear, consisting of a main gear and a nose gear, same as the ATR 42-600. This landing gear configuration was chosen due to its advantages over other configurations such as a tandem landing gear and a tailwheel type landing gear. It enables higher landing speeds because the brakes can be used more forcefully without the risk of nosing over. In addition, the visibility from the flight deck during landing and ground maneuvering is better, and ground-looping is prevented because the center of gravity of the aircraft is forward of the main gear [50]. The landing gear configuration is depicted in Figure XI-8. The main gear has a length of 3.61 ft, and the nose gear has a length of 5.16 ft. The landing gear is estimated to weigh 1782 lbs.

Figure XI-8. Landing Gear Configuration

XII. Systems

This section examines the use of subsystems in the aircraft. In addition to discussing the calibration and generation of the individual subsystem weights, this section will discuss all of the subsystems included on our aircraft, and ways that conventional subsystems can be replaced with state-of-the-art systems deployable by 2035. This section also includes a discussion on autonomous flight systems.

A. Overall Layout

As mentioned in the weights section, the subsystem weights were calibrated to the operating empty weight of the ATR 42-600 using FLOPS' weight multipliers. In addition to calibration to the operating empty weight, the subsystem weights were also verified using methods in Roskam's *Aircraft Design: Part V*, and Nicolai & Carichner's *Fundamentals of Aircraft Design, Volume I* [10, 11]. This calibration was then carried forward to the Songbird-E. On top of the many state-of-the-art systems that the ATR 42-600 uses, the Songbird-E utilizes more futuristic subsystems in order to decrease weight and increase maintainability, efficiency, and reliability. The individual weights of the subsystems are shown in Table XII-1 below. The fuel system weights and engine controls will be discussed separately. All subsystems were placed in the CG analysis, and are placed conventionally, as the aircraft utilizes a standard configuration.

Table XII-1. Subsystem Weights Breakdown

Subsystem	Weight (lbs)
Surface Controls	416
Instruments	179
Hydraulics	329
Electrical	1061
Avionics	817
Furnishings and Equipment	2922
Air Conditioning	414
Anti-Icing	94
Total:	6232

B. Surface Controls

The Songbird-E employs a fly-by-light (FBL) surface control system. The Songbird-E utilizes leading and trailing edge flaps, ailerons, elevators, and a rudder. This system replaces the traditional mechanical controls used on the ATR 42-600. Fly-by-Light, different from fly-by-wire, utilizes fiber optic wiring to send signals to the surface controls system. Use of FBL also helps further electrify the aircraft, helping pave the way for autonomous systems to be added in the future. Not only does it help modernize our aircraft, it also helps us save weight. According to researchers from McDonnell Douglas Aerospace, fly-by-light provides a weight savings of 2,000 lbs for a "commercial widebody" aircraft [52]. The Boeing 747 and 777 were utilized. An average of their TOGWs were taken, and then 1.22% of that was taken to be surface controls weight, as directed by FLOPS analysis. This led to the finding that FBL reduces the FLOPS surface controls weight by 20.5%.

C. Auxiliary Power Unit (APU)

Just as the ATR 42-600 does not include an APU, the Songbird-E also does not. The Songbird-E will mirror the ATR 42-600, and operate the starboard engine in "hotel mode" [36]. Figure XII-1 shows a generic engine of a similar type, to aid in the explanation.
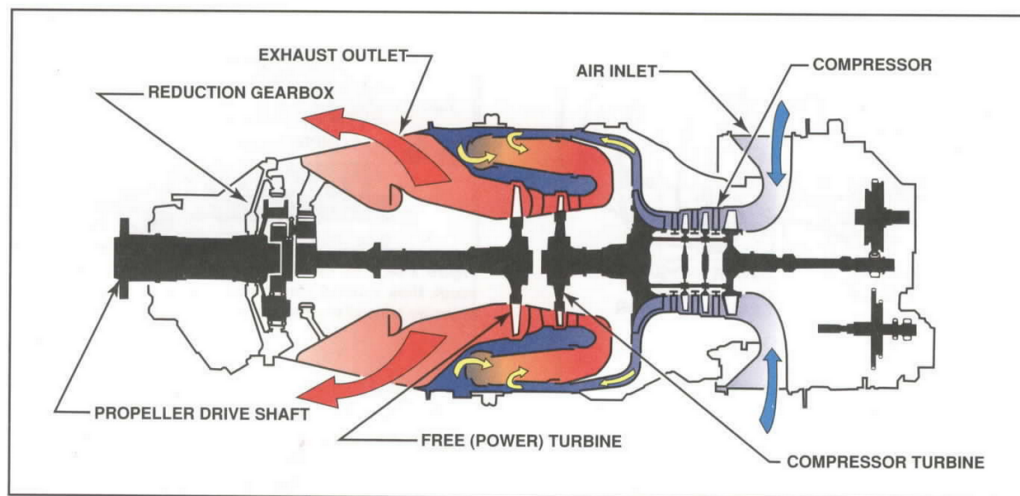
Figure XII-1. Diagram of a Free Turbine Engine [53]

In this type of engine, the propeller, which is driven by the free turbine, rotates independently of the compressor turbine. The starboard propeller is locked with a propeller brake, which allows the turbine to run, providing electrical power without turning the propeller. While it is louder and less efficient, it can save as much as 300 lbs of weight. As the ATR 42-600 already includes the infrastructure in the PW127XT engine weight, our engine, based off

of it, is also assumed to include any necessary infrastructure. Therefore, no APU is included in the FLOPS model, and no additional weight is estimated.

D. Instruments

The Songbird-E utilizes the same cockpit setup as the ATR 42-600. One of the main upgrades from the ATR 42-500 was the modernization of the cockpit, featuring a glass cockpit with 5 LCD screens [54]. The ATR 42-600 also utilizes an advanced flight management system, which helps pilots navigate and operate the aircraft. It also provides efficiency data and recommendations [55]. Also featured is an eye-level head-up display (HUD), which provides important flight information. The instrumentation weight was calibrated to the ATR 42-600 in FLOPS, and the same calibration was implemented in the Songbird-E model. Therefore, all instrumentation is included in the corresponding subsystem weight.

E. Hydraulics

The Songbird-E will utilize a power-by-wire (PBW) system for hydraulics. Power-by-wire utilizes localized hydraulics and actuators that are connected by wiring and electrical power, rather than using a whole-aircraft hydraulic system. Power-by-wire is often paired with fly-by-light systems. There are many benefits outlined for power-by-wire. They include weight savings, improved engine efficiency from elimination of hydraulic bleed air, and simplified and more environmentally-friendly maintenance [52]. In the absence of good quantitative information on weight and efficiency benefits, no weight reductions or performance benefits were accounted for in the current design of the Songbird-E. The FLOPS hydraulics weight estimate was left as-is, even though power-by-wire would likely provide a reduction over the conventional hydraulics system.

F. Electrical

As mentioned in the section on the APU, the Songbird-E will utilize a generator on the turbines to generate AC electricity. This will then be converted to DC through a rectifier in order to power all necessary DC voltage within the aircraft. In addition to the conventionally-powered systems, the new power-by-wire system will utilize power in a different way. The electrical system weight is based off of the calibrated multiplier from the ATR 42-600.

G. Avionics

The avionics for the ATR 42-600 are provided by Thales [54]. Thales' avionics provide both required navigation performance (RNP) and CAT III approach. The aircraft features an automatic dependent surveillance broadcast (ADS-B) system, which provides air traffic data in realtime [55]. The Terrain Awareness and Warning

System (TAWS) alerts the pilots if they are heading towards dangerous terrain. A weather radar also provides pilots with real time weather information to help the pilots with route planning. The aircraft also has a camera-based system, called the enhanced vision system (EVS), which helps the pilots in low-visibility conditions. Overall, the recent renewal of the ATR 42-600 cockpit makes it perfect for continued use in the Songbird-E. These systems also ensure the Songbird-E's ability to meet the RFP requirement of VFR and IFR flight with an autopilot. As the Songbird-E makes use of the ATR 42-600 systems, the calibration for the ATR 42-600's avionics weight holds up.

H. Furnishings & Equipment

Furnishings and equipment is an especially broad area and encompasses many different weights. Included in this is all cabin furnishings, including bulkheads, overhead bins, seats, galley, lavatory, passenger comfort systems (reading lights, etc.), paneling, and environmental systems, among others. In order to reduce weight, a couple future technologies are leveraged.

The first is lightweight aircraft seats. Recaro and Expliseat have both developed seats that utilize netting instead of traditional foams and titanium structures to reduce weight [56, 57]. Though the seats can be more difficult to repair, they are also smaller and more durable, which allows them to be used longer, and to give greater comfort to passengers. Both companies' seats are 40% lighter than traditional seats, reducing their individual seat weight from 15 kg to 9 kg. This leads to a 300 kg (661 lbs) weight reduction, or a 17.3% reduction in furnishings and equipment weight.

Lightweight interior plastics are also utilized on the Songbird-E. Back in 2014, Sabic unveiled polycarbonate aircraft paneling, which is 38.5% lighter than PVC/PMMA, which are traditionally used in aircraft interiors [58]. Plastics are used in many different aspects of the aircraft interior, including floor and ceiling panels, cargo liners, overhead bins, panels, window surrounds, lavatory modules, galleys, food and drink carts, and bulkheads [59]. It is estimated that the Boeing 777 uses more than 11,000 lbs of plastics. Using a TOGW of 766,000 lbs, it is estimated that plastics weigh 1.4% of that aircraft [60]. The same percentage was applied to the Songbird-E, estimating that its plastics weigh 589 lbs. A 38.5% reduction in plastic weight yields a weight savings of about 350 lbs, resulting in a 7.5% decrease in furnishings and equipment weight.

Traditional environmental control systems are utilized on our aircraft and included in the furnishings and equipment weights. This includes oxygen control, life support systems, and ventilation and pressurization systems, among others. As a note, pressurization is accounted for in the fuselage weight.

I. Air-Conditioning

The ATR 42-600 utilizes new, quieter air-conditioning systems. Their state-of-the-art system has 35% more cooling capacity than the previous systems utilized on the ATR 42-300 [42]. The Songbird-E will utilize the same system, as it is quieter and increases passenger comfort. The calibrated ATR 42-600 weight is sufficient for calculating the Songbird-E air-conditioning weight.

J. Anti-Icing

Since turboprops typically have less auxiliary power than jets, and our aircraft utilizes a propeller brake system, permanent thermal protection is not practical [61]. Instead, our aircraft will utilize two anti-icing systems simultaneously. This includes a pneumatic de-icing system on critical exposed portions of the aircraft, and electrical anti-icing protection on parts where pneumatic de-icing is not available. This system is the same structure as the ATR 42-600 and is accounted for in FLOPS' calibrated weight estimation.

K. Engine Controls

The Songbird-E will utilize Full-Authority Digital Engine Control (FADEC) [62]. FADEC is a computerized engine control system that digitally controls all aspects of engine performance, including starting. As mentioned in the propulsion section, where the engine and starting system weights are listed, the weights were calculated using Roskam *Aircraft Design: Part V* [10]. From these formulas, a 50% weight knockdown was taken. This was determined due to weight calibration of the ATR 42-600, an adjustment of the formulas, since the empirical methods are calibrated to 1980s aircraft, and from our use of FADEC. On top of the weight reduction, FADEC optimizes the engines for performance during flight, and reduces the pilot's workload. No efficiency benefit was claimed at this time, though ensuring optimal operation of the engines would provide one.

L. Fuel Systems

There are two fuel tanks, both of which are embedded in the wings. This is common practice in aircraft design and results in little movement of the CG throughout the flight as fuel depletes. The tanks also add extra structure to the wing. The aircraft's fuel tanks were roughly sized to the design mission, with a capacity of 5300 lbs of fuel. This leaves an excess fuel capacity of about 750 lbs, but it was determined that reducing the size of the fuel tanks had little effect on the fuel system weights and so they were left as-is. The larger tanks allow the Songbird-E to provide a longer ferry mission, with little weight penalty. The designed fuel tank accomplished this requirement by having a total volume of 105.8 ft^3. The fuel tank can be seen in Figure XII-2 below.
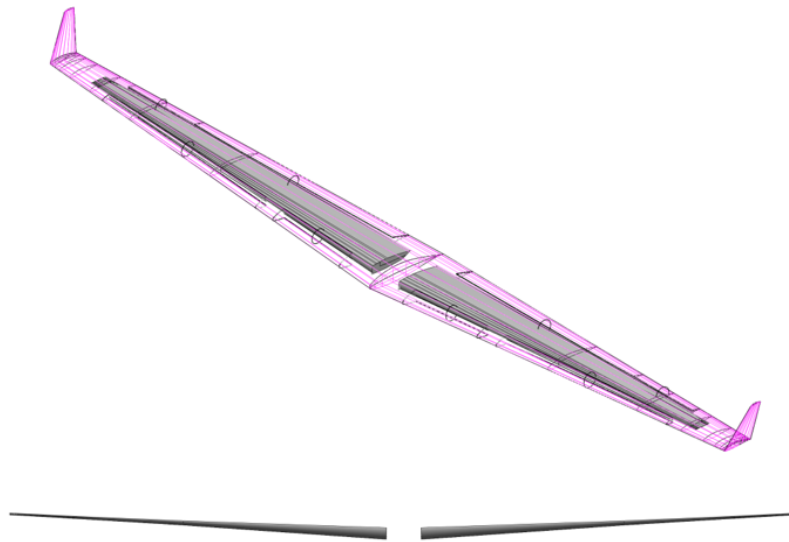
Figure XII-2. Geometric Design of the Fuel Tanks

From FLOPS' weight estimation, the entirety of the fuel system, tanks, and plumbing weighs 160 lbs. This includes all necessary systems. FLOPS also accounts for 225 lbs of unusable fuel and 65 lbs of engine oil. Unusable fuel is often simply fuel that is trapped within the aircraft's fuel systems and lines.

M. Autonomous Flight Capabilities

Due to rising demand for flights and a thus-far inadequate pilot training pipeline, a shortage of qualified pilots is becoming a major concern for airlines. Regional airlines in particular are acutely exposed to this risk. The economic shocks of COVID-19 only further exacerbated this issue [63]. To address this, one solution could be to include autonomous flight systems that could allow the aircraft to be flown by a single pilot, or no pilots at all. Such a system could dramatically reduce the demand for pilots, circumventing constraints imposed by a pilot shortage.

In order for an autonomous flight system to be implemented, it must be able to reliably carry out the tasks that a pilot would normally perform. This includes avoiding aircraft and other obstacles, staying within the operating limits of the aircraft, and navigating to follow a prescribed flight path. Current autopilots already have the capability to do so, or significantly assist pilots in completing these tasks. Therefore, implementing current state of the art autopilot systems will go a long way towards a fully autonomous aircraft. The biggest challenge will be developing systems that can deal with irregular and emergency operations safely and reliably [64]. The primary changes that must be made to the aircraft's design would primarily be software and the addition of the computers necessary to run it, as well as additional redundancy to any systems that provide inputs to the autonomous flight system.

Despite the potential benefits of such a system, the Songbird-E is not designed to enter service as an autonomous aircraft. Given the cost of developing, testing, and getting regulatory approval for such a capability, there is concern regarding whether or not it could be ready for an EIS of 2035. It is believed that the significant research and development costs and potential delays outweigh the potential benefits of focusing efforts on autonomous systems. In addition, customers and passengers would likely be wary of a novel system in control of the aircraft. Therefore, it was decided that advanced, commercially available autopilot systems would be implemented, in conjunction with state-of-the-art subsystems. Together, these systems have many of the capabilities necessary to enable an aircraft to operate autonomously. This allows the aircraft to be retrofitted with an autonomous flight system later in the development stage or after it enters service.

XIII. Repair and Maintenance

An important consideration for airlines is the ease with which the aircraft can be maintained and repaired. This is vital as it is a key determinant of the affordability and reliability of operating the aircraft.

A. Maintenance

In the United States, aircraft maintenance is regulated through various parts of the Code of Federal Regulations. Part 25 Appendix H requires the creation of a maintenance manual as well as a schedule for required maintenance. This includes relatively frequent A checks that must occur multiple times per year as well as more detailed and labor intensive B, C, and D checks. The exact scheduling necessary to ensure continued airworthiness will have to be determined later in the aircraft's development. Maximizing the time in between maintenance intervals is a design goal, as it will help airlines maximize aircraft utilization, and ultimately profitability. This can be achieved by using well-tested parts and manufacturing techniques when possible.

As a point to show reliability, the PW127XT series engines have an overhaul time of 20,000 hours, according to Pratt & Whitney [65]. Accordingly, improvements in reliability and maintainability are expected to be made as technology progresses between now and 2035. As the PW127XT series engines already have high overhaul times, the same or greater should be expected of the turboelectric engines on the Songbird-E.

Compared to existing aircraft in its class, the largest difference that will affect maintainability is the inclusion of the hybrid-electric system. This adds complexity, and therefore more systems that could fail. Because of this system, it is expected that the aircraft will be moderately more expensive to maintain and will have to spend

more time out of service during some of the required maintenance checks. While they must be examined, electric motors are generally low maintenance and should last a long time in this use case. A benefit of the turboelectric architecture that was selected for this aircraft is that it does not require a large battery which would have to be maintained and periodically replaced. The lower maintenance of a turboelectric architecture was a motivation for its selection. This will help keep maintenance costs similar to conventional turboprops, and was a driving force behind selecting a turboelectric system.

By the use of future subsystems, there will be some relief in maintenance. As discussed previously, utilizing a power-by-wire significantly decreases the hassle of the hydraulics system. Using a fly-by-light system also localizes maintenance to be done on the surface control systems. While there will be an increase in maintenance to the propulsion system, decreases in subsystem maintenance should help offset the increases in some manner.

B. Repair

When parts fail, it will be important to ensure that they can be replaced or repaired quickly. In order to make this possible for customers, maintenance, repair, and overhaul centers with spare part warehouses will be positioned nearby all major markets for the aircraft. As a new manufacturer, it will be especially important to demonstrate to potential customers that there will be continuing support for maintenance and repair of the aircraft.

Utilizing cheaper and lightweight parts, as well as keeping repairs simple, is key to repair. Many of the electric propulsion system components are relatively light. Repairs may be somewhat complicated by the high wing, but this is already a problem dealt with in the state-of-the-art aircraft.

XIV. Cost

This section will discuss a full cost analysis of the Songbird-E in comparison to the ATR 42-600, and a cost model developed for it. This section will analyze a business case analysis, the methods used in cost estimation, research, development, test, and evaluation (RDTE) costs, production and unit costs, and operating costs.

A. Business Case Analysis

In a 2022 ATR market forecast, the manufacturer predicted that 620 turboprop aircraft in the 40 to 60 pax range will be purchased between now and 2041 [66]. This forecast was conducted assuming no change in technology or transformative change to business conditions. These assumptions may not be reasonable. If new technologies are implemented in an advanced aircraft to reduce its operating costs, such as is proposed here, more airlines may demand turboprops. In addition, airlines around the world have committed to achieving net-zero carbon

emissions in the coming decades [67]. To achieve this goal, they will need to utilize newer, more efficient aircraft. Current turboprops are significantly more fuel efficient than comparable jet aircraft. Implementing hybrid-electric propulsion could further enhance the environmental benefits of turboprops. Because of this, it is expected that if an aircraft, such as the one proposed here, is brought to market, the total number of 50 pax turboprop aircraft purchased in coming years will exceed ATR's forecast. However, the extent of this difference is difficult to estimate. Therefore, the following cost analysis has been conducted assuming that 300 aircraft will be purchased. This represents a substantial market share of future turboprop demand. For the 15-year production run of the aircraft, this is a rate of approximately two aircraft per month.

B. Cost Estimation Method

Costs were estimated using Advanced Aircraft Analysis (AAA) software [68], which utilizes cost estimation relationships from Roskam's *Aircraft Design: Part VIII* [69]. Key parameters for the model include takeoff gross weight, number and power of engines, number of aircraft to be produced, current and EIS years, desired profit margin, and various correction factors. The model accounts for inflation and other projected cost changes through a Cost Escalation Factor (CEF). In order to validate the model, it was implemented on the ATR 42-600 and compared to publicly-available information on its list price. In addition, the direct operating cost (DOC) output for the ATR 42-600 is shown, however no data was found on this. The results of this are shown in Table XIV-1.

Table XIV-1. ATR 42-600 Model and Cost Validation

	Actual Cost	Modeled Cost	Error
Sale Price ($ Millions)	19.5 [70]	20.7	6.24%
DOC ($/hr)	-	3,450	-

Uncertainty in this model arises from necessary simplifications that have to be made as many specific details of the aircraft are not yet known. For example, the model uses factors to account for the use of advanced materials, use of CAD, and engineering complexity rather than doing a detailed analysis. This will negatively impact the accuracy of the model; however, it appears that the error is at a tolerable level, as the error for the modeled cost of the ATR 42-600 is only about 6.24%.

C. Research, Development, Test, and Evaluation Cost (RDTE)

The RDT&E phase of the program includes the cost of designing the aircraft, building test aircraft, going through the certification process, and preparing for manufacturing. The total RDT&E cost was estimated to be $1.23 billion. Key assumptions made in this phase include that advanced materials would be used in the aircraft, the development would involve novel, costly to develop technologies, and that five test aircraft would be built. Specific data on FAA certification costs were not available. A rough estimate of $100 million for a commercial aircraft was included [71]. In addition, a 15% profit margin was included, as required by the RFP. Figure XIV-1 shows the breakdown of the total RDT&E cost.
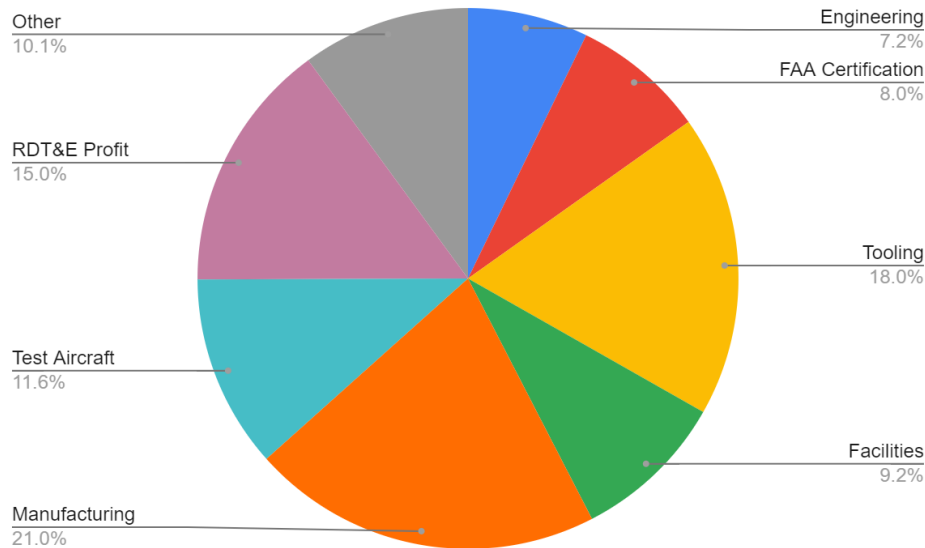
Figure XIV-1. Breakdown of RDT&E Costs

D. Production and Unit Cost

The cost of the manufacturing phase includes labor, quality control, material, and engine costs. It is estimated that the production phase of the program will cost $6.26 billion. The flyaway (marginal) cost of the aircraft is estimated to be $20.9 million. The price at which the aircraft must be sold to achieve a 15% profit margin is $28.1 million. This price is significantly higher than the $20.72 million that is estimated for the ATR 42-600 using this model. As shown in Figure XIV-2, at this price, 171 aircraft must be sold to break even. If the projected 300 aircraft are sold, the production stage profit will be $940 million.
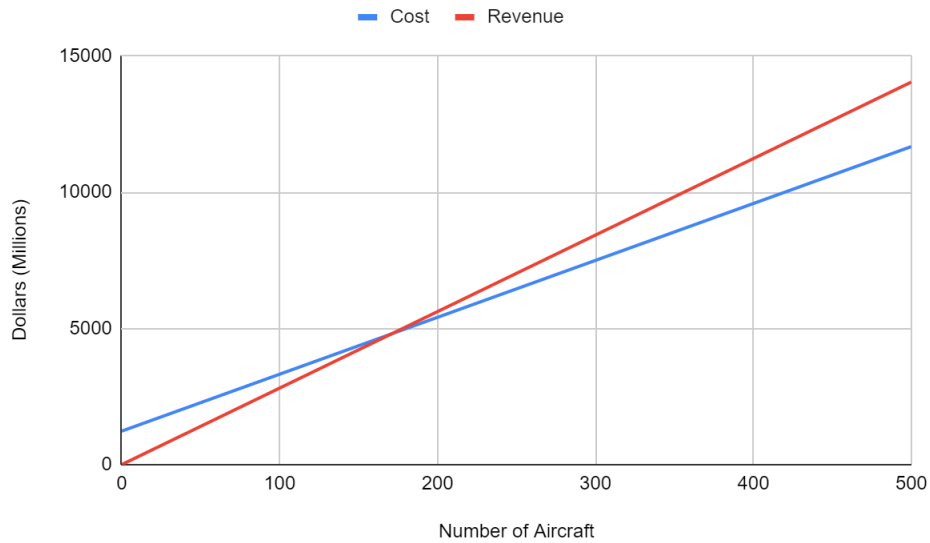
Figure XIV-2. Cost and Revenue

E. Operating Cost

The DOC is the cost to operate the aircraft per flight hour. Key contributors to this cost include the cost of consumables, such as fuel and oil, crew salaries, and maintenance. It is estimated that the DOC for this aircraft will be $2,960 per flight hour. This is about 14% lower than the estimated operating cost of the ATR 42, assuming the same crew salaries and fuel price. Due to this reduced operating cost, it is estimated that a typical regional airline would be able to breakeven on the higher purchase price in only seven years. The breakdown of the DOC is shown in Figure XIV-3. Other operating costs include insurance, depreciation, and navigation fees.
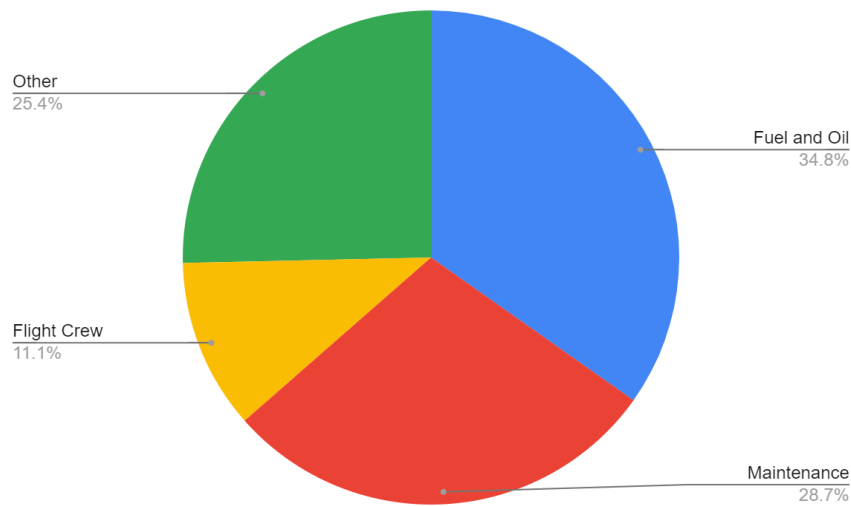
Figure XIV-3. Breakdown of DOCs

XV. Conclusion

Sustainable aviation is a key component of reducing global pollution and emissions. This report has described, in-depth, the iterative design process that created the Songbird-E, which seeks to be the solution in the regional turboprop market. Regional air travel is key for airlines to have service in smaller airports, connecting more people to air transportation, and for connecting people between airports. Regional turboprops are a necessary component of the commercial aviation industry. As there are few competitors left in the regional turboprop market, the Songbird-E seeks to enter and change the game. Seeking to both drive competition and reduce the environmental impact of regional aviation, the AIAA has selected an excellent design point for this year's RFP.

The Songbird-E excels against current competition, achieving a 33.6% reduction in block fuel burn as compared to the ATR 42-600, which is already best-in-class in its efficiency. The Songbird-E also significantly reduces emissions, seeing a 33.6% reduction in CO_2e, as well as a 0.5% reduction in NOX. On top of blowing away the two figures of merit, the Songbird-E exceeds the ATR 42-600 in just about every metric of performance. Its ability to reach smaller runways may bring the Songbird-E into even more destinations, allowing greater equity in access to air transportation. Though it has a higher sticker price, the Songbird-E sees an attractive 14.2% reduction in direct operating cost, meaning that the aircraft pays for itself in about 7 years, which is nothing considering the longevity of current turboprops. While other target requirements could have been met, the Songbird-E meets a design point that maximizes feasible target requirements and minimizes block fuel burn and emissions. The Songbird-E excels in more efficient aerodynamics, state-of-the-art subsystems, and promising future composites.

This report sets forth a viable candidate for a 2035 hybrid-electric, regional turboprop. Our analyses could be repeated, with higher fidelity modeling and tools, to validate much of the work done here. Future work could be conducted to find even more future subsystems to utilize on our aircraft, running high-fidelity CFD simulations to investigate more fully the Songbird-E's aerodynamic benefits, and performing a more in-depth acoustic analysis. More in-depth structural analysis, including aeroelastic flutter, could also help reduce the wing weight. An in-depth trade study would also be done to determine whether our wingspan and aspect ratio are the optimal configuration. The conceptual design of the Songbird-E leaves a definitive concept that could be developed into a tangible, 2035 product, and has the potential to revolutionize the regional turboprop market, and aviation as we know it.
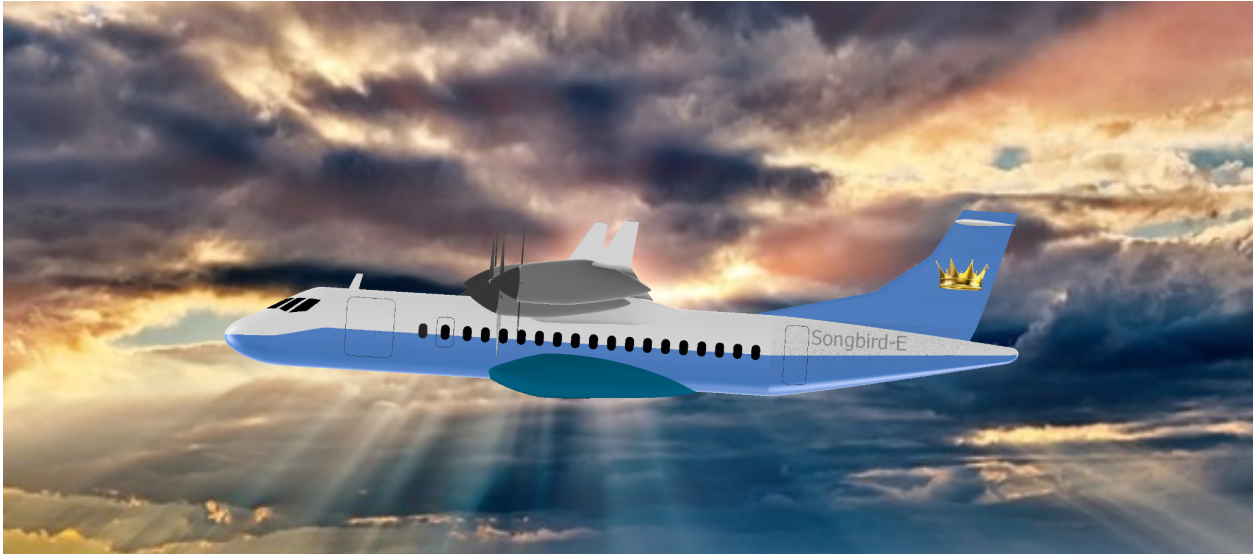
Figure XV-1. Rendered Image of the Songbird-E In Flight

References

[1]   *Guidelines for analysis of Hybrid-Electric Aircraft System Studies*. aiaa.org. (n.d.). Retrieved from
        https://www.aiaa.org/docs/default-source/uploadedfiles/publications/standards/hybrid-electric_properties_at
        tributes.pdf?sfvrsn=c8eb8f11_0

[2]   Transport. IEA. (n.d.). https://www.iea.org/topics/transport

[3]   IEA. (n.d.). *Aviation – analysis*. IEA. https://www.iea.org/reports/aviation

[4]   Announcements, & Announcements. (2022, December 20). *OpenVSP workshop 2023 save the date!*.
        OpenVSP. https://openvsp.org/

[5]   *OpenVSP*. VSPAero Tutorial [OpenVSP]. (n.d.). https://openvsp.org/wiki/doku.php?id=vspaerotutorial

[6]   GmbH, G. (n.d.). *Home*. GasTurb. https://www.gasturb.de/

[7]   *Advanced aircraft analysis: Darcorporation: Aeronautical software*. DARcorporation. (2023a, April 4).
        https://www.darcorp.com/advanced-aircraft-analysis-software

[8]   NASA. (n.d.). *Flight Optimization System (FLOPS) software v.9(LAR-18934-1)*. NASA.
        https://software.nasa.gov/software/LAR-18934-1

[9]   *FlightStream aerodynamic modeling software*. DARcorporation. (2023, April 4).
        https://www.darcorp.com/flightstream-aerodynamics-software/

[10]   Roskam, J. (2004). *Airplane Design Part V: Component Weight Estimation*. DARcorporation.

[11]   Carichner, G. E., & Nicolai, L. M. (2013). *Fundamentals of aircraft and Airship Design*. American Institute
        of Aeronautics and Astronautics.

[12]   American Institute of Aeronautics and Astronautics. (n.d.). Hybrid-electric Regional Turboprop RFP.
        AIAA. American Institute of Aeronautics and Astronautics. (n.d.). Hybrid-electric Regional Turboprop
        RFP. AIAA. Retrieved from
        https://www.aiaa.org/docs/default-source/uploadedfiles/education-and-careers/university-students/design-c
        ompetitions/undergraduate-team-aircraft-design-competition/undergraduate-team-aircraft-design-2021-202
        2---aerial-fire-fighting-aircraft.pdf?sfvrsn=6d6f6ea5_0

[13]   FEAM technical training. (n.d.).
        http://www.feamtechnicaltraining.com/files/ATR%2042%20REFRESHER.pdf

[14]   ATR 42 Cargo. Air Charter Service. (n.d.).
        https://www.aircharterservice.com/aircraft-guide/cargo/atr-france/atr42cargo

[15]   *ATR 42-600*. www.atr-aircraft.com. (n.d.). Retrieved from
        https://www.atr-aircraft.com/wp-content/uploads/2022/06/ATR_Fiche42-600-3.pdf

[16]   Hosking, E.J., Kenny, D.P., McCormick, R.I., Moustapha, S.H., Sampath, P., & Smailys, A.A. (1999). The
        PW100 engine : 20 years of gas turbine technology evolution.

[17]   Gudmundsson, S. (2022). General Aviation Aircraft Design: Applied Methods and procedures.
        Butterworth-Heinemann.

[18]   Pratt & Whitney. (n.d.). PW127XT Engine Series. Pratt & Whitney. https://www.prattwhitney.com/en/products/regional-aviation-engines/pw127xt

[19]   *EASA.IM.E.041 - Pratt and Whitney Canada PW100 series engines*. EASA. (n.d.). Retrieved from https://www.easa.europa.eu/en/document-library/type-certificates/engine-cs-e/easaime041-pratt-and-whitney-canada-pw100-series

[20]   Antcliff, K. R., Guynn, M. D., Marien, T., Wells, D. P., Schneider, S. J., & Tong, M. J. (2016). Mission Analysis and Aircraft Sizing of a Hybrid-Electric Regional Aircraft. 54th AIAA Aerospace Sciences Meeting. https://doi.org/10.2514/6.2016-1028

[21]   NASA. (n.d.). *Updated assessment of turboelectric boundary layer ingestion propulsion applied to a single-aisle commercial transport - NASA technical reports server (NTRS)*. NASA. Retrieved from https://ntrs.nasa.gov/citations/20210016661

[22]   Teeuwen, Y. (2017). *Propeller Design for Conceptual Turboprop Aircraft* (thesis).

[23]   GeneusTM Smart Generator. Safran. (n.d.). https://www.safran-group.com/products-services/geneustm-smart-generator

[24]   *XROTOR Download Page*. web.mit.edu. (n.d.). https://web.mit.edu/drela/Public/web/xrotor/

[25]   NASA. (n.d.). *Propulsion investigation for Zero and near-zero emissions aircraft - NASA technical reports server (NTRS)*. NASA. Retrieved from https://ntrs.nasa.gov/citations/20090023315

[26]   NASA. (n.d.). High-Efficiency Megawatt Motor (HEMM). NASA Glenn Research Center. https://www1.grc.nasa.gov/aeronautics/eap/technology/hemm/https://www1.grc.nasa.gov/aeronautics/eap/technology/hemm

[27]   Husain, E., & Nema, R. S. (1982). Analysis of paschen curves for air, N2 and SF6 using the townsend breakdown equation. *IEEE Transactions on Electrical Insulation*, *EI-17*(4), 350–353. https://doi.org/10.1109/tei.1982.298506

[28]   Schnulo, S. L., Chapman, J. W., Hanlon, P., Hasseeb, H., Jansen, R., Sadey, D., Sozer, E., Jensen, J., Maldonado, D., Bhamidapati, K., Heersema, N., Antcliff, K., Frederick, Z. J., & Kirk, J. (2020). Assessment of the Impact of an Advanced Power System on a Turboelectric Single-Aisle Concept Aircraft. AIAA Propulsion and Energy 2020 Forum. https://doi.org/10.2514/6.2020-3548

[29]   XFLR5. (n.d.). Retrieved from http://www.xflr5.tech/xflr5.htm

[30]   *FLIGHTSTREAM®*. Index. (n.d.). Retrieved from https://researchinflight.com/

[31]   de Vries, R. & Vos, R. (2022). Aerodynamic Performance Benefits of Over-the-Wing Distributed Propulsion for Hybrid-Electric Transport Aircraft. AIAA SCITECH 2022 Forum.

[32]   Blaesser, N. J. (2019). Propeller-wing integration on the parallel electric-gas architecture with Synergistic Utilization Scheme (Pegasus) aircraft. AIAA Scitech 2019 Forum. https://doi.org/10.2514/6.2019-1809

[33]   Lappas, I., & Ikenaga, A. (2019, September 27). *Conceptual design and performance optimization of a tip device for a regional turboprop aircraft*. MDPI. https://www.mdpi.com/2226-4310/6/10/107

[34]   Dieter, S. C. H. O. L. Z. (2018). Definition and discussion of the intrinsic efficiency of winglets. *INCAS BULLETIN*, *10*(1), 117–134. https://doi.org/10.13111/2066-8201.2018.10.1.12

[35]   *ATR 42-600 aircraft: ATR aircraft*. ATR. (2022, July 28). Retrieved from
        https://www.atr-aircraft.com/our-aircraft/atr-42-600/

[36]   *Systems - ATR Training & Flight Operations Services*. TheAirlinePilots. (n.d.). Retrieved from
        https://theairlinepilots.com/forumarchive/atr/atr-systems.pdf

[37]   Palt, K. (n.d.). Boeing 737-900 - specifications - technical data / description.
        https://www.flugzeuginfo.net/acdata_php/acdata_7379_en.php

[38]   *Airplane Glass with Aviation Authority approval*. Aviation Glass. (n.d.).
        https://aviationglass.aero/airplane-glass

[39]   Nickol, C. L., & Haller, W. J. (2016). Assessment of the Performance Potential of Advanced Subsonic
        Transport Concepts for NASA's Environmentally Responsible Aviation Project. 54th AIAA Aerospace
        Sciences Meeting.https://doi.org/10.2514/6.2016-1030

[40]   *First flight in history with 100% sustainable aviation fuel in both engines on a commercial aircraft*. ATR.
        (2022, July 28).

[41]   *ATR 42-600 STOL aircraft: ATR aircraft*. ATR. (2023, March 23).
        https://www.atr-aircraft.com/our-aircraft/atr-42-600s-stol/

[42]   *ATR - Official Website - Air Tahiti*. Official website. (n.d.). Retrieved from https://www.airtahiti.com/en/atr

[43]   *Inpaint_nans*. MathWorks. (n.d.).
        https://www.mathworks.com/matlabcentral/fileexchange/4551-inpaint_nans

[44]   Ahuja, V. FlightStream Aeroacoustics Toolbox: Early Design Acoustics with OpenVSP Geometries. NASA
        OpenVSP Workshop 2021. Early-Design Aeroacoustics Prediction for Distributed Electric Propulsion
        Vehicles using FlightStream (openvsp.org)

[45]   *Stability and Control - Tamkang University*. tku.edt.tw. (n.d.). Retrieved May 3, 2023, from
        https://mail.tku.edu.tw/095980/8_Stability%20and%20Control.pdf

[46]   Napolitano, M. R. (2012). *Aircraft Dynamics*. Wiley.

[47]   J. Roskam, *Airplane design. Part II, Preliminary configuration design and integration of the propulsion
        system*. Lawrence, Kan.: Darcorporation, 2018.

[48]   Frederick, Z. J., Blaesser, N. J., Valdez, F. D., & Hanson, C. (2021). Weight and Balance
        Considerations for Electrified Aircraft Propulsion Applied to the Parallel Electric-Gas Architecture with
        Synergistic Utilization Scheme (Pegasus) Concept. AIAA AVIATION 2021 FORUM.
        https://doi.org/10.2514/6.2021-2449

[49]   Company Profile. ATR. (n.d.). Retrieved from
        https://www.atr-aircraft.com/wp-content/uploads/2021/09/Company-Profile-EN.pdf

[50]   Aircraft Landing Gear Types. Aeronautics Guide. (n.d.).
        https://www.aircraftsystemstech.com/p/landinggear-types-aircraft-landing-gear.html

[51]   *Airfoil Tools: NACA 6412 (NACA6412-IL)*. airfoiltools.com. (n.d.). Retrieved from
        http://airfoiltools.com/airfoil/details?airfoil=naca6412-il

[52]   IEEE Xplore. (n.d.-a). https://ieeexplore.ieee.org/Xplore/dynhome.jsp

[53]   *What is "Hotel mode" on a turboprop engine?* Aviation Stack Exchange. (1960, November 1).
         https://aviation.stackexchange.com/questions/1790/what-is-hotel-mode-on-a-turboprop-engine

[54]   *ATR 42-600 - price, Specs, photo gallery, history*. Aero Corner. (n.d.).
         https://aerocorner.com/aircraft/atr-42-600/

[55]   DefenseBridge. (2023, April 25). *Exploring the features and specifications of the ATR 42-600*.
         DefenseBridge.
         https://defensebridge.com/article/exploring-the-features-and-specifications-of-the-atr-42-600.html

[56]   *Aircraft seats*. RECARO. (n.d.). https://www.recaro-as.com/en/aircraft-seats/economy-class/sl3510.html

[57]   *Home - the world's lightest aircraft seat*. Expliseat. (2021, October 20). https://www.expliseat.com/

[58]   16, P. S. | M. (2016, March 3). *Durable, lightweight PC sheet homes in on aircraft interiors*.
         plasticstoday.com. https://www.plasticstoday.com/durable-lightweight-pc-sheet-homes-aircraft-interiors

[59]   Black, S. (n.d.). *Advanced materials for aircraft interiors*. CompositesWorld.
         https://www.compositesworld.com/articles/advanced-materials-for-aircraft-interiors

[60]   Clark, J., & Kirwan, K. (n.d.). *777 Freighter: Greater Efficiency for Long-Haul Operators*. Boeing.
         https://www.boeing.com/commercial/aeromagazine/articles/qtr_02_09/article_02_1.html

[61]   *ATR Cold Weather Operations*. (n.d.). Retrieved May 3, 2023, from
         https://theairlinepilots.com/forumarchive/atr/atr-cold-weather-operations.pdf

[62]   *What is FADEC?* Baesystems.com. (n.d.). Retrieved from
         https://www.baesystems.com/en-us/definition/what-is-fadec

[63]   Murray, G., & Green, J. (n.d.). After Covid-19, Aviation Faces a Pilot Shortage. OliverWyman.
         Retrieved from
         https://www.oliverwyman.com/our-expertise/insights/2021/mar/after-covid-19-aviation-faces-a-pilot-shortage.html

[64]   Mathur, A., Panesar, K., Kim, J., Atkins, E. M., & Sarter, N. (2019). Paths to Autonomous Vehicle
         Operations for Urban Air Mobility. AIAA Aviation 2019 Forum. https://doi.org/10.2514/6.2019-3255

[65]   *PW127XT engine series | Pratt & Whitney*. prattwhitney.com. (n.d.). Retrieved May 3, 2023, from
         https://www.prattwhitney.com/en/products/regional-aviation-engines/pw127x

[66]   Turboprop Market Forecast 2022-2041. ATR. (2022). Retrieved from
         https://www.atr-aircraft.com/wp-content/uploads/2022/07/ATR_Market-Forecast_2022_Digital_HD.pdf

[67]   Our Commitment to Fly Net Zero by 2050. IATA. (n.d.).
         http://www.iata.org/en/programs/environment/flynetzero/

[68]   *Advanced aircraft analysis: Darcorporation: Aeronautical software*. DARcorporation. (2023, April 4).
         Retrieved from https://www.darcorp.com/advanced-aircraft-analysis-software/

[69]   Roskam, J. (2018). Airplane Design Part VIII: Airplane Cost Estimation: Design, Development,
         Manufacturing and Operating. DARcorporation.J. Roskam, *Airplane Design Part VIII: Airplane Cost
         Estimation: Design, Development, Manufacturing and Operating*. Lawrence, KS: DARcorporation, 2018.

[70]   ATR 42-600 Specs, Interior, Cockpit, and Price. Airplane Update. (n.d.). Retrieved from
         https://www.airplaneupdate.com/2019/08/atr-42-600.html

[71]   Siemens. (n.d.). Aerospace engineering services company uses Simcenter Star-CCM+ to reduce aircraft certification cost. Siemens. Retrieved from
https://resources.sw.siemens.com/en-US/case-study-tlg-aerospace